# STUDIES ON BARIUM TITANATE BASED 0- 3 COMPOSITES

SUBMITTED BY

CHEUNG MAN CHIU

FOR THE DEGREE OF MASTER OF PHILOSOPHY

AT

DEPARTMENT OF APPLIED PHYSICS

THE HONG KONG POLYTECHNIC UNIVERSITY

AUGUST 1999

# Acknowledgments

First, I am deeply indebted to my chief supervisor Prof. Helen. L.W. Chan and co-supervisor Prof. C.L. Choy for their valuable comments, supervision and encouragement throughout the period of my research work.

I am grateful to Dr. Q.F. Zhou for his skilful assistance and suggestion in the sol-gel process and film preparation. I would like to thank Mr. D.M. Lei from the Department of Physics of Zhongshan University in Guangzhou, China, for his technical assistance and advice in the bulk ceramic fabrication. Furthermore, thanks to Dr. K.W. Kwok for his help in the LIPP measurements and advice.

Thanks are also due to Dr. Bernd Ploss and Dr. Beatrix Ploss, Mr. M.N. Yeung of the Materials Research Centre, the research personnels and technicians of our departments for their helpful discussion and technical support during the period of my study.

I gratefully acknowledge the financial support from the Honk Kong Polytechnic University. Last, but not least, I would like to thank my family and friends for their encouragement and support.

# Abstract

Fabrication and characterizations of barium titanate $BaTiO_3$ based 0-3 composites are presented and discussed. Two types of composites are studied. First, barium titanate powder prepared by a mixed oxide route is dispersed into a poly(vinylidene fluoride-trifluoroethylene) P(VDF-TrFE) copolymer matrix to form ceramic/polymer composites. The second type of ceramic/ceramic composite is fabricated by mixing a sol-gel $BaTiO_3$ powder into a $BaTiO_3$ sol-gel matrix.

$BaTiO_3$/P(VDF-TrFE) 0-3 composites with various ceramic volume fractions are fabricated. The dielectric permittivity and loss of the 0-3 composites are measured as functions of temperature. These data are used to estimate the electric field experienced by the ceramic phase during poling and used to optimize the poling temperature. After the poling process, the pyroelectric and piezoelectric properties of the 0-3 composites were measured and compared to model calculations. The polarization distributions of the composites were also studied using the laser induced pressure pulse (LIPP) method.

$BaTiO_3$/$BaTiO_3$ ceramic/ceramic composite films are fabricated by a modified sol-gel process. Nano-sized $BaTiO_3$ powder are dispersed in a $BaTiO_3$ sol-gel matrix to form a 0-3 composite solution. Films are prepared by spin coating many layers (8 layers with thickness about 16 μm) on stainless steel substrates and annealed at various temperatures. The crystallization of the 0-3 composite film is studied by X-ray

diffraction. The dielectric permittivity and the ferroelectric properties of the films are also measured.

The major findings of the project included:

(1) Barium titanate ($BaTiO_3$) powders with size in the nanometer range were prepared by a sol-gel process and coprecipitation method. The average particle size of the powder prepared by a sol-gel process and coprecipitation method was 100 nm and 300 nm, respectively. $BaTiO_3$ ceramic, with grain size $\geq$ 1 μm, were prepared by sintering the sol-gel derived powder and the coprecipitation derived powder. The dielectric permittivity and the ferroelectric hysteresis loop were measured as functions of temperature. The room temperature (25 °C) dielectric permittivity, pyroelectric and piezoelectric properties were also measured as functions of the poling field. The results will be submitted for publication.

(2) Barium titanate/polyvinylidene fluoride-trifluoroethylene [$BaTiO_3$/P(VDF-TrFE)] 0-3 composites with different volume fractions of ceramic were fabricated. The permittivities and electrical resistivities of the composites were measured as functions of temperature. These data were then used to find the electric field experienced by the ceramic phase and hence the optimum poling temperature. The pyroelectric and piezoelectric properties of the composites were measured and compared to model calculations. The results are published in *Ferroelectrics*, Vol.224, pp.113-120 (1999).

(3) Barium titanate ($BaTiO_3$) 0-3 ceramic/ceramic composite thick films (~16μm) for ultrasonic transducer applications were fabricated by a modified sol-gel process. Nano-sized $BaTiO_3$ powder was dispersed in a sol-gel matrix of $BaTiO_3$ to form a 0-3 composite solution. Films were prepared by spin coating and then annealed at various temperatures. The crystallization of the composite film was studied by X-ray diffraction. The dielectric permittivity and the ferroelectric properties of the film were also measured. The results will be published in *Proceedings 1999 Spring Meeting Symposium* and in *Nano Structured Materials*.

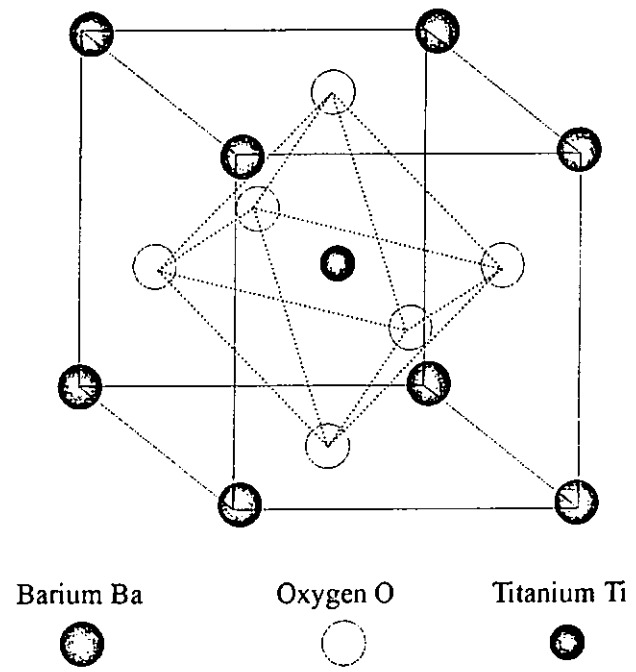


Fig. 1.1 The perovskite ($ABO_3$) structure of $BaTiO_3$ above its Curie point [2].

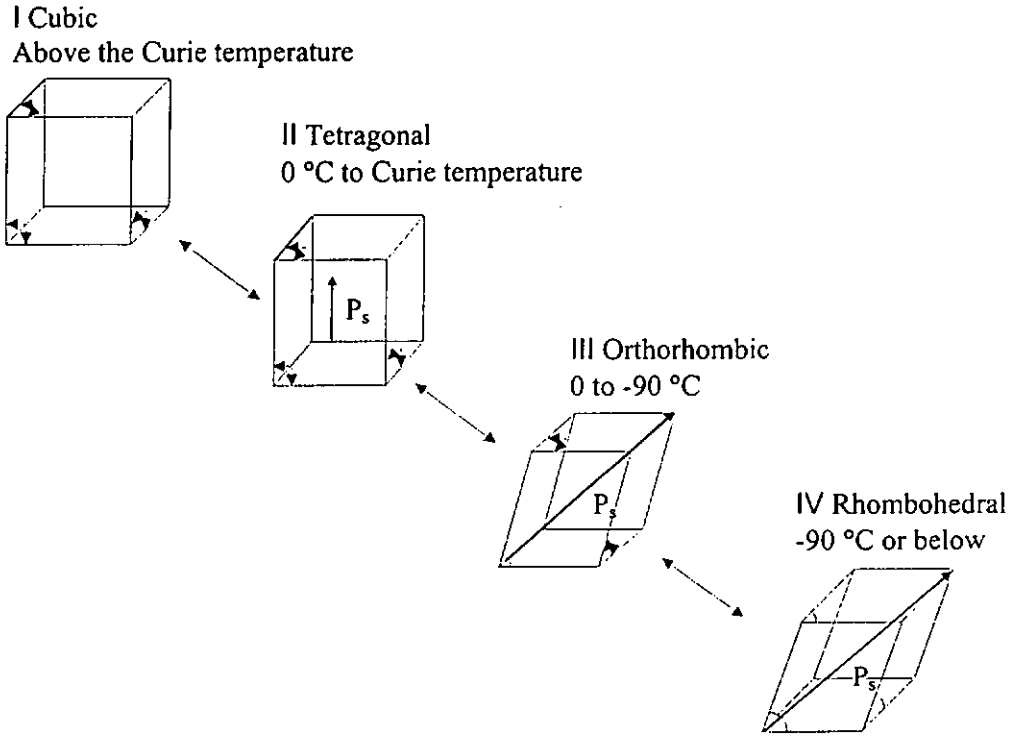


Fig. 1.2 Phase changes of a $BaTiO_3$ unit cell into different polymorphs. The arrow shows the direction of polarization [1,2].

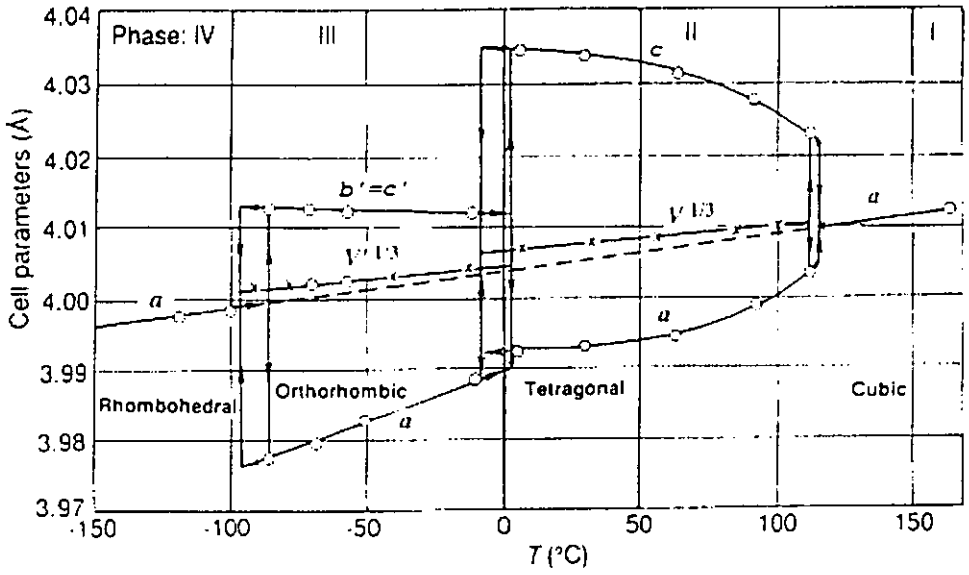


Fig. 1.3 Lattice parameters of $BaTiO_3$ as a function of temperature. V is the volume of unit cell and b', c', V' are cell parameters of the pseudo-cubic unit cell [2].

### 1.1.2 Ferroelectric Properties

An important characteristic of a ferroelectric ceramic is the hysteresis loop, i.e. the polarization P as a doubled-valued function of the applied field as shown in Fig. 1.4. By applying an a.c. electric field across a ferroelectric sample, dipoles begin to line up with the field. As the field is large enough to align all the domains in the positive direction, saturation polarization is obtained. When the field strength decreases, the polarization decreases. As the field is removed, some of the domains will remain aligned in the positive direction. The sample will exhibit a remanent polarization $P_r$. The polarization cannot be removed until the field in the negative direction reaches a certain value called the coercive field $E_c$. The field increases in the negative direction will cause a complete alignment of the dipoles in the negative direction. The cycle can

be completed by reversing the field direction once again. At higher temperature, narrower loop and smaller coercive field will be obtained. This is due to the higher mobility of ferroelectric domains in the sample at higher temperatures. Above the Curie temperature, the ferroelectric behavior disappears. The area of the hysteresis loop is related to the energy of polarization.

Generally, ferroelectric materials with high values of remanent polarization $P_r$ are useful piezoelectric materials. The $P_r$ of $BaTiO_3$ single crystal is ~ 25 $\mu C/cm^2$ while $P_r$ of well-poled $BaTiO_3$ ceramics is ~ 8 $\mu C/cm^2$ [1].

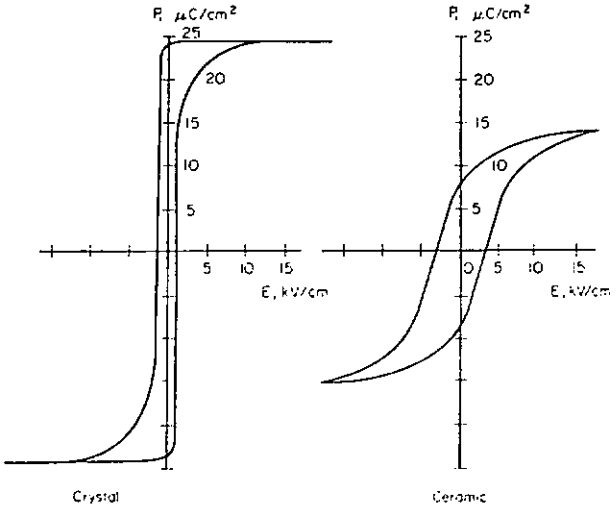


Fig. 1.4 Hysteresis loops of $BaTiO_3$ single crystal and ceramic [1].

### 1.1.3 Poling

Before poling, ferroelectric ceramics do not exhibit any piezoelectric and pyroelectric properties due to random orientations of the domains in the ceramics. During poling, a d.c electric field is applied across a ferroelectric material and the domains are reoriented. After poling, a remanent polarization and strain remained in the sample and the sample will exhibit piezoelectric and pyroelectric effect. Fig. 1.5 shows the schematic drawings of the poling process for a piezoelectric ceramic.

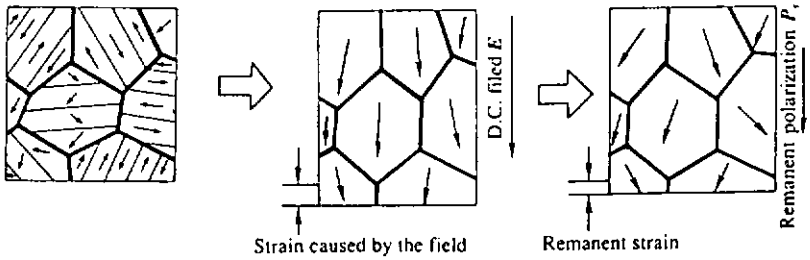


Fig. 1.5 Illustration of the poling process for a piezoelectric ceramic [2].

| | c/a ratio | Pyroelectric coefficient, p ($\mu C/m^2K$) | Piezoelectric coefficient, $d_{33}$ (pC/N) | Remanent polarization, $P_r$ ($\mu C/cm^2$) |
|---|---|---|---|---|
| Single crystal | 1.010 | 200 | 85.6 | 26 |
| Ceramic | 1.010 | 235 | 191 | 8 |

Table 1.1 Summaries of the properties of $BaTiO_3$ single crystal and ceramic [1,2].

### 1.1.4 Grain Size Effect

The grain size effect of a $BaTiO_3$ ceramic have a pronounced influence on the ferroelectric and the dielectric properties.

According to Artl, G. et al. (1985) [3], the tetragonality of $BaTiO_3$ ceramic is about 1.010 when the grain size of the ceramic is greater than 1.5 μm. As the grain size decreases smaller than 1 μm, the tetragonality also decreases. McNeal, M.P. et al. (1998) [4] reported the similar trend. When the grain size of the $BaTiO_3$ ceramic equal to 0.26 μm, the c/a ratio becomes 1 and it has a cubic structure.

In ISAF'94 meeting, Bell, A.J. [5] presented an informative chronological review of the grain size effects in $BaTiO_3$. Figs. 1.6(a) and 1.6(b) show the grain size effect on the room temperature dielectric permittivity as determined by Artl, G. et al. (1985) [3] and Shaikh, A.S. et al. (1989) [6], respectively. Artl, G. et al. also found that the room temperature dielectric permittivity of $BaTiO_3$ ceramic maximized for the grain size between 0.7 to 1 μm, whereas Shaikh, A.S. et al. reported that the dielectric permittivity of $BaTiO_3$ ceramic maximized at 0.4 μm.

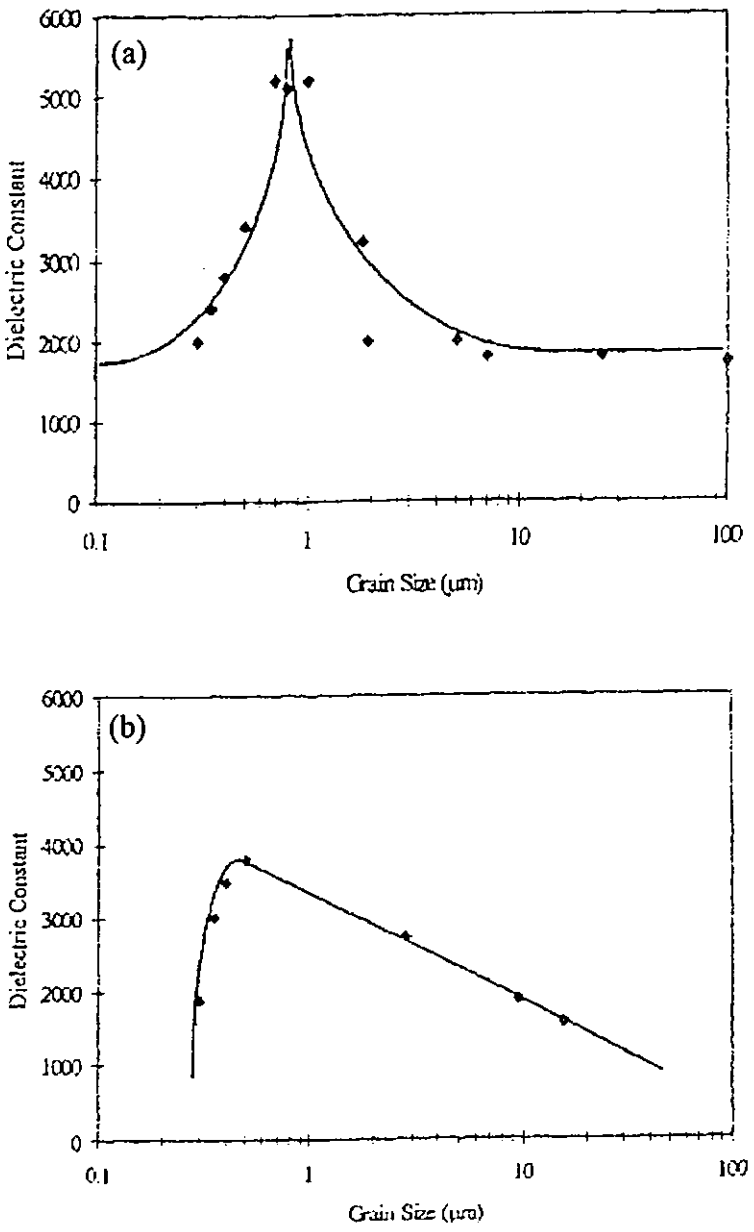


Fig. 1.6 Grain size effect on the room temperature dielectric permittivity of $BaTiO_3$ ceramic of (a) Artl, G. et al. [3] and (b) Sharikh, A.S. et al. [6].

## 1.2 Literature Review on P(VDF-TrFE) Copolymer

In the past few decades, polyvinylidene fluoride PVDF and its copolymers with trifluorethylene, poly(vinylidene fluoride-trifluoroethylene) P(VDF-TrFE), have attracted special attention from researchers since Kawai [7] first demonstrated the piezoelectricity of PVDF in 1969. PVDF has no Curie transition below its melting point while P(VDF-TrFE) has an observable Curie temperature $T_c$ and the location of $T_c$ depends on the mol% of TrFE present in the copolymer.

PVDF consists of a repeating unit of $-CH_2CF_2-$. It has three major crystalline phases, they are the α, β and γ-phase. β-phase is the preferred polar with piezoelectric activity because the dipoles of $CH_2$ and $CF_2$ oriented perpendicular to the molecular chain of the polymer.

Three crystalline phases of PVDF:

α-phase (Fig. 1.7a), it is the most common polymorph. Two chains pack in antiparallel directions which results in the cancellation of the dipole moment and it is non-polar. Another polar version similar to the α-phase is called the δ-phase (Fig. 1.7b).

β-phase (Fig. 1.7c), the chain backbone has an all-trans planar zigzag conformation. All chains are oriented in the same direction with the dipoles pointing in the same direction. As a result, β-phase PVDF is polar.

γ-phase (Fig. 1.7d), the chain backbone has a $T_3GT_3G'$ conformation (T: Trans, planar, G: gauche, non-planar). The molecular chains are packed parallelly in the noncentrosymmetric polar crystal.

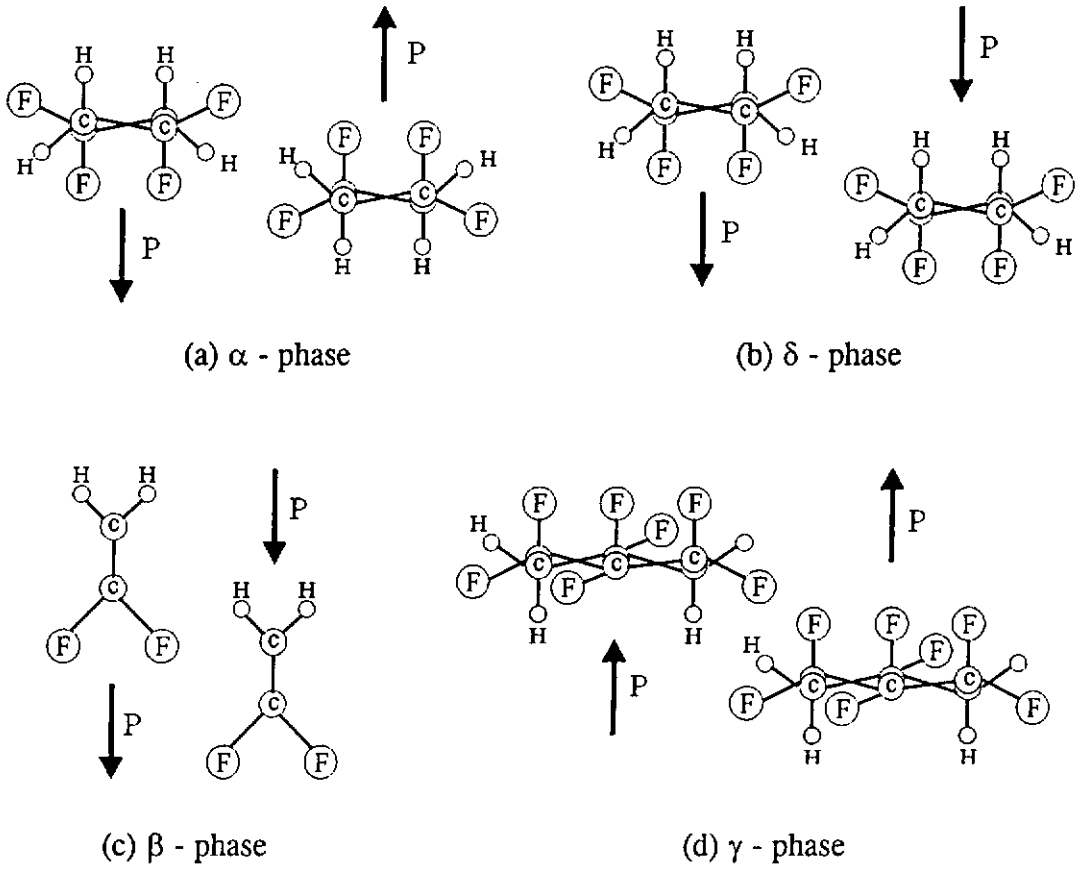


Fig. 1.7 Molecular arrangement in unit cells of (a) α, (b) δ, (c) β and (d) γ -phase of PVDF. Arrows indicate the dipole directions normal to the molecular axes [8].

Among the four crystalline phases, only the α-phase is non-polar. But the α-phase can be converted into other polar phases by mechanical drawing or by applying a high electric field. (see Fig. 1.8) [9,10].

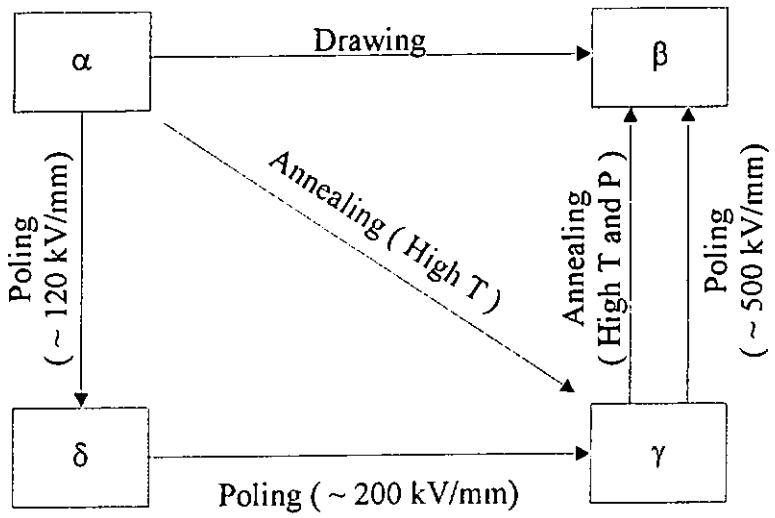


Fig. 1.8 The crystalline transformations among polymorphs of PVDF by poling, thermal treatments or by mechanical drawing.

P(VDF-TrFE) is a random copolymer with monomer units ($-CH_2CF_2-$) and ($-CHCF_3-$) which exhibits net dipole moments (see Fig. 1.9). In TrFE, there are three fluorine atoms, thus TGTG' conformation is formed and enhance the all-trans conformation of the β-phase. So, P(VDF-TrFE) copolymers crystallize directly into the polar β-phase when the VDF content is in the ranges of 50 to 83 mol% [11,12]. The copolymer used in the present work has 70 mol% VDF. It is ferroelectric with Curie temperatures of 105 °C upon heating and 70 °C upon cooling. The Curie transition of the copolymer is below its melting temperature (153 °C). In the early 80's, many researchers were interested in P(VDF-TrFE) copolymers because this copolymers were reported to be piezoelectric and pyroelectric without the need of mechanical stretching. Hence, it can be spin coated onto a silicon substrate, can be poled in situ and used in integrated piezoelectric and pyroelectric sensors [11,12].

# Table of Contents

# Table of Figures

# List of Tables

# CHAPTER ONE

# INTRODUCTION AND REVIEW

Piezoelectric ceramics such as barium titanate ($BaTiO_3$), lead titanate ($PbTiO_3$) and lead zirconate titanate ($PbZr_{(1-x)}Ti_xO_3$) have been used in transducer applications for many years. However, these ceramic can find new applications when it is combined with a polymer or a ceramic sol-gel matrix. One of the most attractive features of ceramic/polymer 0-3 composites is that it can be fabricated into various forms, such as thin film, extruded bars or a specific molded shape. By dispersing ceramic powder into a sol-gel matrix, thicker films (> 10 μm) can be fabricated. Films with thickness up to several microns or higher have potential for applications such as pyroelectric infrared sensors, microelectromechanical systems (MEMS), high frequency ultrasonic transducer, etc.

## 1.1 Literature Review on Barium Titanate

Barium titanate ($BaTiO_3$) is one of the first lead-free piezoelectric ceramic developed and is still widely used. Since the early 1940's, many reports about $BaTiO_3$ have been published and many research works are still in progress. In recent years, there is an urgency of finding lead-free ceramics with good properties for various piezoelectric

applications for environmental protection. $BaTiO_3$ is one of the candidate that has this potential. $BaTiO_3$ has been used extensively in fabricating capacitor and as PTCR (Positive Temperature Coefficient of Resistance) ceramics. These applications are outside the scope of the present study and will not be discussed in the present work.

### 1.1.1 Crystal Structure

One of the basic structures of barium titanate is a perovskite form which is ferroelectric in a certain temperature range. Most of the useful ferroelectric ceramic, such as barium titanate ($BaTiO_3$), lead titanate ($PbTiO_3$), lead zirconate titanate ($PbZr_{(1-x)}Ti_xO_3$ PZT), etc, have a perovskite structure. Perovskite type ceramics have the general chemical formula $ABO_3$, where "A", "B" and "O" represent a cation with a larger ionic radius, a cation with a smaller ionic radius and oxygen, respectively. Fig. 1.1 shows a perovskite unit cell of $BaTiO_3$ above its Curie point.

Barium titanate has a paraelectric phase (cubic structure) above its Curie temperature (the Curie temperature of $BaTiO_3$ is in between 120 –130 °C [1-3]). When barium titanate is in the temperature range of 0 °C to the Curie temperature, it is tetragonal with tetragonality of about 1.010 [3]. For temperatures below 0 °C, barium titanate is orthorhombic. Barium titanate becomes rhombohedral at temperatures below –90 °C. Fig. 1.2 shows the phase changes of $BaTiO_3$ against temperature.

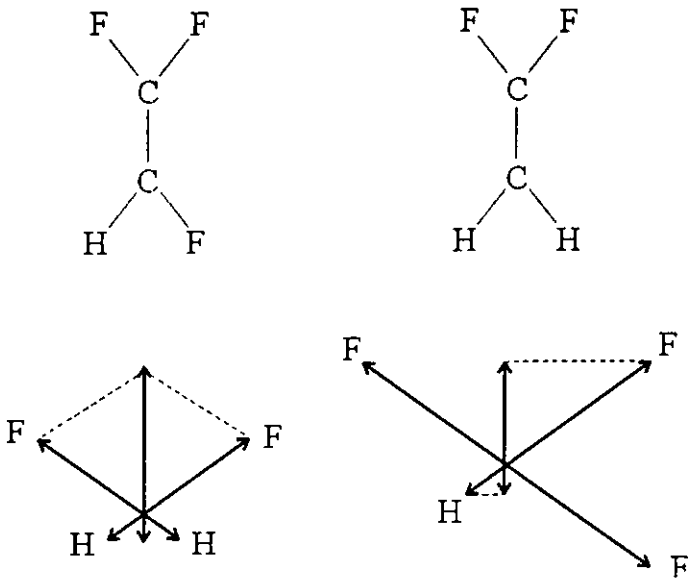


Fig. 1.9 Dipole moment of VDF and TrFE units [13].

## 1.3 Literature Review on 0-3 Composites

A composite material has a chemically and/or physically distinct filler phase distributed within a matrix phase. A composite generally has different and/or better characteristics than those of the constitutive components. Also the composite has improved properties to meet specific design requirements. The idea of connectivity of the composite was introduced by Newnham et al. in 1978 [14]. It was used to describe the possible arrangements for diphasic materials. In a diphasic system, there are ten possible combinations which are indicates with two digits to denote the connectivity of the filler and the matrix respectively.(i.e. 0-0, 0-1, 0-2, 0-3, 1-1, 1-2, 1-3, 2-2, 2-3 and 3-3 connectivities represented in Fig. 1.10). The digits "0" to "3" correspond to the dimensions of the phase that are continuous. 0-3 composite is a commonly used connectivity in which filler particles dispersed in a 3-dimensionally connected matrix.

Another commonly used system is the 1-3 composites. In the present study, we shall concentrate on the 0-3 pattern (Fig. 1.11).

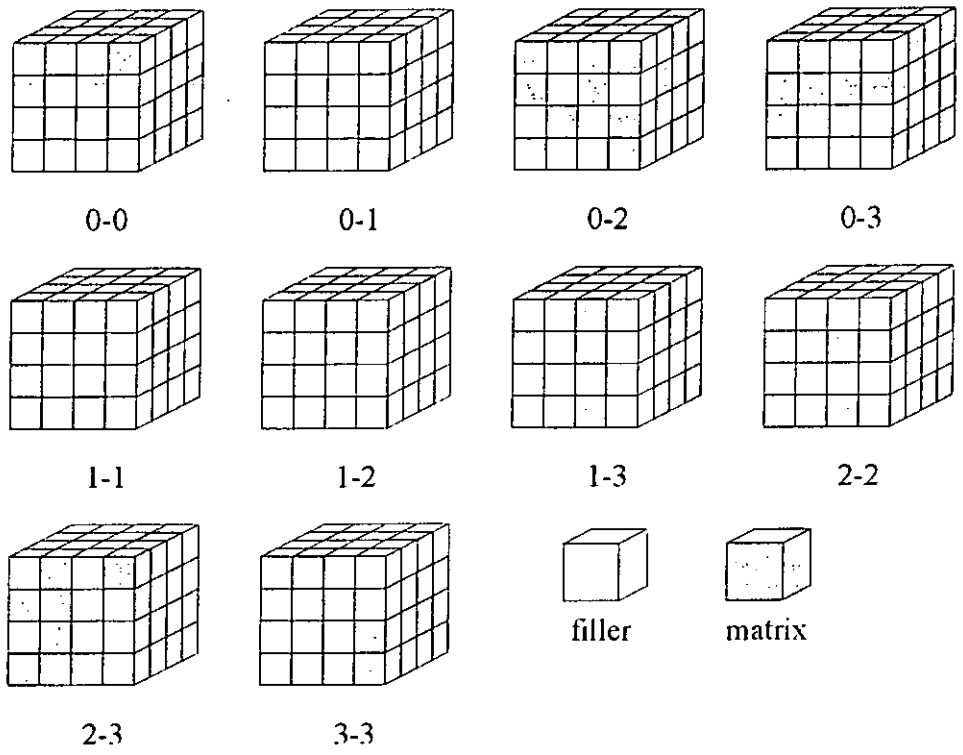


Fig. 1.10 Connectivity patterns in a diphasic composite system [14].

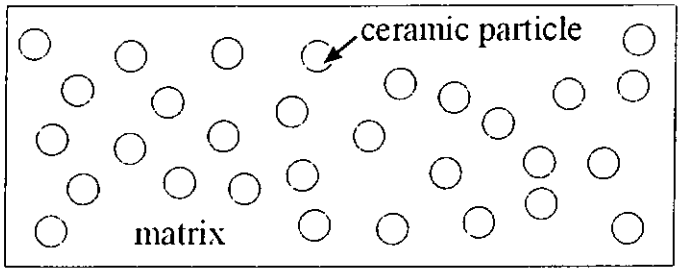


Fig. 1.11 Schematic diagram of a composite with a 0-3 connectivity.

### 1.3.1 Ceramic/Polymer 0-3 Composites

Dispersion of ceramic powder into a polymer matrix to form composites has been studied in the past twenty years [14-16]. Conventional piezoelectric materials such as lead titanate ($PbTiO_3$), lead zirconate titanate ($PbZr_{(1-x)}Ti_xO_3$) are the most popular choices in transducer applications. These materials provide a high electromechanical coupling factor ($k_t$ = 0.4-0.5), a wide range of dielectric permittivity, low dielectric and mechanical losses but also have large acoustic impedance (acoustic impedance Z = density × velocity of sound, ~ $37 \times 10^6$ kg/m$^2$s or 37 MRayl). So, it is difficult for PZT to have an acoustic impedance match with a soft media such as tissues and water. Ferroelectric polymer polyvinylidene fluoride (PVDF) and its copolymer with trifluoroethylene (P(VDF-TrFE)) [17] have advantage in this aspect as they which have a low acoustic impedance (Z ~ 4 Mrayl) that can match better to water or soft tissues (Z ~ 1.5 Mrayl). However, these polymers have a low electromechanical coupling factor and high dielectric losses which limits the application of these materials.

Composites can be formed by combining ceramic and polymer [18]. Combining a piezoelectric ceramic and a polymer to form a flexible ferroelectric composite can produce desirable properties [16] and it is easy to fabricate composites into different forms, such as thin film, molded shapes, extruded bars and fibers.

Various combinations of ceramic/polymer 0-3 composites have been studied. PZT, $BaTiO_3$, $PbTiO_3$, PLZT, etc are the main filler materials and PVDF, P(VDF-TrFE) with various molar ratio of PVDF and PTrFE , epoxy, etc are the matrix [14-16,18-30]. For the

composite of $BaTiO_3$ and P(VDF-TrFE) (70/30), no work has been reported in the literature.

### 1.3.2 Ceramic/Ceramic 0-3 Composites

In recent years, ferroelectric thin film of thickness ≤ 0.2 μm have been used in non-volatile memory and dynamic access memory applications [31,32]. However, the preparation of thicker ferroelectric films (up to several μm or higher) which have potential applications in pyroelectric infrared sensors, in microelectromechanical systems (MEMS), ultrasonic high frequency transducers, etc are still in the research stage [33].

Various deposition techniques such as sputtering [34], pulse laser deposition [35], sol-gel processing [36,37], etc have been used for ferroelectric film fabrications. Among the various techniques, sol-gel processing has attracted considerable interest because it can be used to produce large area homogeneous films with high purity (in stoichiometric ratio) at low costs and low processing temperatures. However, it is difficult to prepare films up to several microns using conventional sol-gel methods. Recently, a modified sol-gel method has been developed for preparing lead zirconate titanate films of thickness up to 60 μm [38]. In this method, films are made by dispersing nano-sized ceramic particles in a sol-gel matrix of the same kind of materials. The resulting coating is in a 0-3 pattern and is sometimes referred to a "ceramic/ceramic 0-3

composite". To-date no work has been reported in the literature on $BaTiO_3/BaTiO_3$ 0-3 composites.

## 1.4 Scope of Present Study

The present study can be separated into two parts. The first part is the study of barium titanate/ polyvinylidene fluoride-trifluoroethylene $BaTiO_3$/P(VDF-TrFE) 0-3 composites and the second part is the study of barium titanate $BaTiO_3$ ceramic/ceramic 0-3 composites.

In a $BaTiO_3$/P(VDF-TrFE) 0-3 composite, the ceramic powder was prepared by the mixed oxide route and samples with various ceramic volume fraction were fabricated by compression molding (thickness ~ 0.4 to 0.7 mm). The frequency dependence and the temperature dependence of dielectric permittivity $\varepsilon'$ and $\varepsilon''$ of $BaTiO_3$ ceramic, P(VDF-TrFE) and 0-3 composites were obtained by measuring the capacitance of the samples. The Bruggeman model was used to model the dielectric permittivity of the diphasic 0-3 composites. A poling process was used to induce the pyroelectric and the piezoelectric properties. The piezoelectric and pyroelectric properties and the polarization distributions in the 0-3 composites were measured. The result of the pyroelectric coefficient p and the piezoelectric coefficient $d_{33}$ are compared to model calculations.

To prepare a ceramic/ceramic 0-3 composite, a sol-gel method was used to prepare the $BaTiO_3$ nano-sized ceramic powder. The ceramic powder was then dispersed into a

$BaTiO_3$ solution to form a $BaTiO_3$ complex solution. The 0-3 composite films were fabricated on stainless steel substrates by spin-coating. The films were annealed at different temperatures. The crystallization process of the powder and the composite film was studied by X-ray diffraction. The dielectric permittivity and the ferroelectric properties of the film were also measured.

## 1.5 Outline of Thesis

This thesis contains seven chapters. Chapter one gives a brief introduction on the barium titanate, ceramic/polymer 0-3 composites and ceramic/ceramic composites. Fabrication of the barium titanate ceramic is described in chapter two. Three types of $BaTiO_3$ powder were prepared; the first type was prepared by a mixed oxide route and the two types of nano-sized $BaTiO_3$ powder were prepared by sol-gel process and a co-precipitation method, respectively. In chapter three, characteristics of the barium titanate are presented. Chapters 4 and 5 describe the structure, dielectric properties, the pyroelectric and the piezoelectric properties of the P(VDF-TrFE) copolymer and the $BaTiO_3$/P(VDF-TrFE) 0-3 composites with various ceramic volume fraction. Chapter 6 reports the fabrication method and the characteristics of the ceramic/ceramic 0-3 composites. Finally, chapter seven gives the conclusion.

# CHAPTER TWO

# FABRICATION OF BARIUM TITANATE CERAMICS

## 2.1 Introduction

In this chapter, fabrication processes of $BaTiO_3$ powder and ceramics are described. Three fabrication methods were used to prepare the $BaTiO_3$ powder. These were the mixed oxide route, the sol-gel process and the co-precipitation method. The powder prepared by the mixed oxide method was used to prepare barium titanate/polyvinylidene fluoride-trifluoroethylene [$BaTiO_3$/P(VDF-TrFE)] 0-3 composites. Detailed descriptions of the properties of the ferroelectric P(VDF-TrFE) copolymer and the $BaTiO_3$/P(VDF-TrFE) 0-3 composites are given in chapters 4 and 5. The powder prepared by a sol-gel process was also used in preparing barium titanate ($BaTiO_3$) 0-3 ceramic/ceramic composite thick films and the details are given in chapter 6. Properties of the $BaTiO_3$ ceramic discs prepared using powder derived by the three different methods are reported in chapter 3.

## 2.2 Preparation of $BaTiO_3$ Powder

### 2.2.1 Mixed Oxide Route

$BaTiO_3$ powder and the ceramic disc were prepared by Mr. D.M. Lei from the Department of Physics of Zhongshan University in GuangZhou, China using the conventional mixed oxide process [1]. It has a tetragonal structure with a = b= 3.976 Å and c= 4.017 Å as determined by X-ray diffraction (XRD). The c/a ratio was 1.010.

$BaTiO_3$ powder were made by reacting $BaCO_3$ and $TiO_2$ in air. The $BaTiO_3$ was initially formed at the $BaCO_3$-$TiO_2$ grain boundaries. In this process, $BaTiO_3$ reacted with $BaCO_3$ to form $Ba_2TiO_4$ until all the $BaCO_3$ was used up. Then the $Ba_2TiO_4$ reacted with the remaining $TiO_2$ to form $BaTiO_3$.

$$BaCO_3 + TiO_2 \xrightarrow{\text{Calcined at 1000 °C/ 8 h}} BaTiO_3 + CO_2\,(gas)$$

The ceramic powder used as filler in the ceramic/polymer 0-3 composite was obtained by grinding a sintered ceramic block in a ball-milling machine. The particle size of the powder is about 1 μm as determined by scanning electron microscopy (SEM) and the crystallite size is 52.2 nm as determined by X-ray diffraction method [39].

### 2.2.2 Sol-gel Process

To prepare $BaTiO_3$ powder by a sol-gel method [40], the process involved the mixing of titanium isopropoxide and barium acetate in deionized water under continuous stirring at room temperature. The amount of titanium isopropoxide and barium acetate was in a molar ratio of 1:1. In order to avoid precipitation, small amounts of acetic acid and acetylacetone were added. These sols were relatively stable and gel in a few days. The $BaTiO_3$ gels was dried at 100 °C for about 24 h and then annealed at 800 °C for 2 h to obtain the $BaTiO_3$ powder. Fig. 2.1 shows the procedure for preparing the $BaTiO_3$ powder by the sol-gel process. The particle size of the powder was about 100 nm and the crystallite size is 46.4 nm, it is much smaller than the size of the powder prepared by the mixed oxide route.

### 2.2.3 Co-precipitation Method

The $BaTiO_3$ powder prepared by co-precipitation method was supplied by Prof. Z.Z. Huang from the Shanghai Institute of Ceramics. To prepare $BaTiO_3$ powder by a co-precipitation method [41], the mixed solution of barium chloride and titanium tetrachloride was titrated dropwise into an oxalic acid while being vigorously stirred. The amount of barium chloride and titanium tetrachloride was in a molar ratio of 1:1. The quantity of the oxalic acid was 20 % in excess the stoichiometric amount required for precipitates. The resulting $BaTiO_3$ precipitates were washed repeatedly using

deionized water and were dried at 80 °C. The particle size of the powder was about 300 nm and the crystallite size is 68.8 nm.

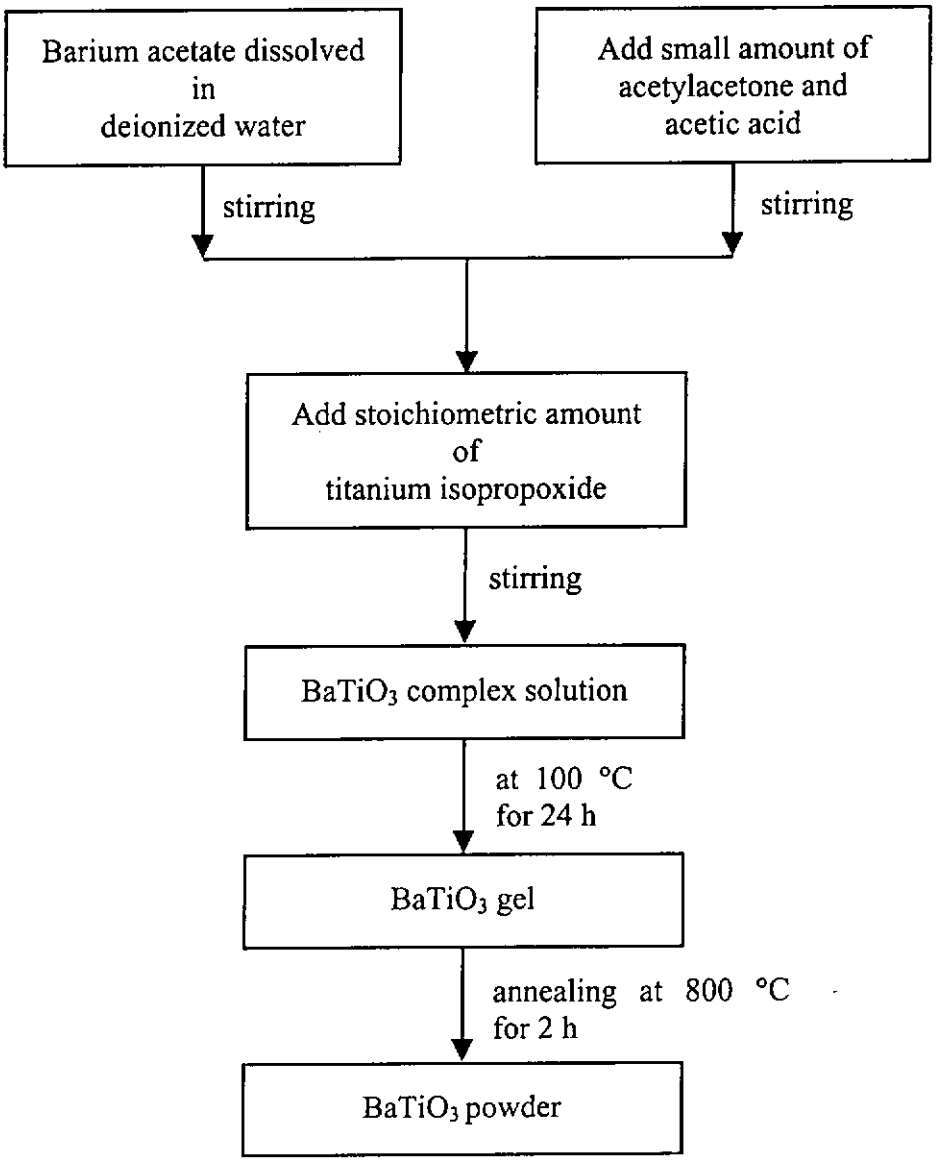


Fig. 2.1 Flowchart showing the procedures for preparing $BaTiO_3$ powder by a sol-gel process.

## 2.3 Fabrication of $BaTiO_3$ Ceramic Discs

### 2.3.1 Compression Molding

The powder prepared by the mixed oxide route and the sol-gel process were fabricated into discs by compression molding. About five weight percent polymer binder solution, polyvinyl alcohol (PVA), was added to the ceramic powder. It allows the powder to be shaped easily. The PVA and the powder were mixed continuously to produce a homogeneous mixture. The mixture was put into a stainless steel mold and uniaxially pressed into a disc shape at a pressure of about 160 MPa at room temperature. The dimension of the disc was about 20 mm in diameter and 1.1 mm thick. Then the disc was heat-treated at 750 °C for 1 h in a programmable temperature controlled furnace to remove the organic binder. The heat-rate should be relatively slow during the binder burn-out. After the polymer binder was burnt off, the ceramic discs were sintered at a higher temperature.

The ceramic disc fabricated with the powder prepared by the mixed oxide route was sintered at 1320 °C for 1 h with a heating rate of 10 °C/min. After sintering, the geometry of the ceramic disc was reduced to 17 mm in diameter and 0.9 mm thick.

The ceramic disc fabricated with the powder prepared by the sol-gel process was sintered at 1150 °C, 1200 °C and 1320 °C for 1 h. Lower sintering temperature can be used due to the smaller particle size of the powder obtained from the sol-gel process

(~ 100 nm). The driving force during sintering is much larger than that of the powder (> 1 μm) obtained from a mixed oxide route.

### 2.3.2 Roll-pressed Method

The powder prepared by co-precipitation method was fabricated into disc shape by a roll-pressed method. About 14 wt% of polyvinyl alcohol PVA was added to the powder, then the mixture were continuously pressed by a roller to mix and flatten the mixture. Finally, the mixture was pressed into a 0.5 mm thick sheet. Similar to the compression molded disc, the ceramic disc prepared by the roll-pressed method were heat-treated at 750 °C for 1 h to remove the polymer binder and then sintering at a higher temperature. The $BaTiO_3$ ceramic discs fabricated by this method were sintered at 1250, 1280, 1300 and 1320 °C for 1 h.

# CHAPTER THREE

# CHARACTERIZATION OF BARIUM TITANATE CERAMIC

## 3.1 Introduction

The $BaTiO_3$ powder used to fabricate the ceramic discs was prepared by three different methods. They are the mixed oxide route, sol-gel process and the co-precipitation method. Preparations of the ceramic samples using these three different types of powders are described in chapter 2.

The structures of the three groups of ceramic samples were studied with the scanning electron microscope (SEM) and X-ray diffraction (XRD). The ferroelectric hysteresis (D-E) loops were measured with a standard Sawyer-Tower bridge circuit [42]. Fig. 3.1 shows the experimental set-up of the D-E loop measurement which is computer controlled. The D-E loops of the three groups of samples were measured at various temperatures at 60 Hz.

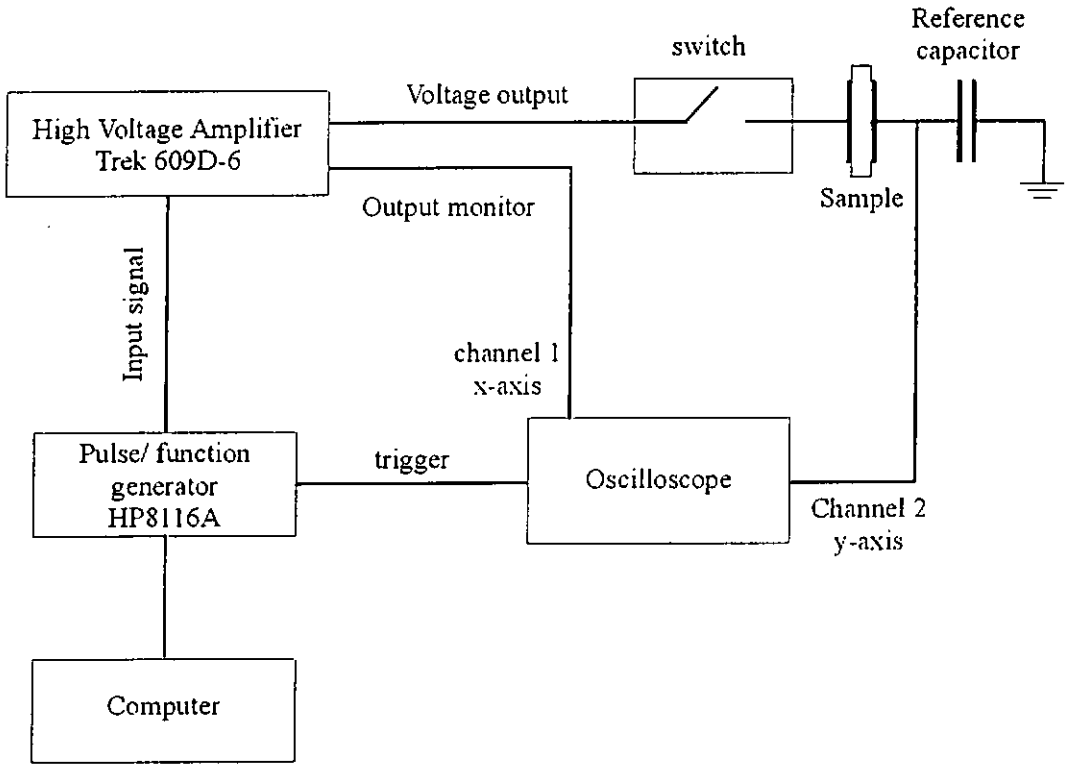


Fig. 3.1 Schematic diagram of the experimental set-up for D-E hysteresis loop measurement.

After poling with various d.c. field, the pyroelectric coefficient p, piezoelectric coefficient $d_{33}$ and the dielectric permittivity ε' of the samples were measured. The p was measured by the digital integration method [43]. The piezoelectric coefficient $d_{33}$ was directly measured by a Pennebaker model 8000 piezo $d_{33}$ tester. The dielectric permittivity ε' was measured at 1 kHz using a HP4194A impedance analyzer. The data will be used as references in the 0-3 composite modeling.

### 3.1.1 Poling Procedure

All the samples were poled using the following procedure. First, the ceramic disc was heated to 90 °C inside an oil bath. Then an electric field $E_0$ was applied for 30 min. Finally, the sample was cooled to 45 °C with the electric field kept on.

## 3.2 Properties of Bulk $BaTiO_3$ Prepared by Sintering Powder Obtained from the Mixed Oxide Route

This ceramic is called $BaTiO_3$ (oxide) in subsequent work.

### 3.2.1 Structures and Microstructures

Fig. 3.2 shows the x-ray diffraction (XRD) pattern of the $BaTiO_3$ (oxide) ceramic. The lattice constants "a" and "c" were found to be 4.004 Å and 4.044 Å, respectively. The c/a ratio is about 1.010. Fig. 3.3 shows the SEM micrographs of the surface of the $BaTiO_3$ (oxide) sample showing that it has an average grain size of ~ 20 μm. In all the SEM measurements, the ceramic samples were polished and thermally etched at a temperature 50 °C below the sintering temperature. The $BaTiO_3$ (oxide) was sintered at 1320 °C which is a sintering temperature commonly used [1,44,45] in a mixed oxide route. The density of the $BaTiO_3$ (oxide) is 5702 kg/m$^3$ which is closed to the reported value ρ ~ 5700 kg/m$^3$ [1,2,46].

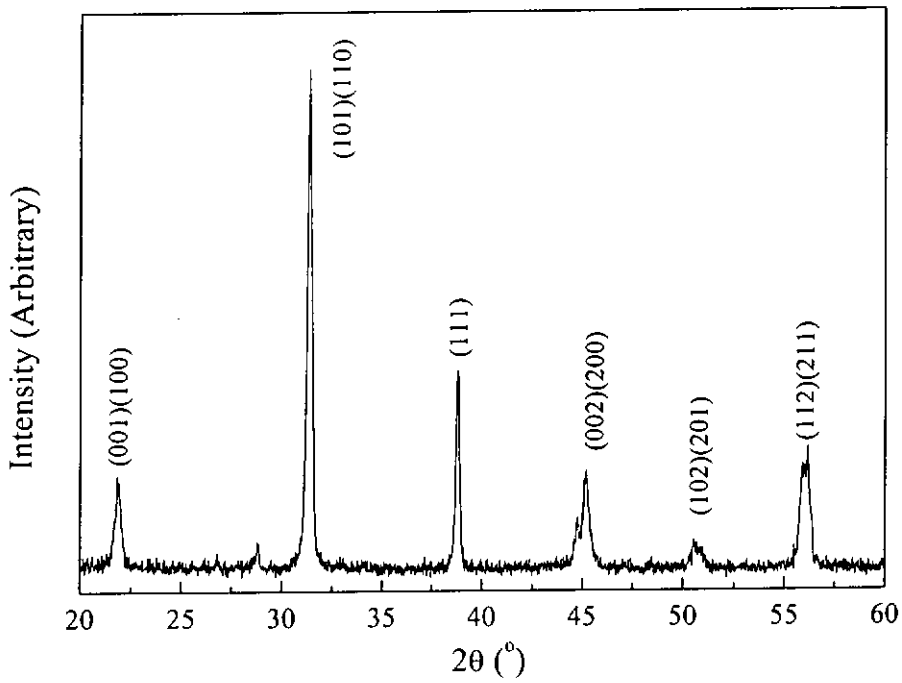


Fig. 3.2 XRD patterns of $BaTiO_3$ (oxide) ceramic sintered at 1320 °C.

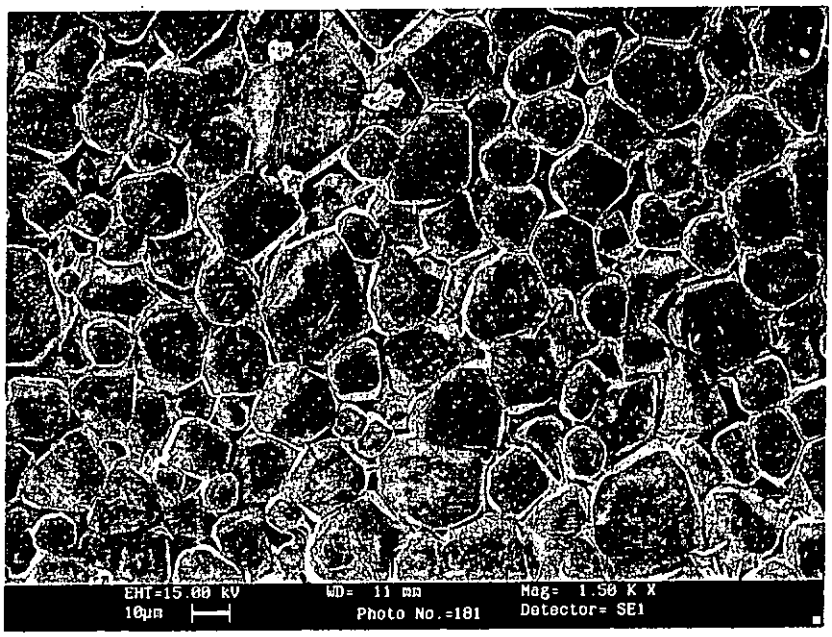


Fig. 3.3 SEM micrograph of $BaTiO_3$ (oxide) ceramic sintered at 1320 °C.

### 3.2.2 Dielectric Properties

Fig. 3.4 shows the dielectric permittivity ε' (square symbol) and ε" (circle symbol) of the $BaTiO_3$ (oxide) as functions of temperature. The solid and the open symbols represent heating and cooling, respectively. Two phase transition points were found at 20 °C and 130 °C. The ceramic has tetragonal structure within the temperature range of 20 to 130 °C. The room temperature (25 °C) dielectric permittivity ε' and ε" at 1 kHz was 1160 and 17.7, respectively.

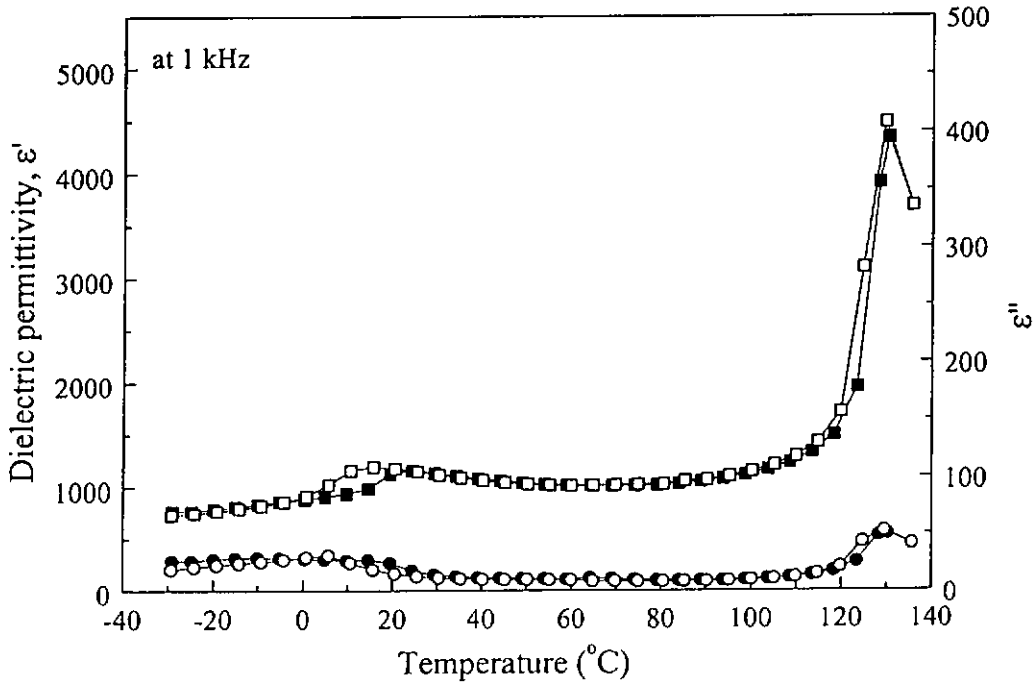


Fig. 3.4 Dielectric permittivity ε' (square symbol) and ε" (circle symbol) of $BaTiO_3$ (oxide) sintered at 1320 °C as a function of temperature upon heating (solid symbol) and cooling (open symbol).

### 3.2.3 Ferroelectric Hysteresis Loop

Fig. 3.5 shows the ferroelectric hysteresis loop of $BaTiO_3$ (oxide) ceramic at various temperatures. The maximum applied electric field was 4.5 kV/mm. At room temperature (25 °C), spontaneous polarization $P_s$, remanent polarization $P_r$, and coercive field $E_c$ were 13 $\mu C/cm^2$, 5 $\mu C/cm^2$ and 0.5 kV/mm respectively. Results obtained from the hysteresis measurements for the sample at various temperatures are shown in Fig. 3.5. $BaTiO_3$ (oxide) has a Curie transition at 130 °C (and $P_r$ is almost 0 at 130 °C). Comparing the saturation polarization $P_s$, remanent polarization $P_r$ and the coercive field $E_c$ at various temperatures (see Fig. 3.6), $P_s$, $P_r$ and $E_c$ decrease as the temperature increases. This is due to the higher mobility of a ferroelectric domain in the sample at higher temperatures.

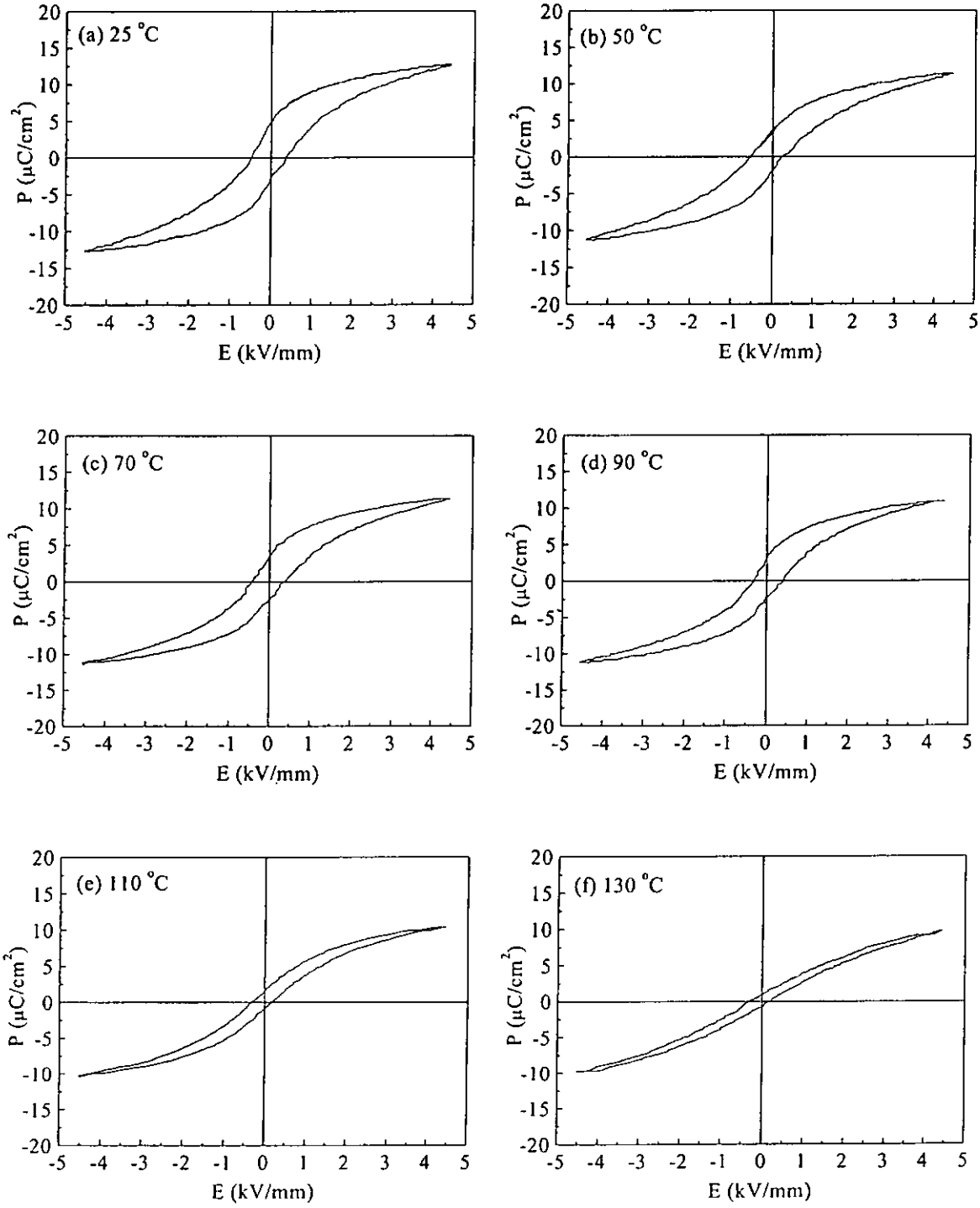


Fig. 3.5 Ferroelectric hysteresis loops (measured at 60 Hz) of $BaTiO_3$ (oxide) ceramic sintered at 1320 °C at various temperatures.

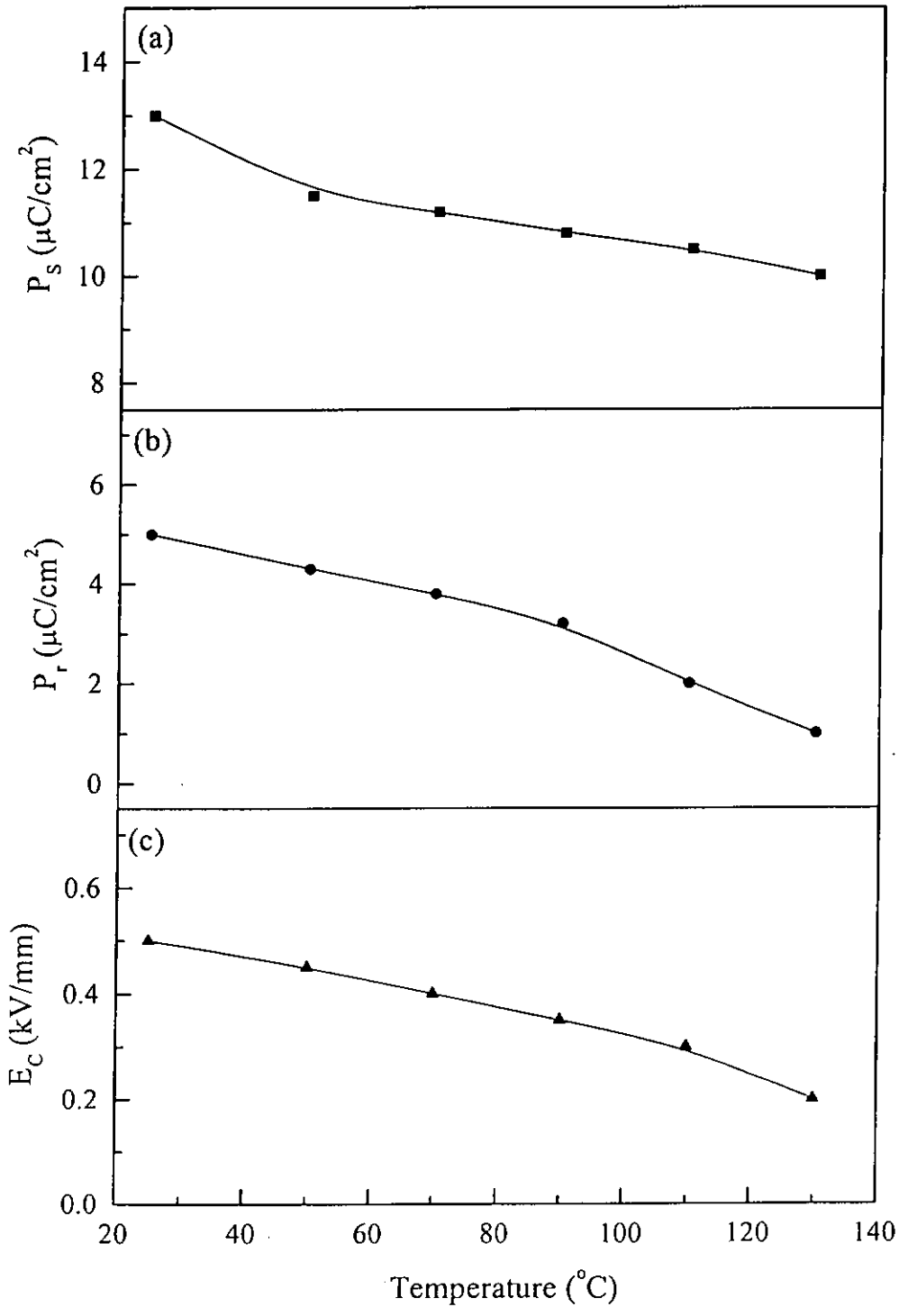


Fig. 3.6 Spontaneous polarization $P_s$, remanent polarization $P_r$ and coercive field $E_c$ of $BaTiO_3$ (oxide) ceramic sintered at 1320 °C as functions of temperature.

### 3.2.4 Piezoelectric and Pyroelectric Properties

The bulk $BaTiO_3$ (oxide) ceramic was poled by the procedure described in 3.1.1. After poling, the sample was annealed in a short-circuited condition at 50 °C for 3 h. Fig. 3.7 shows the dielectric permittivity ε' of $BaTiO_3$ (oxide) poled as various fields. The dielectric permittivity ε' decreases from 1160 (unpoled sample) to 1075 (poled with E = 5 kV/mm) which may be due to the domain orientation after poling. The room temperature pyroelectric coefficient p and piezoelectric coefficient $d_{33}$ poled at different field were shown in Figs. 3.8 and 3.9, respectively. Both p and $d_{33}$ increase as the poling field increases and tends to saturate when the field is about 3 kV/mm. The maximum p and $d_{33}$ were 235 $\mu C/m^2K$ and 175 pC/N, respectively.

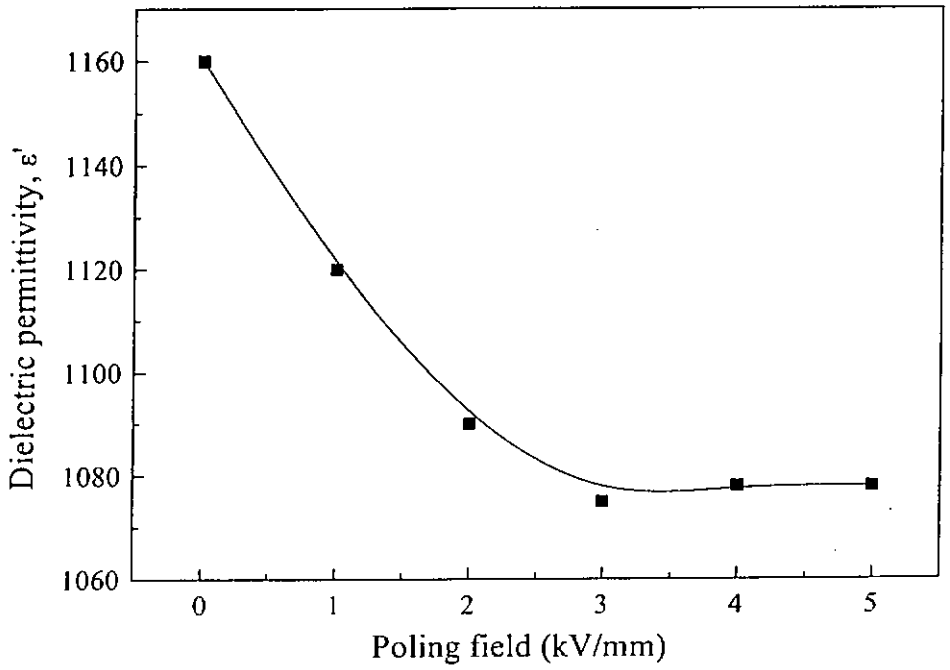


Fig. 3.7 Dielectric permittivity ε' of $BaTiO_3$ (oxide) ceramic sintered at 1320 °C poled at various fields.

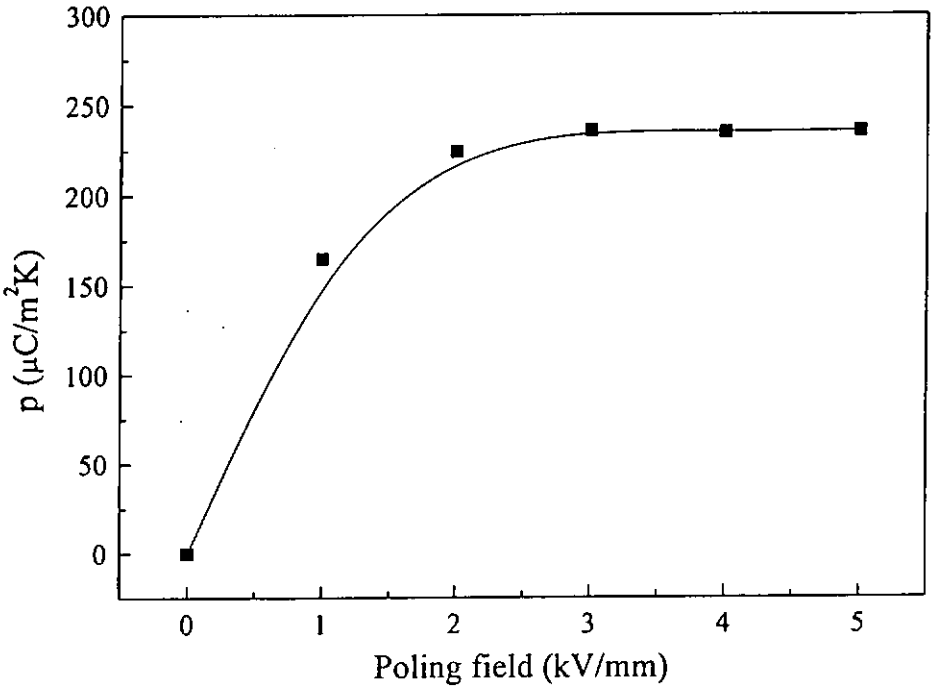


Fig. 3.8 Pyroelectric coefficient p of $BaTiO_3$ (oxide) ceramic sintered at 1320 °C poled at various fields.

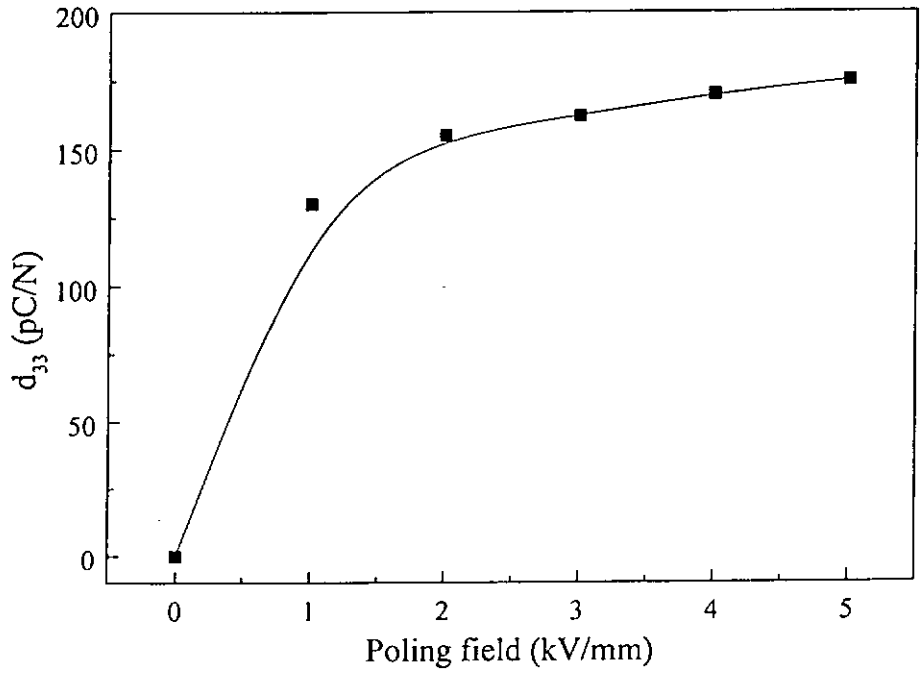


Fig. 3.9 Piezoelectric coefficient $d_{33}$ of $BaTiO_3$ (oxide) ceramic sintered at 1320 °C poled at various fields.

## 3.3 Properties of Bulk $BaTiO_3$ Prepared by Sintering Powder Obtained from a Sol-Gel Process

This ceramic is called $BaTiO_3$ (sol-gel) in subsequent work.

### 3.3.1 Structures and Microstructures

Fig. 3.10 and Fig. 3.11 show the XRD patterns and the SEM micrographs of the bulk ceramic (sol-gel) sintered at 1150 °C, 1200 °C and 1320 °C, respectively. The c/a ratio, average grain size and density of $BaTiO_3$ (sol-gel) ceramics sintered at various temperatures were listed in Table 3.1. Comparing the SEM micrographs, the grain size of the ceramic sintered at 1150 °C is ~ 2 μm which is smaller than the ceramic sintered at 1200 °C (~ 5 μm) and sintered at 1320 °C (~ 10 μm). Densities of the $BaTiO_3$ (sol-gel) ceramics sintered at 1150 °C, 1200 °C and 1320 °C are 5574 $kg/m^3$, 5649 $kg/m^3$ and 5685 $kg/m^3$, respectively. As we are interested in the properties of $BaTiO_3$ ceramic with small grain size for potential thin film applications, in subsequent study, properties of the $BaTiO_3$ (sol-gel) sintered at 1200 °C are evaluated.

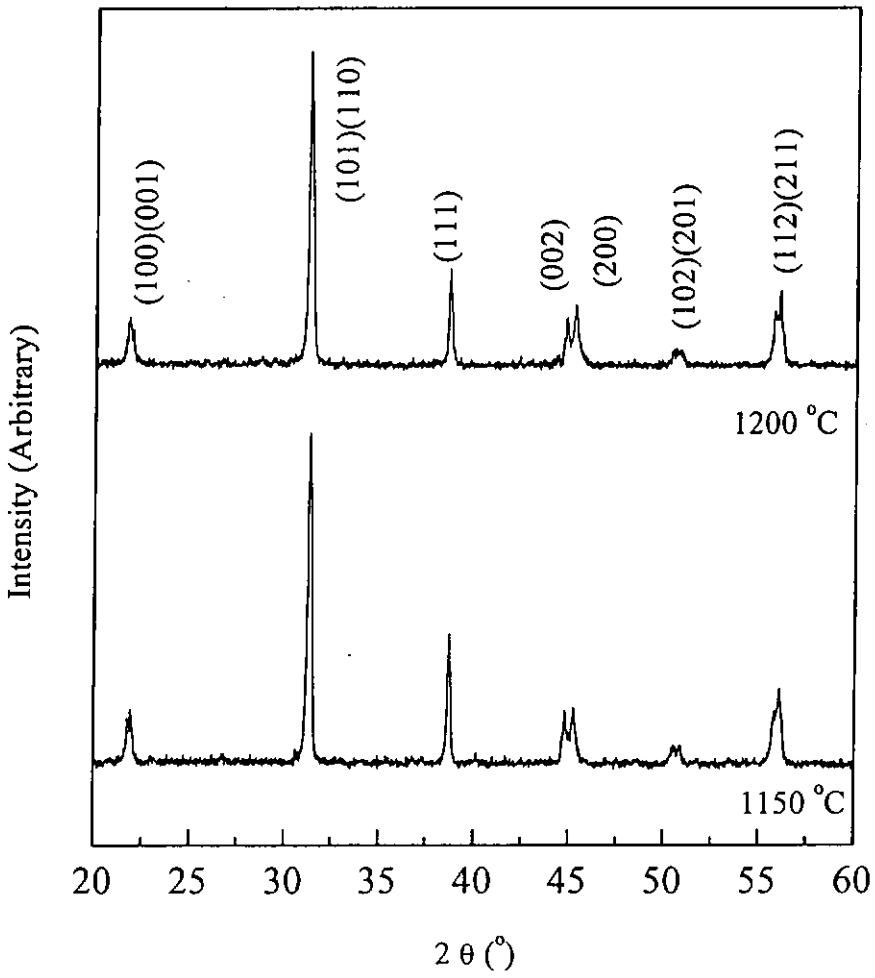


Fig. 3.10 XRD patterns of $BaTiO_3$ (sol-gel) ceramic sintered at 1150 °C and 1200 °C.

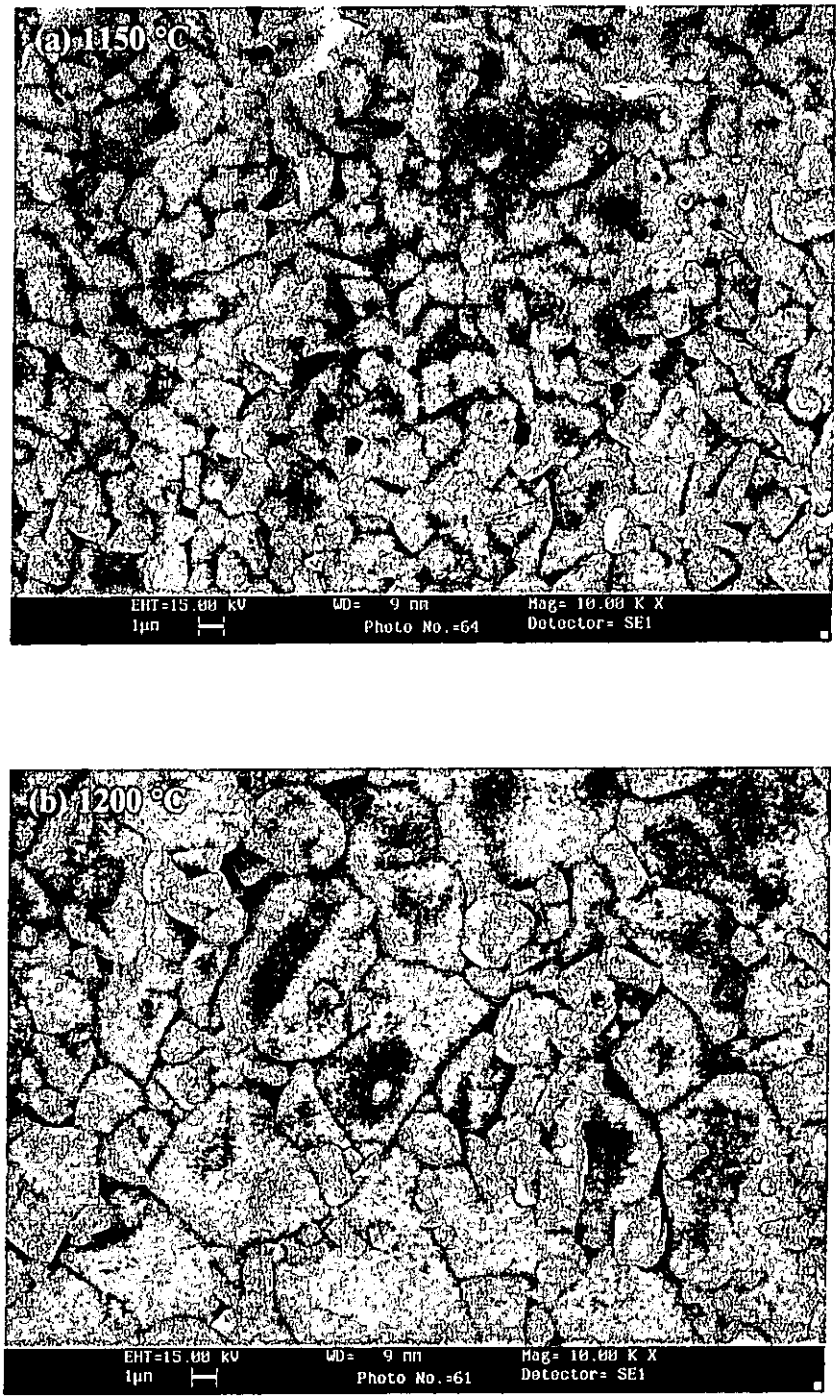


Fig. 3.11 SEM micrographs of $BaTiO_3$ (sol-gel) ceramic sintered at (a) 1150 °C and (b) 1200 °C.

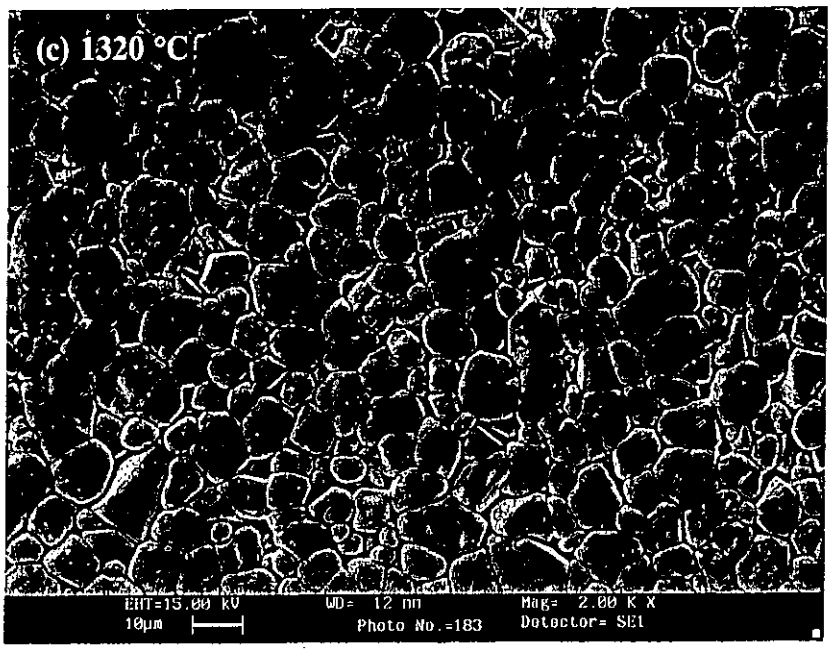


Fig. 3.11 SEM micrographs of $BaTiO_3$ (sol-gel) ceramic sintered at (c) 1320 °C.

| Sintering temperature (°C) | c/a ratio | Average grain size (µm) | Density ($kg/m^3$) | ε' (1 kHz) | ε" (1 kHZ) |
|---|---|---|---|---|---|
| 1150 | 1.009 | 2 | 5574 | 2075 | 181.9 |
| 1200 | 1.010 | 5 | 5649 | 1905 | 63.3 |
| 1320 | 1.010 | 10 | 5685 | 1825 | 114.4 |

Table 3.1 The c/a ratio, the average grain size, density and dielectric permittivity ε' and ε" of the $BaTiO_3$ (sol-gel) ceramics sintered at various temperatures. All the values are measured at 25 °C.

### 3.3.2 Dielectric Properties

Fig. 3.12 shows the dielectric permittivity ε' (square symbol) and ε" (circle symbol) of the $BaTiO_3$ (sol-gel) sintered at 1200 °C as functions of temperature. The solid and the open symbols represent heating and cooling, respectively. The phase transition points were found at 20 °C and 130 °C which is the same as that obtained for $BaTiO_3$ (oxide) ceramic. The room temperature dielectric permittivity ε' and ε" at 1 kHz was 1905 and 63.3, respectively which is higher than that of $BaTiO_3$ (oxide) presumably due to grain size effect [3,6].

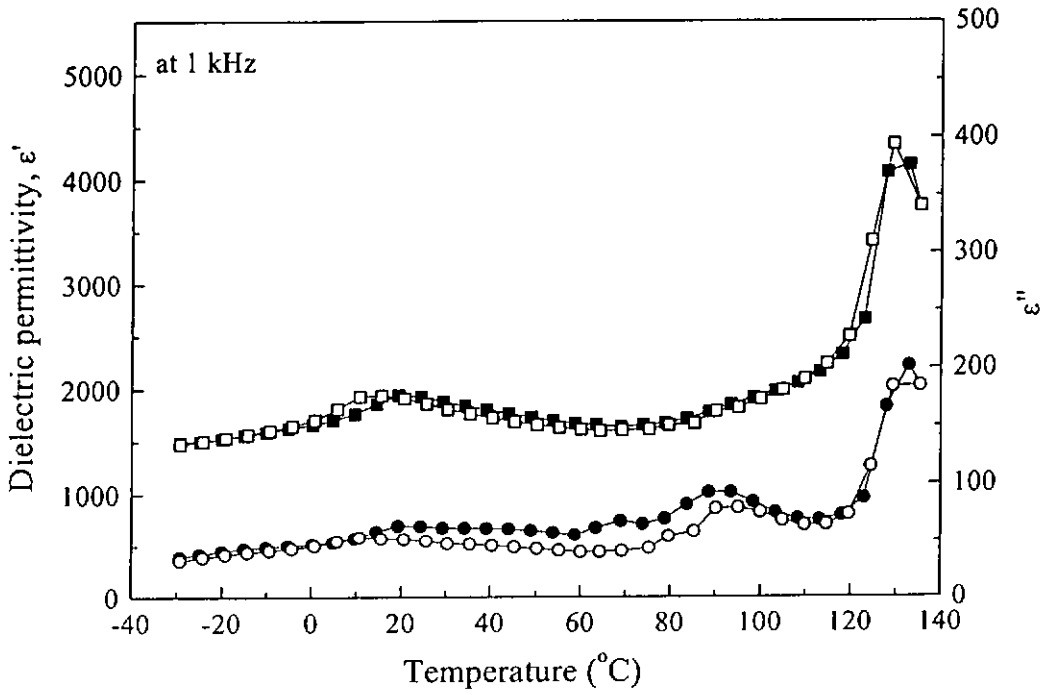


Fig. 3.12 Dielectric permittivity ε' (square symbol) and ε" (circle symbol) of $BaTiO_3$ (sol-gel) ceramic sintered at 1200 °C as functions of temperature upon heating (solid symbol) and cooling (open symbol).

### 3.3.3 Ferroelectric Hysteresis Loop

Ferroelectric hysteresis loop of the bulk $BaTiO_3$ (sol-gel) ceramic sintered at 1200 °C was measured at various temperatures (Fig. 3.13). The maximum applied field was 4 kV/mm. The room temperature spontaneous polarization $P_s$, remanent polarization $P_r$ and the coercive field $E_c$ are 16.8 $\mu C/cm^2$, 6.5 $\mu C/cm^2$ and 0.8 kV/mm, respectively. Fig. 3.14 shows the result of $P_r$, $P_s$, and $E_c$ decrease when the temperature increases. Compared with $BaTiO_3$ (oxide), $BaTiO_3$ (sol-gel) has higher $P_s$, $P_r$ and $E_c$.

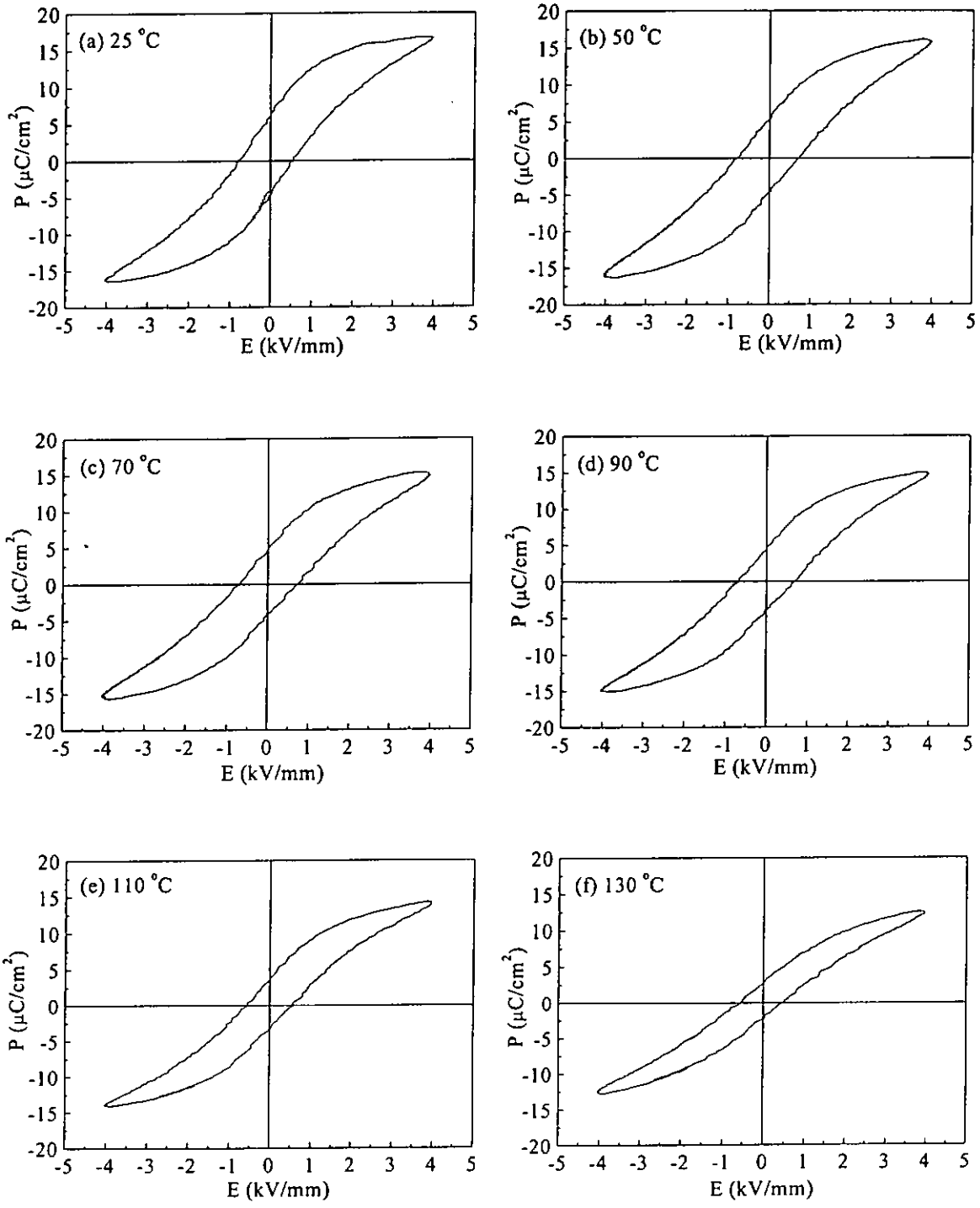


Fig. 3.13 Ferroelectric hysteresis loop (measured at 60 Hz) of $BaTiO_3$ (sol-gel) ceramic sintered at 1200 °C at various temperatures.

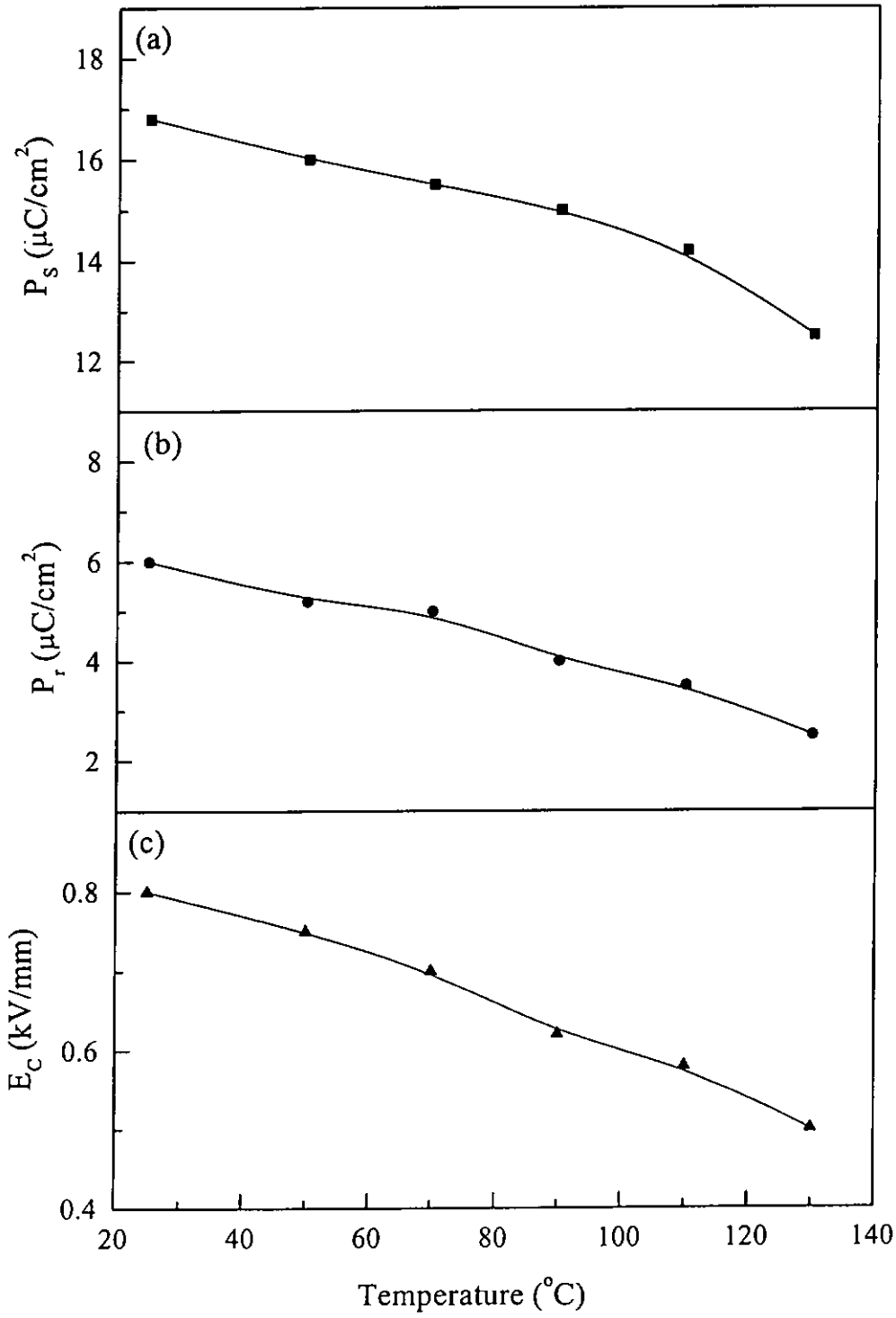


Fig. 3.14 Spontaneous polarization $P_s$, remanent polarization $P_r$ and coercive field $E_c$ of $BaTiO_3$ (sol-gel) ceramic sintered at 1200 °C as functions of temperature.

### 3.3.4 Piezoelectric and Pyroelectric Properties

Figs. 3.15 to 3.17 show the dielectric permittivity ε', pyroelectric coefficient p and piezoelectric coefficient $d_{33}$ of the $BaTiO_3$ (sol-gel) ceramic sintered at 1200 °C poled with various fields. From the graphs, ε', p and $d_{33}$ have constant values when poled at 3 kV/mm which is similar to $BaTiO_3$ (oxide) ceramic. The dielectric permittivity ε' was reduced from 1905 for an unpoled sample to 1880 for the sample poled at E = 5 kV/mm. The pyroelectric coefficient p and the piezoelectric coefficient $d_{33}$ have the maximum values of 117 $\mu C/m^2K$ and 110 pC/N, respectively which are smaller compared with $BaTiO_3$ (oxide) ceramic.

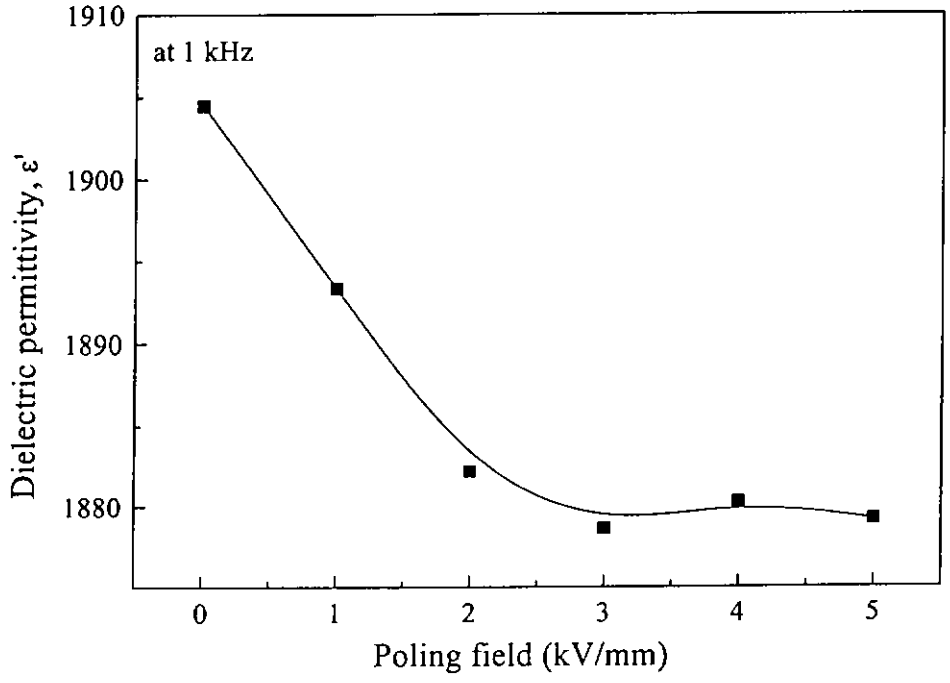


Fig. 3.15 Dielectric permittivity ε' of $BaTiO_3$ (sol-gel) ceramic sintered at 1200 °C poled at various fields.

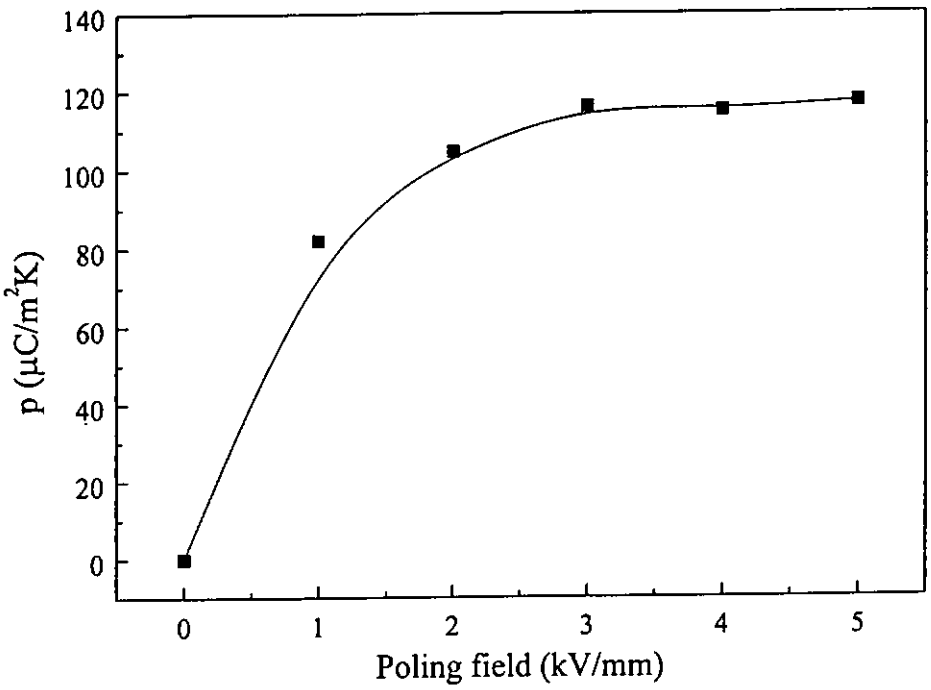


Fig. 3.16 Pyroelectric coefficient p of $BaTiO_3$ (sol-gel) ceramic sintered at 1200 °C poled at various fields.

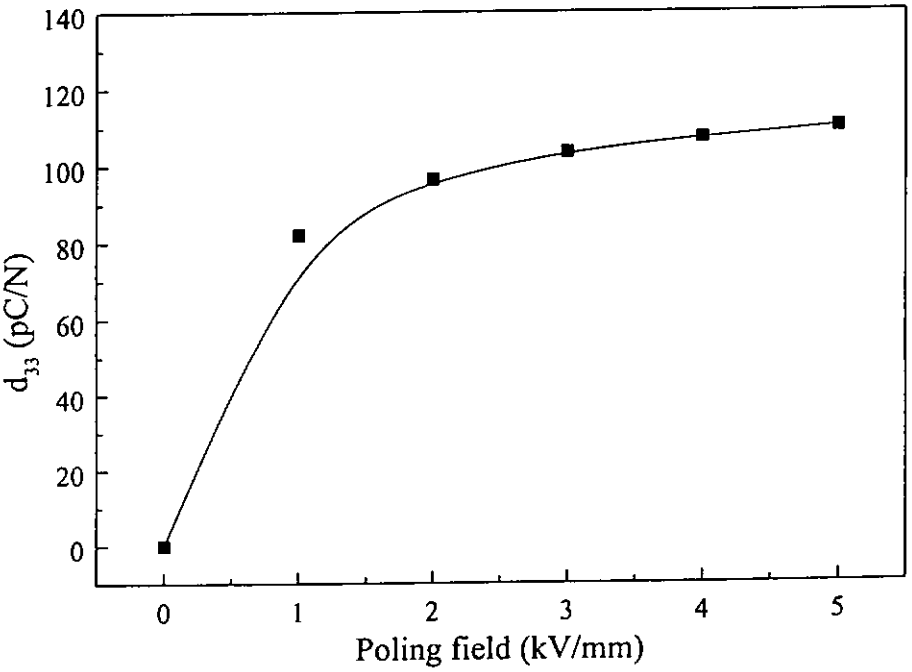


Fig. 3.17 Piezoelectric coefficient $d_{33}$ of $BaTiO_3$ (sol-gel) ceramic sintered at 1200 °C poled at various fields.

## 3.4 Properties of Bulk $BaTiO_3$ Prepared by Sintering Powder Obtained from a Co-precipitation Method

This ceramic is called $BaTiO_3$ (co-precipitation) in subsequent work.

The samples prepared by the roll-press method were sintered at different temperatures. The grain size, XRD patterns, tetragonality (c/a ratio) and dielectric permittivity ε'of the roll pressed ceramic were measured as functions of the sintering temperature.

### 3.4.1 Structures and Microstructures

The grain size of the ceramics increases as the sintering temperature is increased. Fig. 3.18 shows the average grain size as a function of sintering temperature. The sample sintered at 1320 °C has the largest average grain size (~ 1 μm) and have the highest density (ρ = 5717 g/cm$^3$). Fig. 3.19 shows the SEM micrographs of the roll-pressed $BaTiO_3$ (co-precipitation) ceramic sintered at (a) 1250 °C, (b) 1280 °C, (c) 1300 °C and (d) 1320 °C.

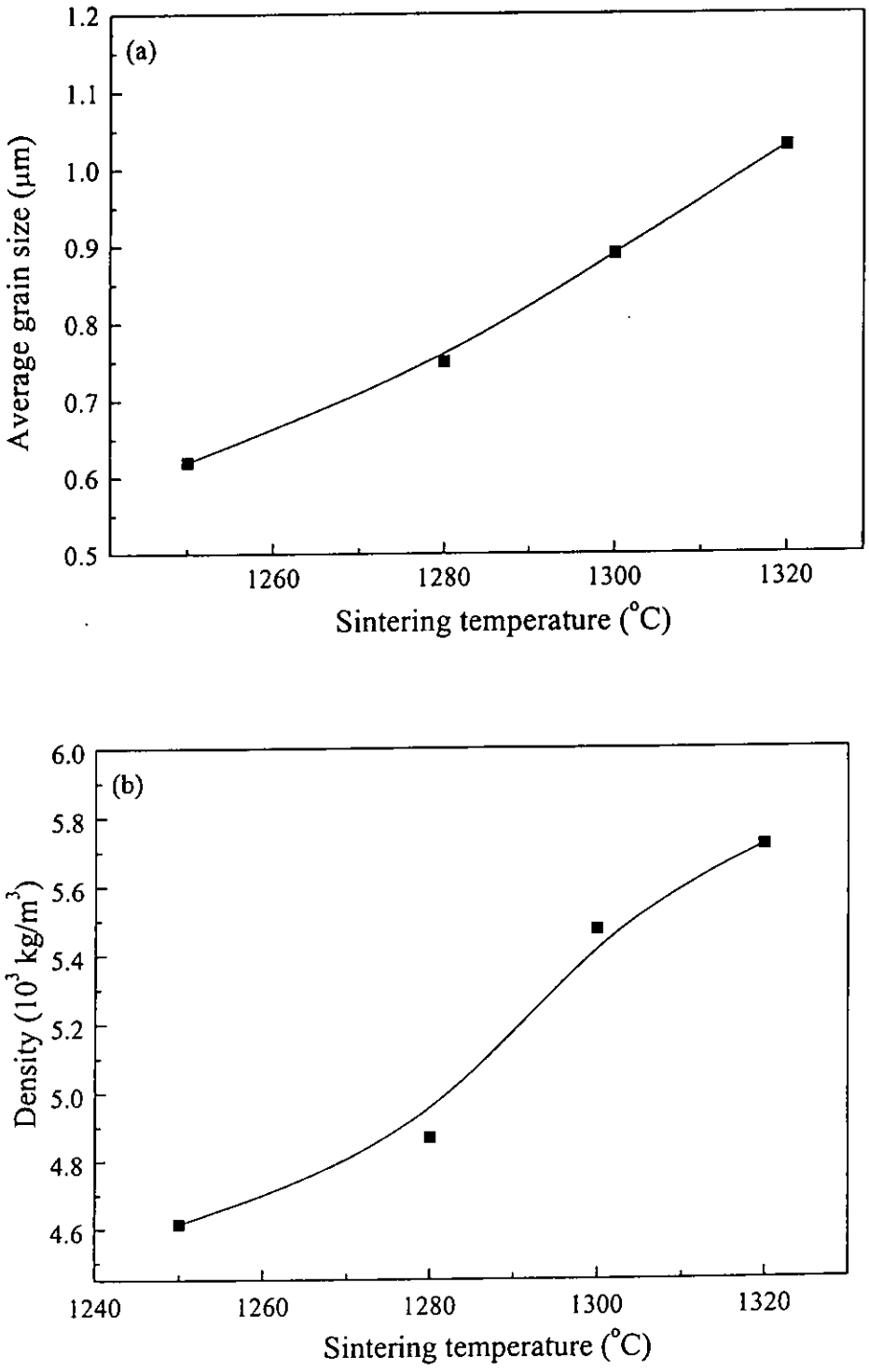


Fig. 3.18 (a) Average grain size and (b) density of $BaTiO_3$ (co-precipitation) ceramic as a function of sintering temperature.

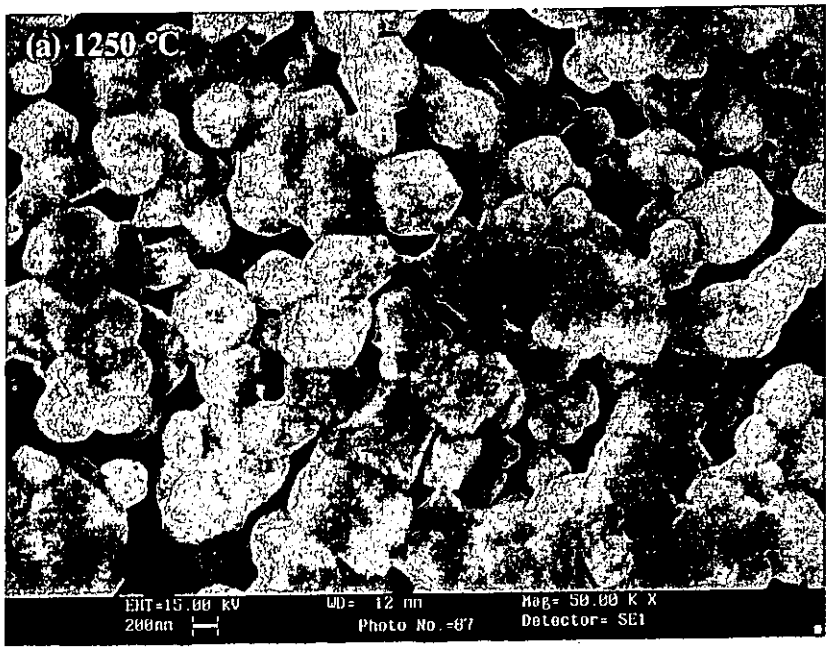


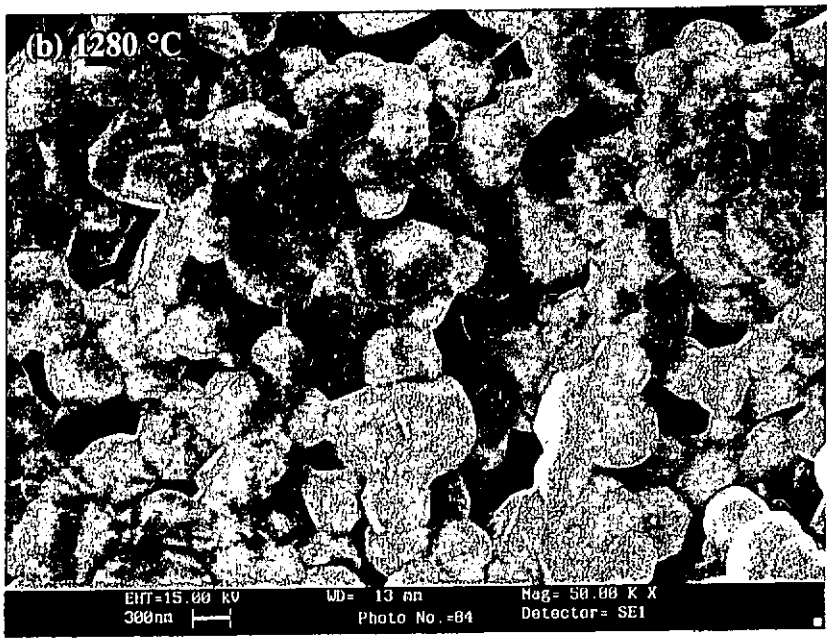


Fig. 3.19 SEM micrographs of $BaTiO_3$ (co-precipitation) ceramic sintered at (a) 1250 °C, (b) 1280 °C.

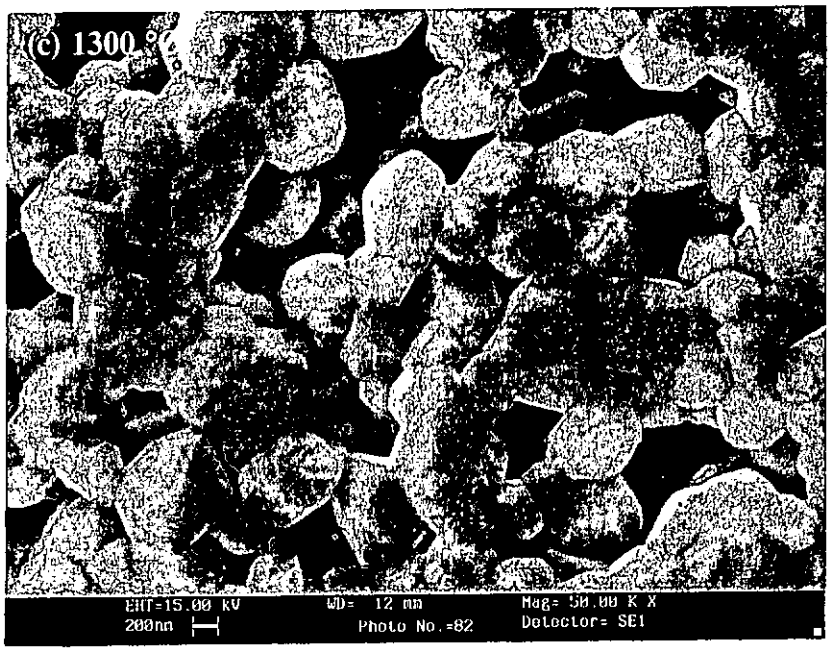


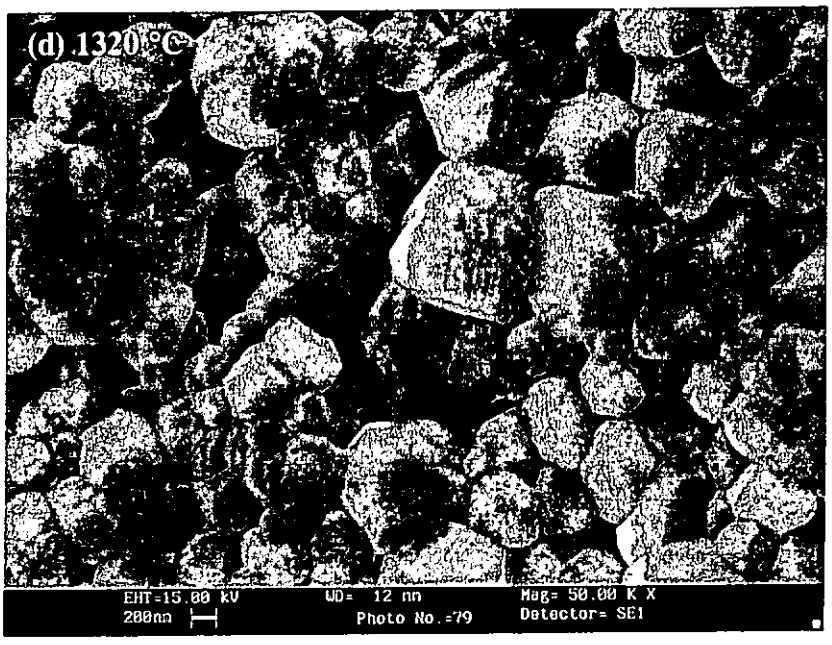


Fig. 3.19 SEM micrographs of $BaTiO_3$ (co-precipitation) ceramic sintered at (c) 1300 °C and (d) 1320 °C.

Fig. 3.20 shows the XRD patterns of $BaTiO_3$ (co-precipitation) ceramic sintered at various temperatures. The calculated tetragonality (c/a ratio) was shown in Fig. 3.21. The tetragonality of the $BaTiO_3$ (co-precipitation) ceramic was increased at the sintering temperature increased (or the grain size of the ceramic increased). When sintered at 1320 °C, the tetragonality of the ceramic was 1.0085 that is a little bit smaller than the reported value c/a = 1.010 [2]. It is noted that as the grain size increases, the tetragonality also increases. The tetragonality of $BaTiO_3$ ceramic should be proportional to the grain size and saturated at 1.010, a value closed to that reported by Mark P. McNeal et al. [4].

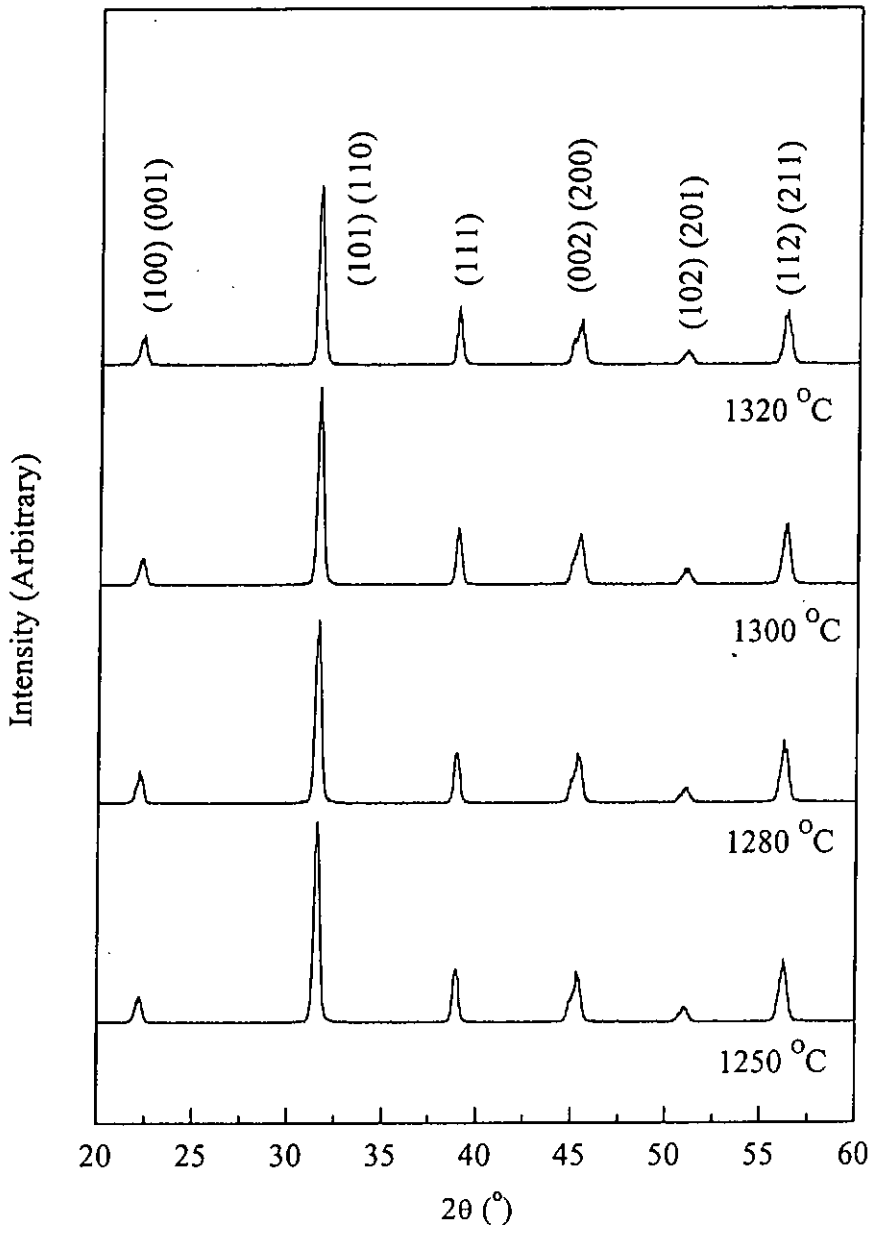


Fig. 3.20 XRD patterns of $BaTiO_3$ (co-precipitation) ceramic at various sintering temperatures.

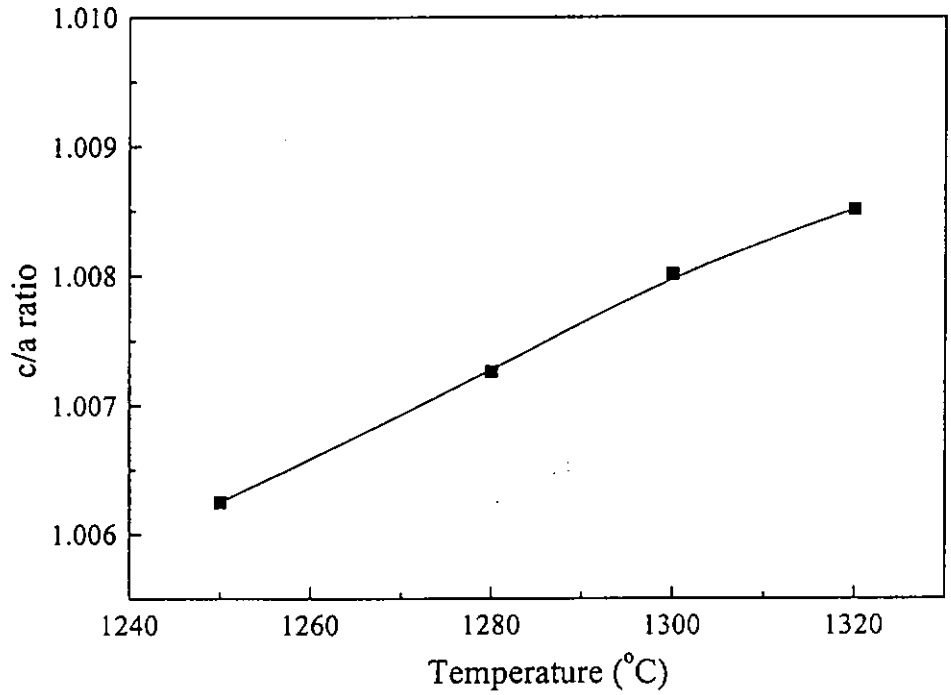


Fig. 3.21 Tetragonal (c/a ratio) of $BaTiO_3$ (co-precipitation) ceramic as a function of sintering temperature.

### 3.4.2 Dielectric Properties

The dielectric permittivity as a function of sintering temperature was shown in Fig. 3.22 and it indicated that the room temperature dielectric permittivity ε' maximized at the ceramic sintered at 1300 °C (the average size ~ 890 nm). Fig. 3.23 shows the dielectric permittivity ε' (square symbol) and ε" (circle symbol) of $BaTiO_3$ (co-precipitation) ceramic sintered at 1320 °C as a function of temperature. The Curie points were found at 20 °C and 130 °C. It is the same as the $BaTiO_3$ (oxide) and the $BaTiO_3$ (sol-gel). The room temperature dielectric permittivity ε' and ε" at 1 kHz was 2130 and 100, respectively.

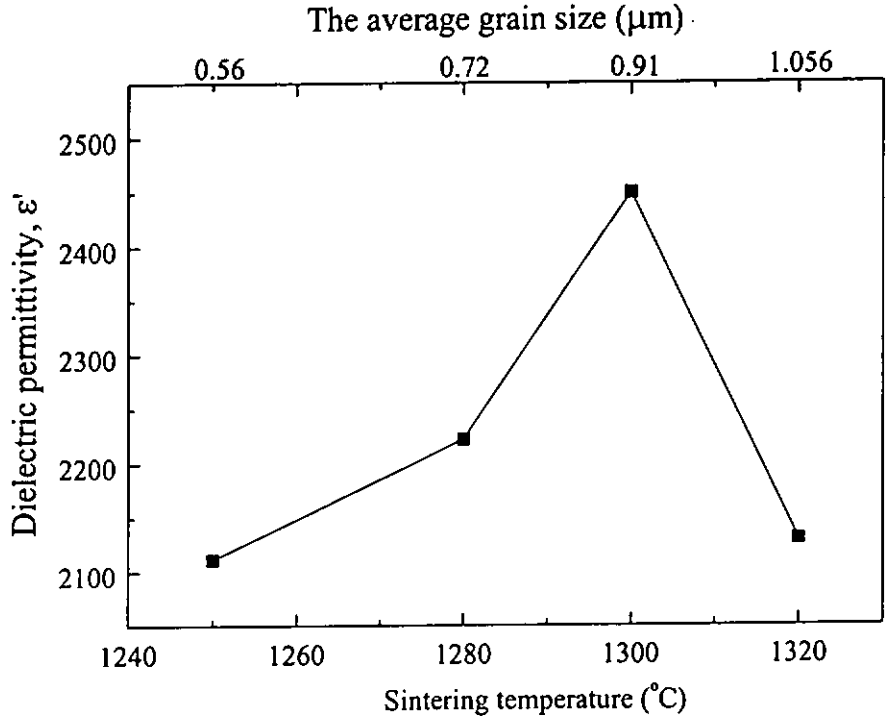


Fig. 3.22 Room temperature (25 °C) dielectric permittivity ε' of $BaTiO_3$ (co-precipitation) as a function of sintering temperature.

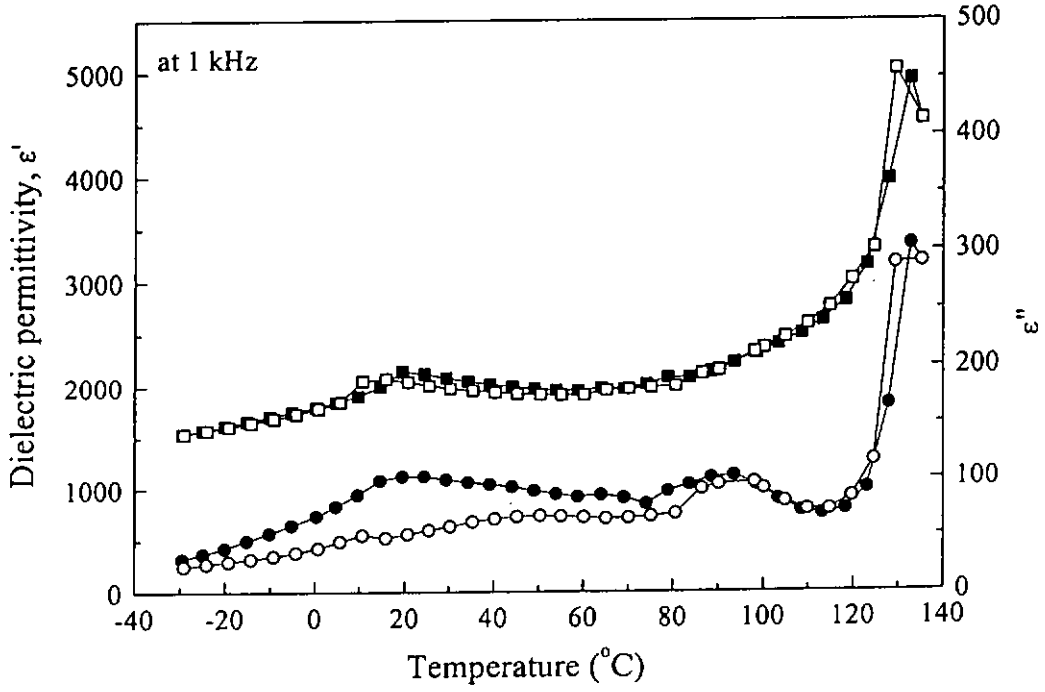


Fig. 3.23 Dielectric permittivity ε' (square symbol) and ε" (circle symbol) of $BaTiO_3$ (co-precipitation) sintered at 1320 °C as functions of temperature upon heating (solid symbol) and cooling (open symbol).

### 3.4.3 Ferroelectric Hysteresis Loop

The ferroelectric hysteresis loop of $BaTiO_3$ (co-precipitation) ceramic sintered 1320 °C was measured at various temperatures. The value of the $P_s$, $P_r$ and $E_c$ was decreased when the temperature rises. It was similar to the results in the previous section. The D-E loops of $BaTiO_3$ (co-precipitation) ceramic sintered at 1320 °C was measured at various temperatures and shown in Fig. 3.24. The maximum applied field was 4 kV/mm. The room temperature spontaneous polarization $P_s$, remanent polarization $P_r$ and the coercive field $E_c$ are 19 $\mu m/cm^2$, 6 $\mu m/cm^2$ and 0.5 kV/mm, respectively. Fig. 3.25 shows $P_s$, $P_r$ and $E_c$ decrease as the temperature increases and $P_r$ is almost 0 at 130 °C.

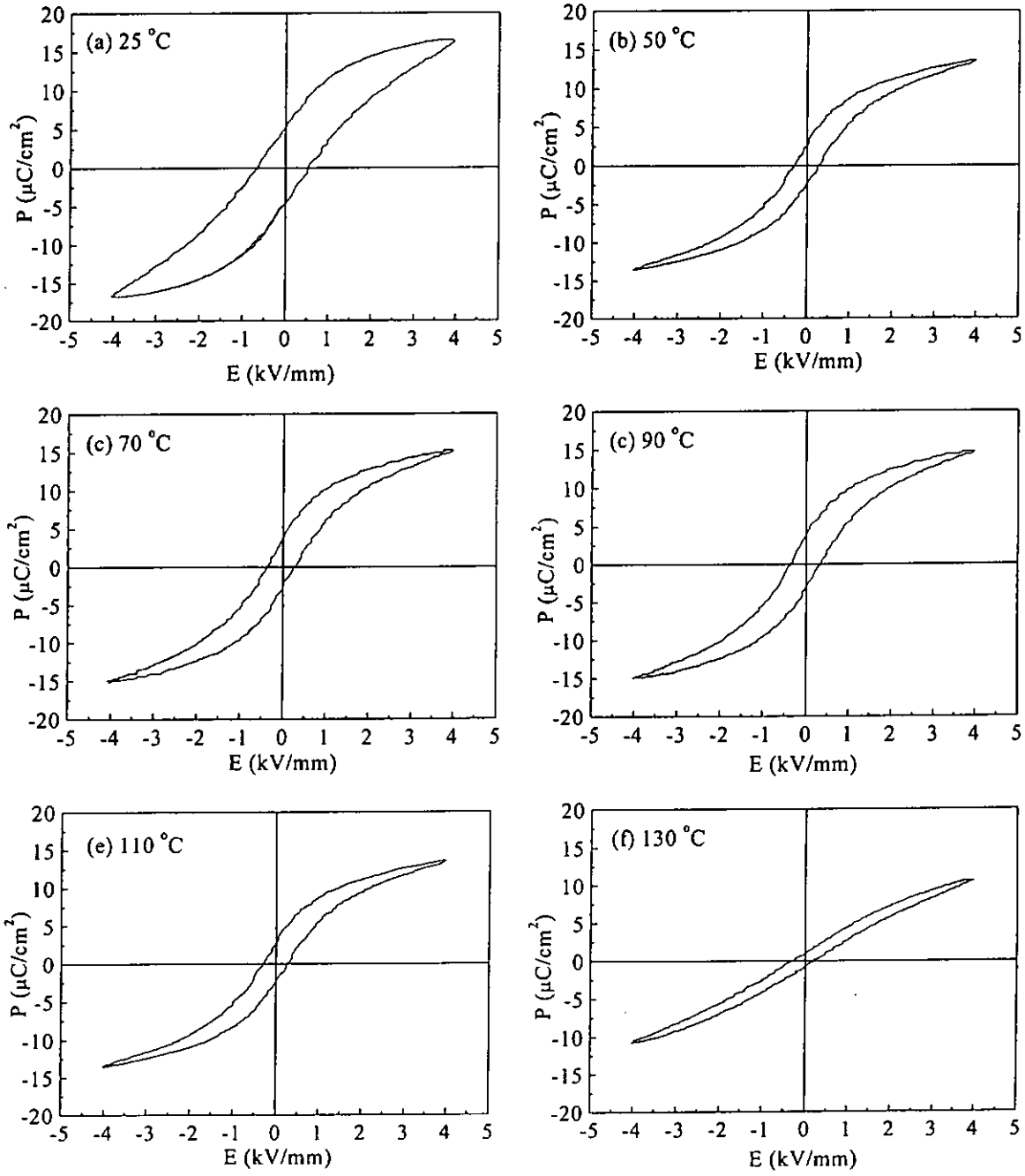


Fig. 3.24 Ferroelectric hysteresis loops measured at 60 Hz of $BaTiO_3$ (co-precipitation) ceramic sintered at 1320 °C at various temperatures.

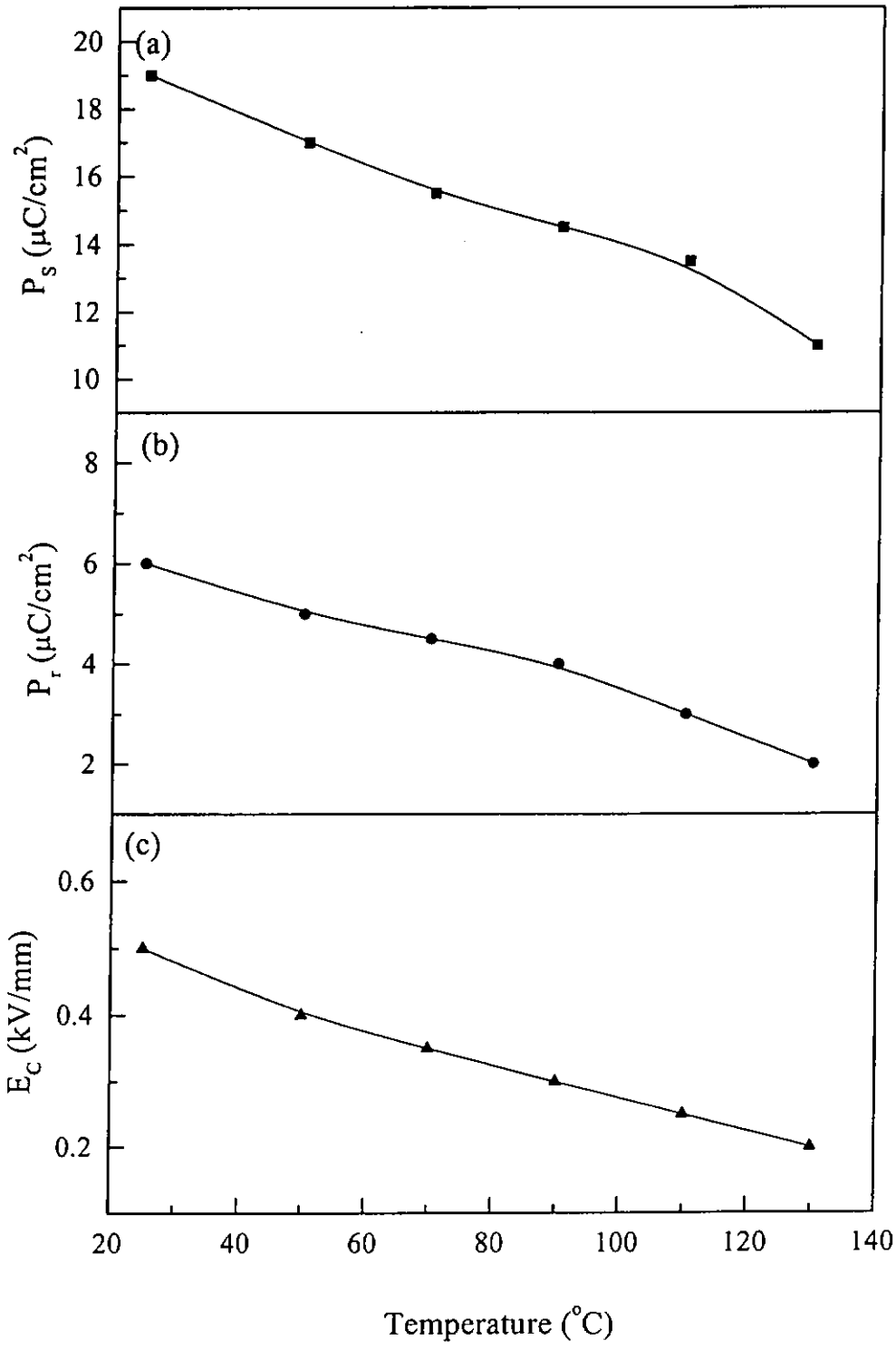


Fig. 3.25 Spontaneous polarization $P_s$, remanent polarization $P_r$ and coercive field $E_c$ of $BaTiO_3$ (co-precipitation) ceramic sintered at 1320 °C as functions of temperature.

### 3.4.4 Piezoelectric and Pyroelectric Properties

$BaTiO_3$ (co-precipitation) ceramic sintered at 1320 °C was poled at various fields and the dielectric permittivity ε', piezoelectric coefficient $d_{33}$ and pyroelectric coefficient p as a function of poling field are shown from Fig. 3.26 to Fig. 3.28, respectively. The dielectric permittivity ε' was decreased from 2130 (unpoled sample) to 1960 (poled with E = 5 kV/mm). The pyroelectric coefficient p and the piezoelectric coefficient $d_{33}$ were 157 $\mu C/m^2K$ and 147 pC/N, respectively when $BaTiO_3$ (co-precipitation) ceramic poled at 5 kV/mm. Both ε', p and $d_{33}$ tends to saturate when the poling field is about 3 kV/mm.

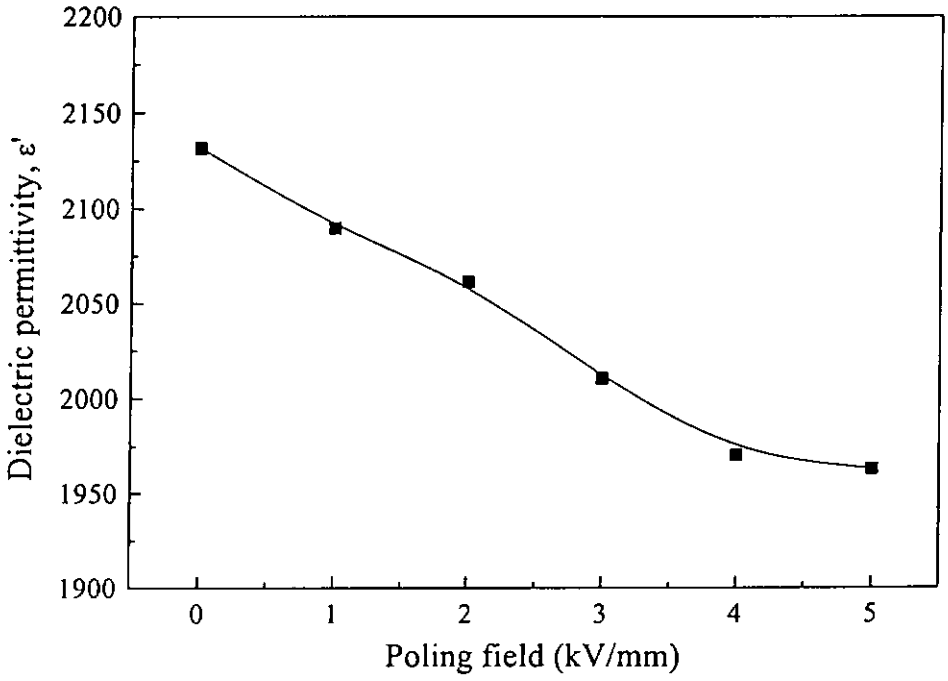


Fig. 3.26 Dielectric permittivity ε' of $BaTiO_3$ (co-precipitation) ceramic sintered at 1320 °C poled at various fields.

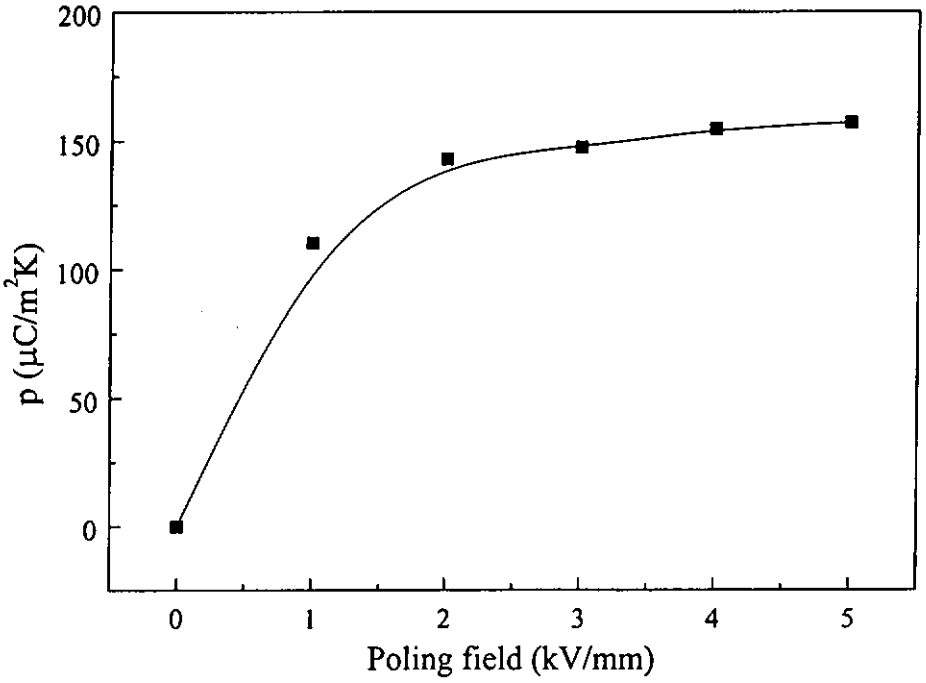


Fig. 3.27 Pyroelectric coefficient p of $BaTiO_3$ (co-precipitation) ceramic sintered at 1320 °C poled at various fields.

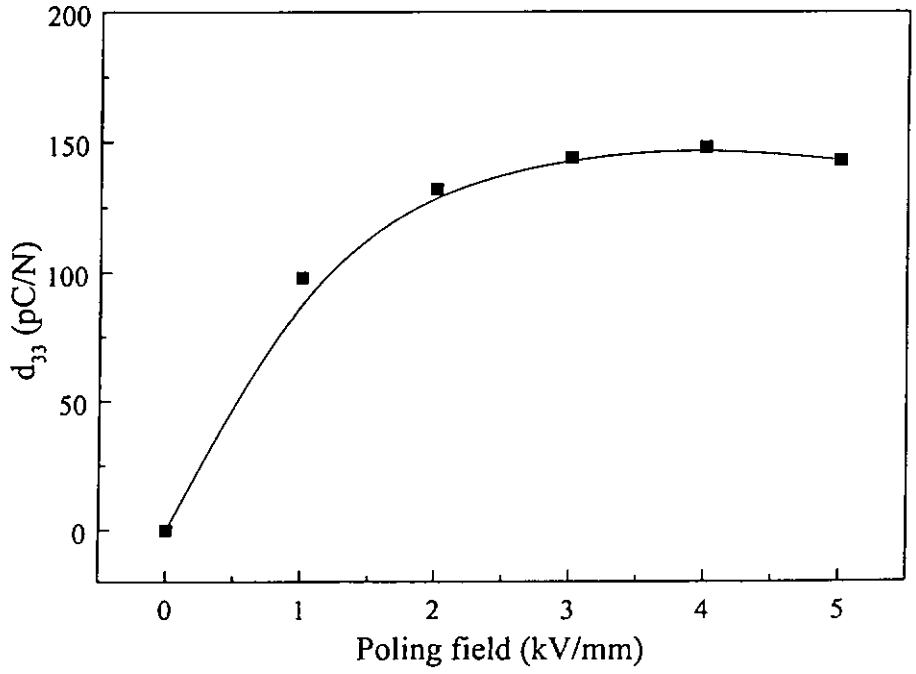


Fig. 3.28 Piezoelectric coefficient $d_{33}$ of $BaTiO_3$ (co-precipitation) ceramic sintered at 1320 °C poled at various fields.

# CHAPTER FOUR

# FERROELECTRIC P(VDF-TrFE) COPOLYMER

## 4.1 Introduction

In the following discussion, we will concentrate on the copolymer with 70 mol% of VDF and 30 mol% of TrFE. The samples were fabricated by a compression molding process. Thickness of the copolymer was about 0.8 mm. Air-dried silver paint was applied to both sides of the samples and they act as the electrodes for poling and for electrical measurements.

Structures of the copolymer were studied by using X-ray diffraction (XRD Philips x'pert XRD system). The phase transitions were obtained by using a differential scanning calorimetry DSC (Perkin Elmer DSC7 thermal analyzer). The dielectric permittivity ε' and ε" were measured by a HP4194A impedance analyzer connected to a temperature controlled oven. The pyroelectric coefficient p was measured by the digital integration method [43] and the piezoelectric coefficient $d_{33}$ was measured using a Pennebaker model 8000 piezo $d_{33}$ tester (American Piezo-Ceramic Inc.). These results would be used as a reference in the model calculation for the $BaTiO_3$/P(VDF-TrFE) 0-3 composites in Chapter 5.

## 4.2 Preparation of the P(VDF-TrFE) Copolymer Sample

The copolymer P(VDF-TrFE)(70-30) pellet was supplied by Piezotech Co. in France. The samples were fabricated by compression molding. The copolymer pellets were placed inside a cylindrical stainless steel mold. Then the mold was heated in between two hot plates of a temperature controlled hydraulic machine (model 2699, CARVER Inc.). First, the temperature was increased to 210 °C. Then a pressure of 10 MPa was applied for 1 h. After this, the sample was cooled to room temperature with the pressure kept on. The samples were cut into disc form with a high precision diamond saw. Finally, the samples were polished and annealed at 130 °C for 2 h. The sample thickness was about 0.8 mm. Fig. 4.1 shows the schematic set-up for the compress-molding.

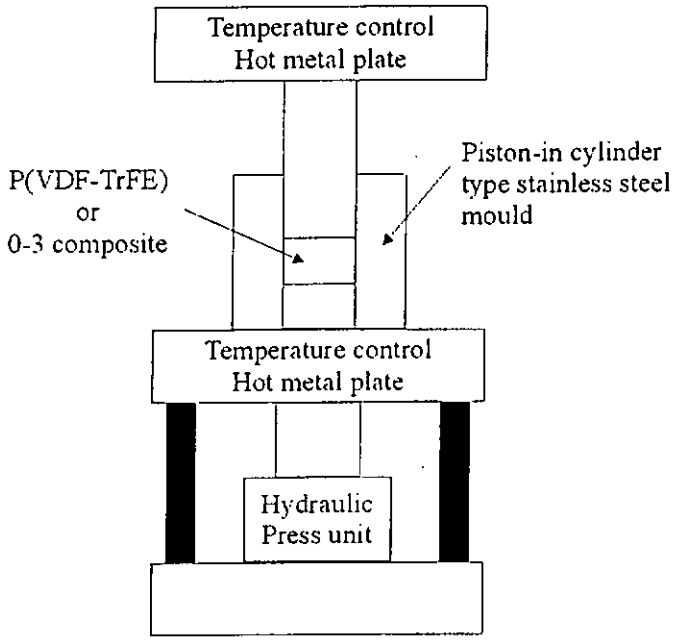


Fig. 4.1 Schematic set-up for the compression molding.

## 4.3 Experimental Results and Discussions

### 4.3.1 XRD Analysis

Fig. 4.2 shows the XRD pattern of P(VDF-TrFE). The sample was annealed at 130 °C for 3 h. The copolymer was assumed to have quasi-hexagonal structure [13] which is similar to the polar β-PVDF. A sharp peak was found at $2\theta$ = 19.7 ° and a broad shoulder at its low angle side. The peak corresponded to the (110) and (200) planes. The diffraction curves observed could be resolved into two Gaussian peaks, C (crystalline) and N (non-crystalline), as shown in Fig. 4.2(b). The degree of crystallinity $X_c$ of P(VDF-TrFE) can be evaluated from the ratio of area C to the sum of the area of C and N. A value of $X_c$ = 0.68 was obtained.

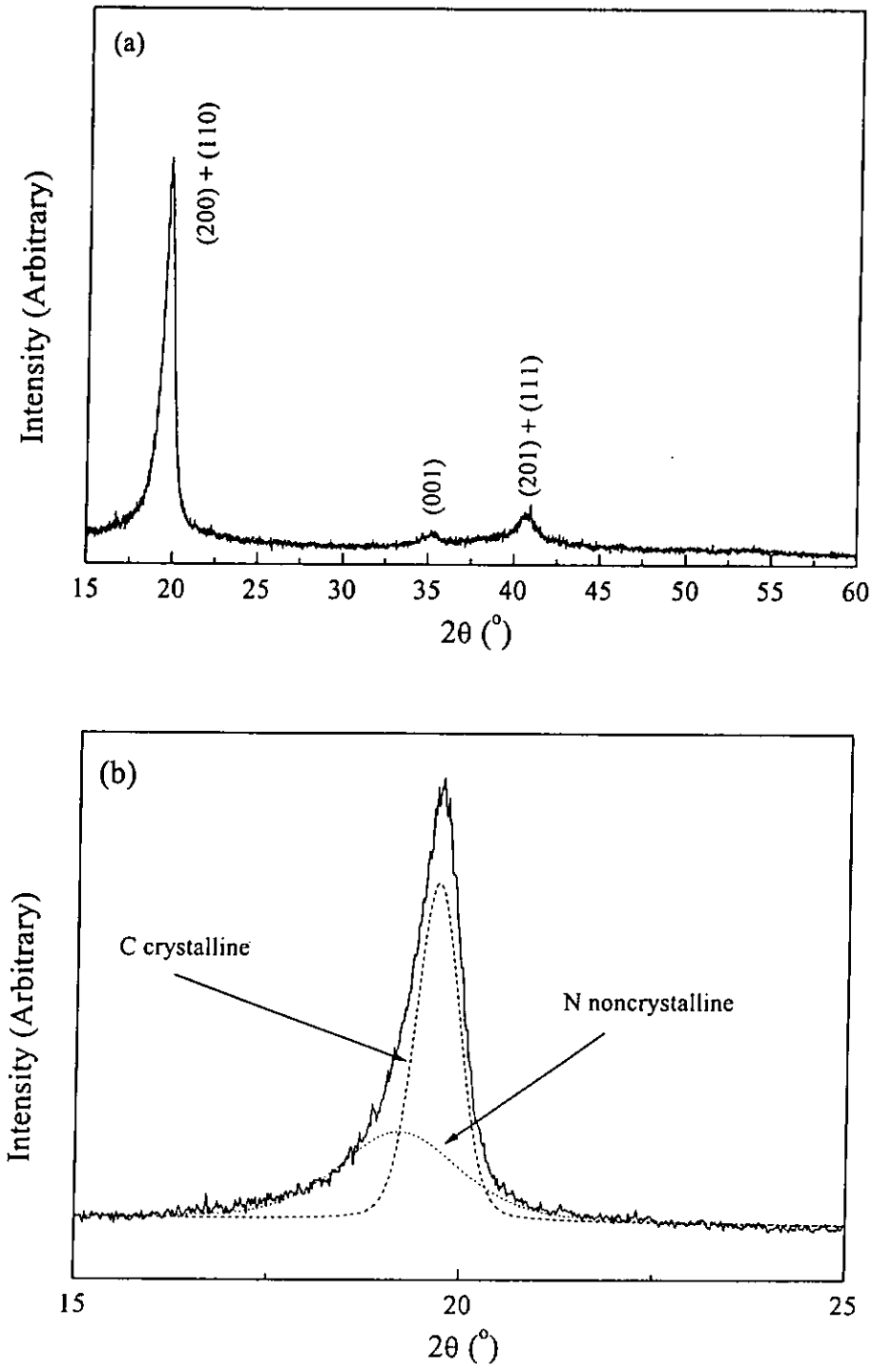


Fig. 4.2 XRD pattern of P(VDF-TrFE) (70/30).

### 4.3.2 Phase Transitions

The copolymer phase transition temperature (or Curie temperature $T_c$) was measured by differential scanning calorimetry DSC (Perkin Elmer DSC7 thermal analyzer). Fig. 4.3 shows the DSC data of P(VDF-TrFE) upon heating and cooling. Fig. 4.3(a) shows the Curie temperature $T_c\uparrow$ and melting temperature $T_m$ at 104.6 °C and 153 °C respectively upon heating. Upon cooling, an endothermic peak is found at the crystallization temperature $T_s$ (135.5 °C). At 59.5 °C and 65.5 °C, another two peaks appear which are the paraelectric-to-ferroelectric transition temperature $T_c\downarrow$. A thermal hysteresis upon heating and cooling is observed.

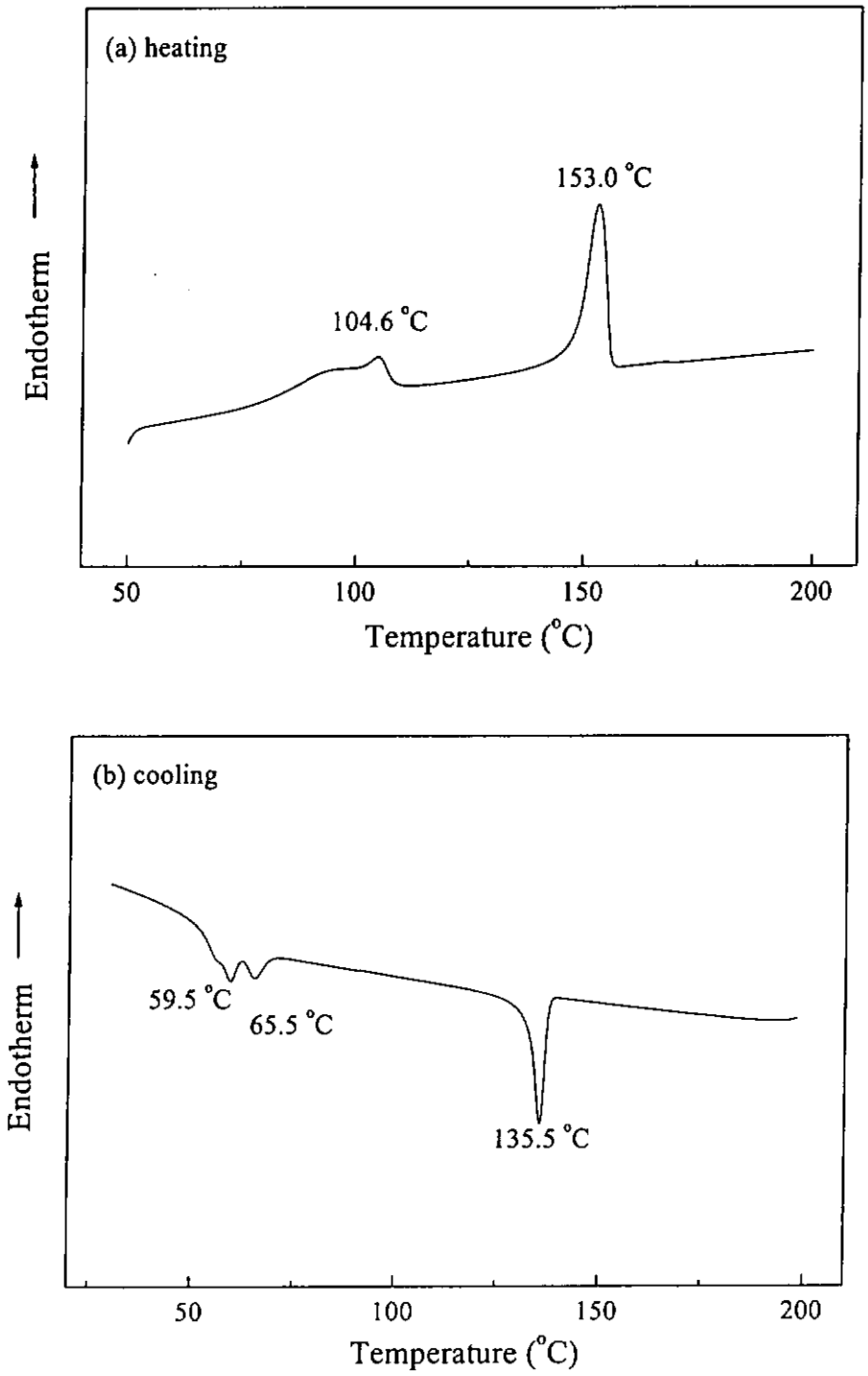


Fig. 4.3 DSC endotherms of P(VDF-TrFE) (70/30) (a) upon heating and (b) upon cooling.

### 4.3.3 Dielectric Properties

The dielectric permittivity ε' and ε" of an unpoled P(VDF-TrFE) copolymer were measured from -30 °C to 135 °C in the frequency range of 100 Hz to 10 MHz by a HP4194A Impedance Analyzer.

#### 4.3.3.1 Dielectric properties as functions of temperature

Fig. 4.4 shows the dielectric permittivity ε' and ε" at 1 kHz as a function of temperature upon heating and cooling. From Fig. 4.4(a), relaxation peaks are found at 107 °C and 70 °C upon heating and cooling, respectively. These are related to the paraelectric-to-ferroelectric transition temperature $T_c$. The copolymer shows a thermal hysteresis in that transition temperature upon heating and cooling similar to the DSC result. The room temperature dielectric permittivity ε' and ε" are 10 and 0.15 at 1 kHz. From Fig. 4.4(b), two relaxation processes are observed at -15 °C and 110 °C. The low temperature β process may be ascribed to the cooperative local motions of the short chain segments in the non-crystalline regions [47]. The high temperature process is the relaxation associated with the ferroelectric phase transition.

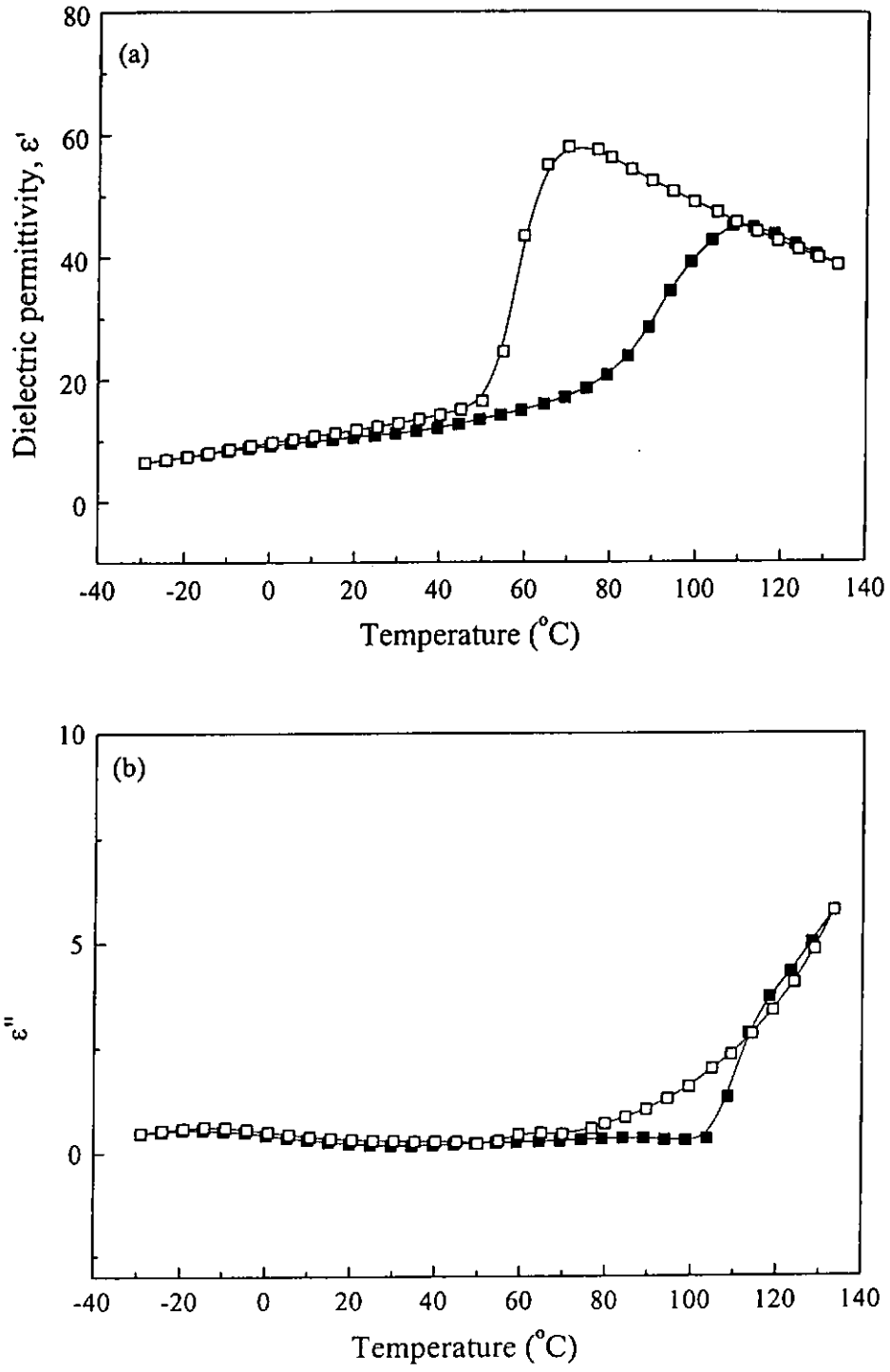


Fig. 4.4 Dielectric permittivity (a) ε' (square symbol) and (b) ε" (circle symbol) of P(VDF-TrFE) (70/30) at 1 kHz as a function of temperature upon heating (solid symbol) and cooling open symbol).

### 4.3.3.2 Frequency dispersion

Fig. 4.5 shows the dielectric permittivity ε' and ε" as a function of frequency measured at -20,0, 30, 50, 70, 100 and 130 °C. From Fig. 4.5(a), for f > 1 kHz, ε' has a maximum value near 110 °C where a ferroelectric phase transition occurs in the crystalline regions. Fig. 4.5(b) shows that at low temperature, the ε" peak is lower and broad. As the temperature increases the ε" peaks become sharper and higher. At 110 °C and 130 °C, ε" rise sharply in the low frequency range (f < 10 kHz) due to d.c. conductivity. The β relaxation occurs at frequency $f_m$. When the temperature is low, e.g. at -20 °C, $f_m$ ~ 1 kHz. As temperature increases, $f_m$ shifts to higher frequency and near room temperature, e.g. at 30 °C, $f_m$ ~ 5 MHz. Hence, if P(VDF-TrFE) is used as ultrasonic transducer near room temperature which operates at the MHz range, this β relaxation may adversely affect its performance.

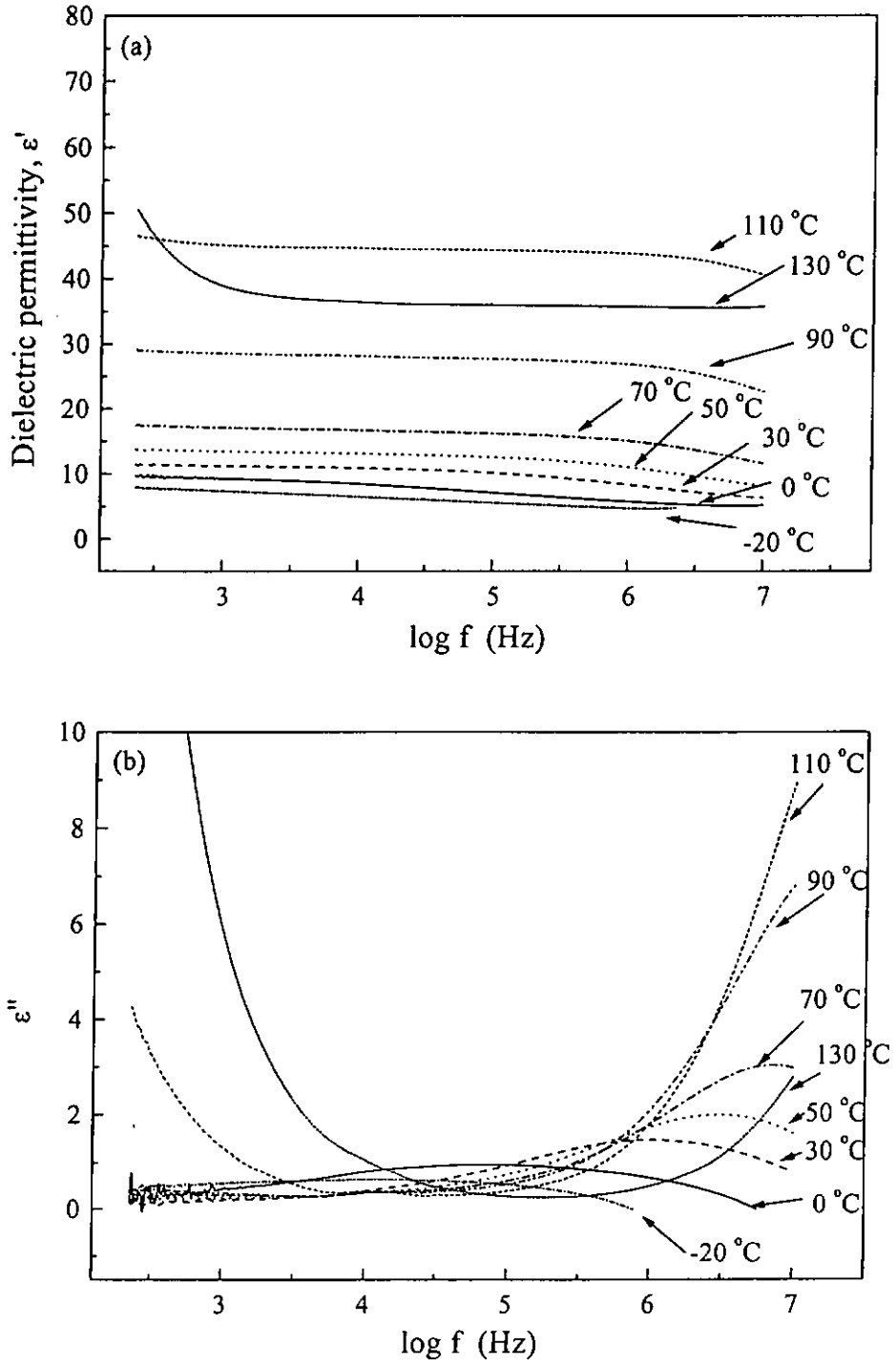


Fig. 4.5 Dielectric permittivity (a) ε' and (b) ε'' of P(VDF-TrFE) as a function of frequency at various temperatures.

The relaxation time τ, it is determined from the ε" peak frequency $f_m$ by the equation

$$\tau = \frac{1}{2\pi f_m} \tag{4.1}$$

The relaxation time τ decreases with the temperature increases. Fig. 4.6 shows the logarithm of τ as a function of the reciprocal of absolute temperature 1/T [48]. From the slope, the activation energy of the relaxation is estimated to 13.45 kcal/mol which is close to the reported value for P(VDF-TrFE) (70/30) copolymer [48].

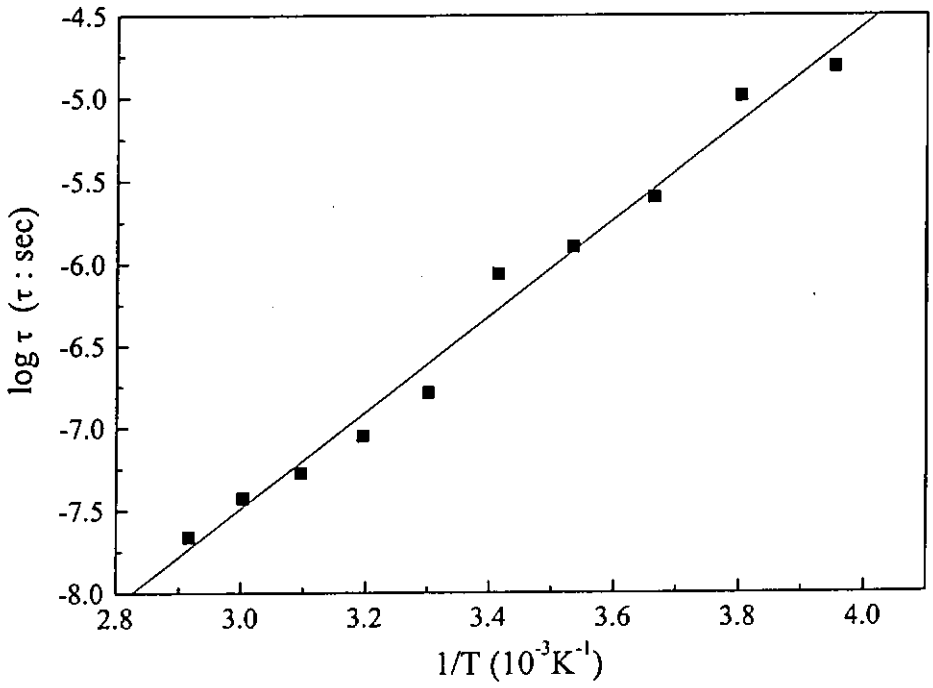


Fig. 4.6 Plots of log τ as a function of 1/T for P(VDF-TrFE) (70/30).

### 4.3.4 Piezoelectric and Pyroelectric Properties

For an unpoled ferroelectric material, it does not exhibit a net macroscopic polarization and have no pyroelectric and piezoelectric activities. This is due to the random distribution of the dipoles. To bring out the pyroelectric and piezoelectric activities, a poling process is needed. During poling, a high electric field is applied across the thickness of the ferroelectric sample to align the dipoles of the samples [19-21,48]. After poling, the ferroelecrtric materials would exhibit pyroelectric and piezoelectric activities. A larger degree of dipole orientations in the sample will result in higher pyroelectric and piezoelectric activities.

In this work, P(VDF-TrFE) samples were poled by a d.c. electric field. An electric field E = 20 kV/mm was applied at 95 °C for 2 h. Then the sample was cooled to ~ 45 °C with the field kept on. After poling, the pyroelectric p and piezoelectric $d_{33}$ coefficients were measured. Fig. 4.7 shows the pyroelectric coefficient $p_p$ of P(VDF-TrFE) (measured by the digital integration method) as a function of temperature. At room temperature (25 °C), the pyroelectric coefficient $p_p$ was 28 $\mu C/m^2K$ and the piezoelectric coefficient $d_{33p}$ was -28 pC/N which was directly measured by a Pennebaker model 8000 piezo $d_{33}$ tester (American Piezo-Ceramic Inc.). These values of $p_p$ and $d_{33p}$ will be used in subsequent composite modeling.

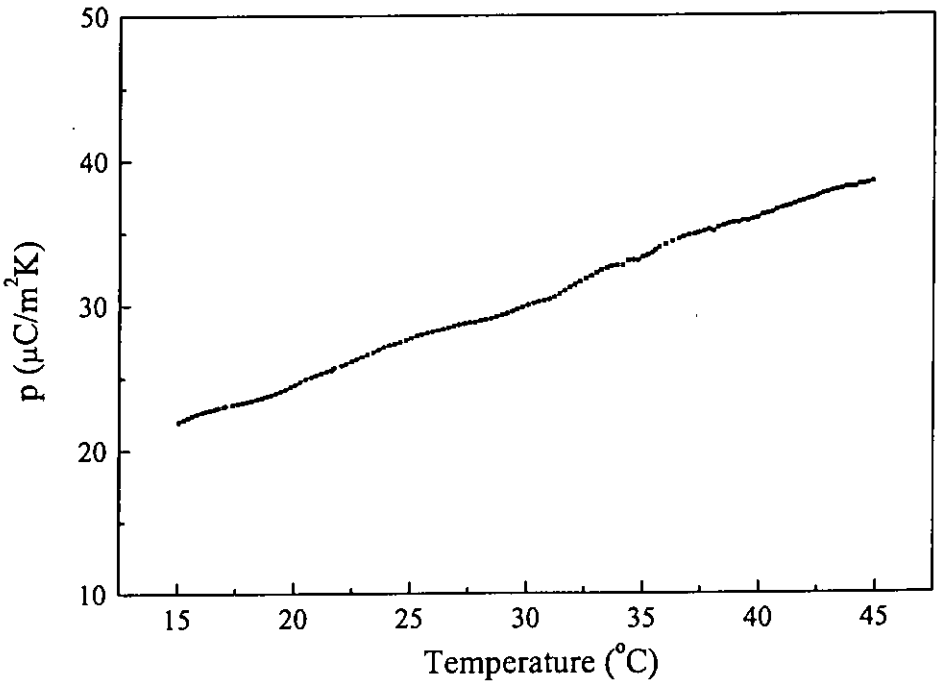


Fig. 4.7 Pyroelectric coefficient p of P(VDF-TrFE) (70/30) as a function of temperature.

# CHAPTER FIVE

# $BaTiO_3$/P(VDF-TrFE) 0-3 COMPOSITES

## 5.1 Introduction

Barium titanate/polyvinylidene fluoride- trifluoroethylene [$BaTiO_3$/P(VDF-TrFE)] 0-3 composites with different ceramic volume fractions were fabricated. The preparation method of the $BaTiO_3$ powder and the characteristics of the $BaTiO_3$ were discussed in chapters 2 and 3, respectively. The room temperature (25 °C) dielectric permittivity $\varepsilon_c$' and $\varepsilon_c$" of $BaTiO_3$ (oxide) was 1160 and 17.7 at 1 kHz. The pyroelectric $p_c$ and piezoelectric $d_{33c}$ coefficients at 25 °C are 235 $\mu C/m^2K$ and 175 pC/N, respectively. The P(VDF-TrFE) copolymer was supplied by Piezotech in France. It consists of 70 mol% of VDF and 30 mol% TrFE. The room temperature (25 °C) dielectric permittivity $\varepsilon_p$' and $\varepsilon_p$" was 10 and 0.15 at 1 kHz. The pyroelectric $p_p$ and piezoelectric $d_{33p}$ coefficients at 25 °C are 28 $\mu C/m^2K$ and -28 pC/N, respectively. The values will be used as references in 0-3 composites modeling.

Phase transitions of the 0-3 composites were measured by DSC (Perkin Elmer DSC7 thermal analyzer). The dielectric permittivity $\varepsilon$' and $\varepsilon$" of the composites were measured as functions of temperature. These data were used to find the electric field experienced by the ceramic phase and hence to optimize the poling temperature [22].

The pyroelectric p and piezoelectric $d_{33}$ coefficients of the composites were measured by the digital integration method and a Pennebaker model 8000 piezo $d_{33}$ tester, respectively and compared to model calculation [23]. The laser induced pressure pulse (LIPP) [24,49-52] method was used to study the polarization distributions in the 0-3 composites.

## 5.2 Sample Preparation

To prepare $BaTiO_3$/P(VDF-TrFE) 0-3 composites, the copolymer was dissolved in acetone at room temperature. To prepare composites with different ceramic volume fraction $\phi$, appropriate amounts of $BaTiO_3$ ceramic powder were added to the copolymer solution. The $BaTiO_3$ powder was prepared by the mixed oxide route and has an average grain size of 1 to 3 μm. Then the mixture was placed in an ultrasonic bath for 1 h to ensure the ceramic powder was dispersed homogeneously in the copolymer matrix. Finally the 0-3 composite solution was poured onto a glass plate and left for the solvent to evaporate. A composite sheet was formed. The sheet was placed in an oven at about 120 °C for 2 h to allow the solvent to evaporate completely. The dried composite sheet was torn into small pieces. These were molded into a cylinder by compression-molding at 210 °C, under a pressure of 10 MPa for 1 h. Then the sample was cooled to room temperature with the pressure kept on. After the sample was molded, it was cut into thin discs between 0.4 to 0.7 mm thick using a high precision diamond saw. Diameter of the disc was 19 mm. The sample discs were polished and

painted with air-dried silver paint, which act as the conductive electrodes. The schematic set-up for compression-molding was shown in Fig. 4.4 (Chapter 4).

The ceramic volume fraction $\phi$ of the 0-3 composite was calculated using the relation

$$\rho = \phi\rho_c + (1-\phi)\rho_p \tag{5.1}$$

where $\rho$, $\rho_c$ and $\rho_p$ are the density of the composite, ceramic and copolymer, respectively. The densities of the samples were measured using Archemedes principle. Composites with $\phi > 0.5$ cannot be successfully fabricated as the polymer cannot encapsulate all the ceramic particles properly and it will crack and breakdown during poling.

## 5.3 Structures and Microstructures of 0-3 Composites

The fracture surfaces of the composite samples were examined by SEM in order to examine the particle dispersion within the copolymer matrix. Fig. 5.1 shows the micrographs of (a) P(VDF-TrFE) and $BaTiO_3$/P(VDF-TrFE) 0-3 composites with various ceramic volume fraction $\phi$: (b) $\phi$ = 0.10 and (c) $\phi$ = 0.21 (d) $\phi$ = 0.31, (e) $\phi$ = 0.41 and (f) $\phi$ = 0.49. From the micrographs, we can see that the $BaTiO_3$ particles dispersed rather uniformly in the copolymer matrix.

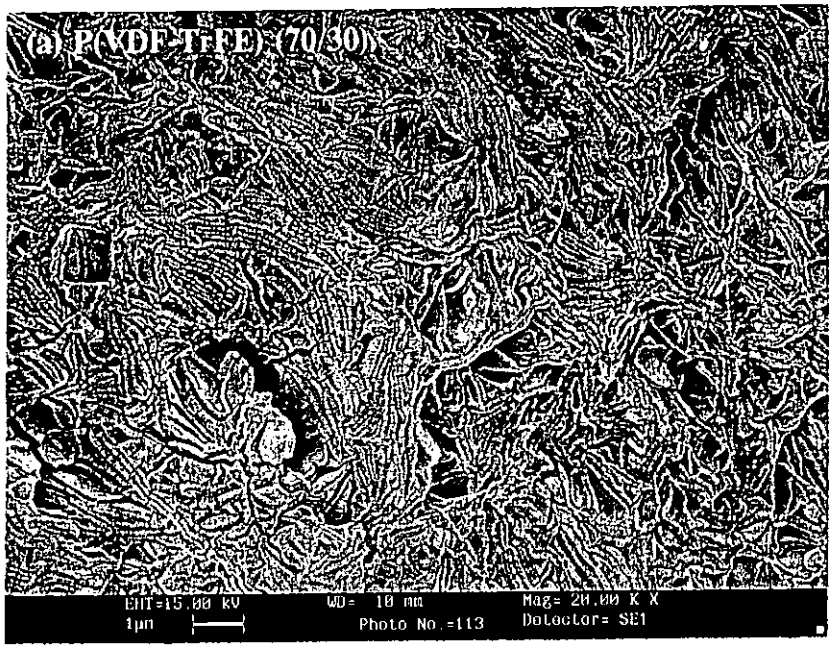


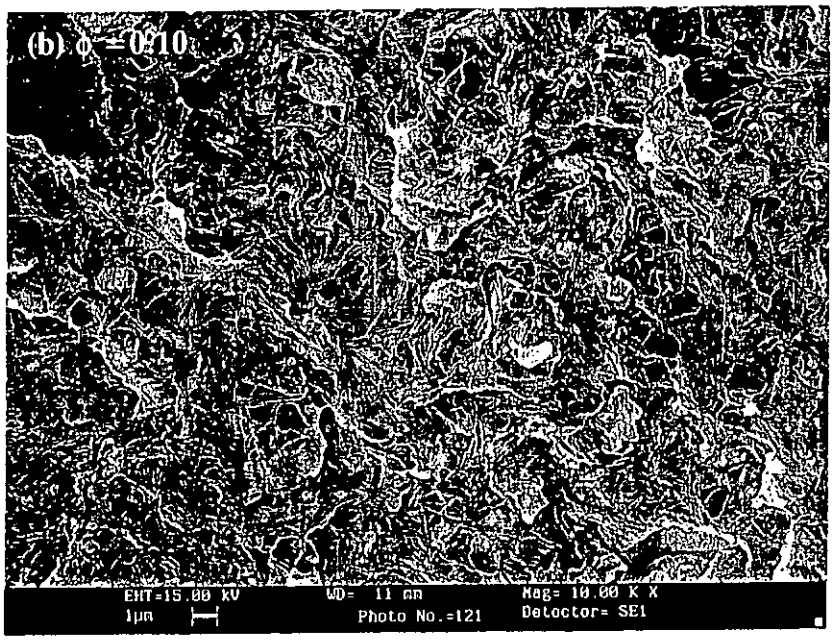


Fig. 5.1 SEM micrographs of the fractured surface of $BaTiO_3$/P(VDF-TrFE) 0-3 composites with $\phi$ equal to (a) 0 (PVDF-TrFE) (70/30) and (b) $\phi = 0.10$.

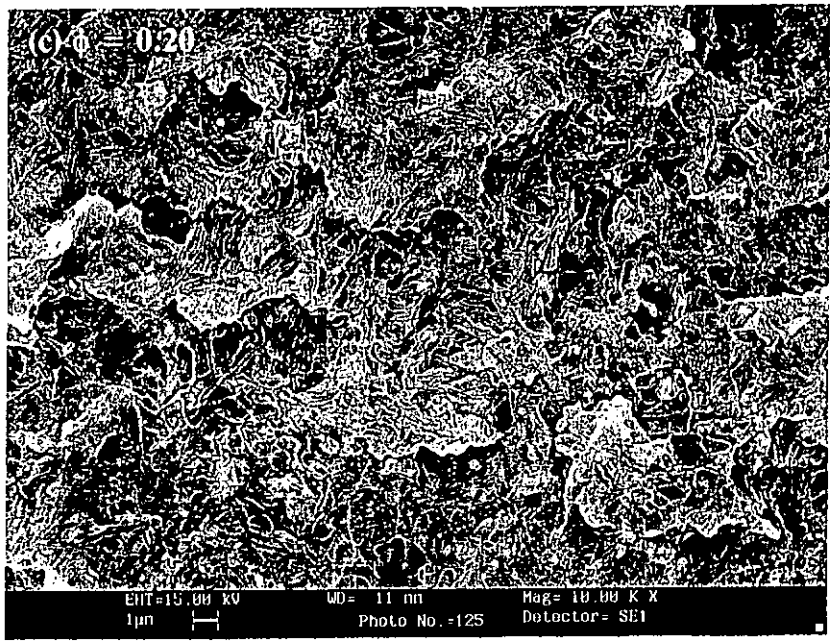


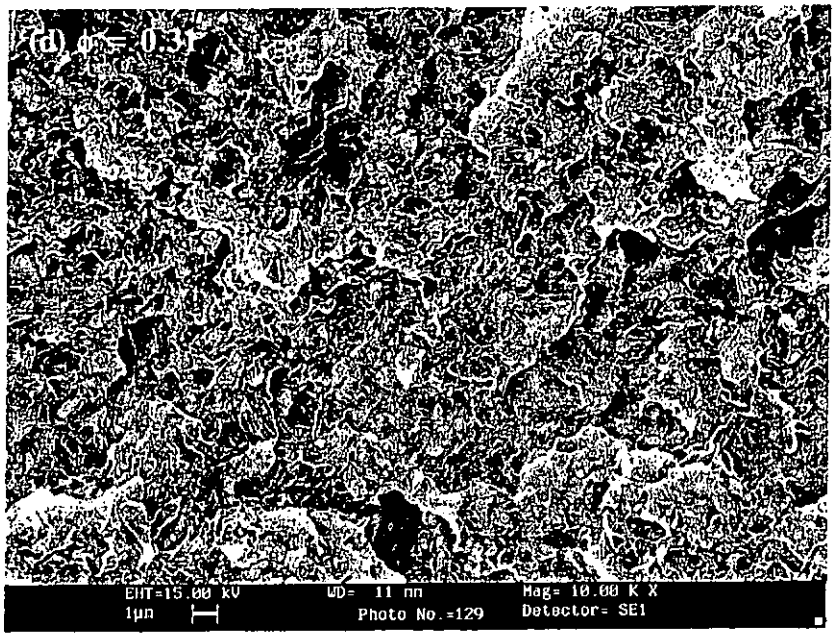


Fig. 5.1 SEM micrographs of the fractured surface of the $BaTiO_3$/P(VDF-TrFE) 0-3 composites with $\phi$ equal to (c) 0.21 and (d) 0.31.

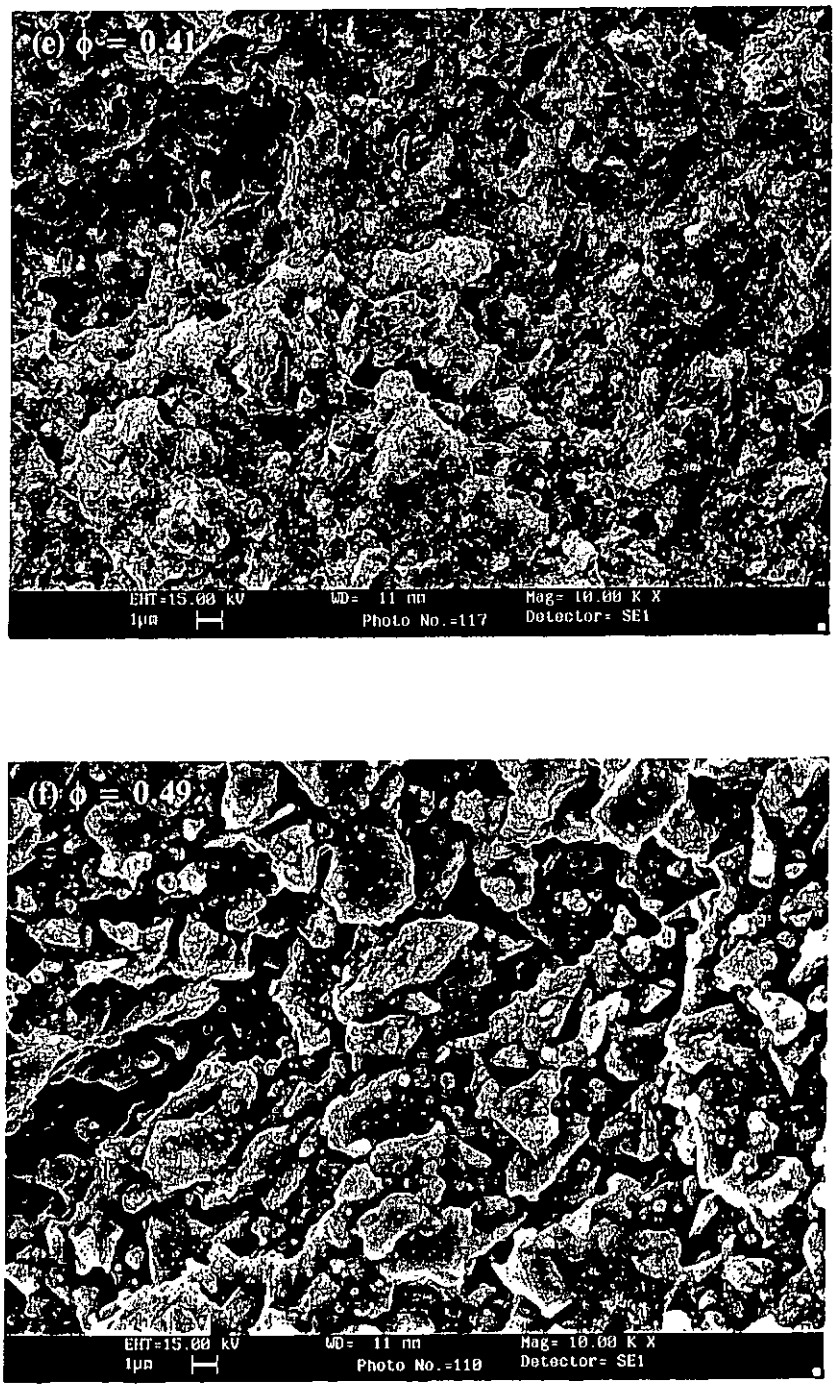


Fig. 5.1 SEM micrographs of the fractured surface of the $BaTiO_3$/P(VDF-TrFE) 0-3 composites with $\phi$ equal to (e) 0.41 and (f) 0.49.

Fig. 5.2 shows the XRD patterns of P(VDF-TrFE) copolymer, 0-3 composite ($\phi$ = 0.31) and $BaTiO_3$ ceramic. The XRD patterns showed that all the reflection peaks of the ceramic were present. The reflection peak at $2\theta$ = 19.7 ° ($(110)_p$ and $(200)_p$ planes of P(VDF-TrFE)) still existed but the peaks of P(VDF-TrFE) at $2\theta$ = 35.2 ° ($(001)_p$ plane) and 40.9 ° ($(201)_p$ and $(111)_p$ planes) cannot be observed probably due to their small intensity compared to the ceramic peaks. XRD patterns for $BaTiO_3$/P(VDF-TrFE) 0-3 composites with other values of $\phi$ are similar to that shown in Fig. 5.2 (b).

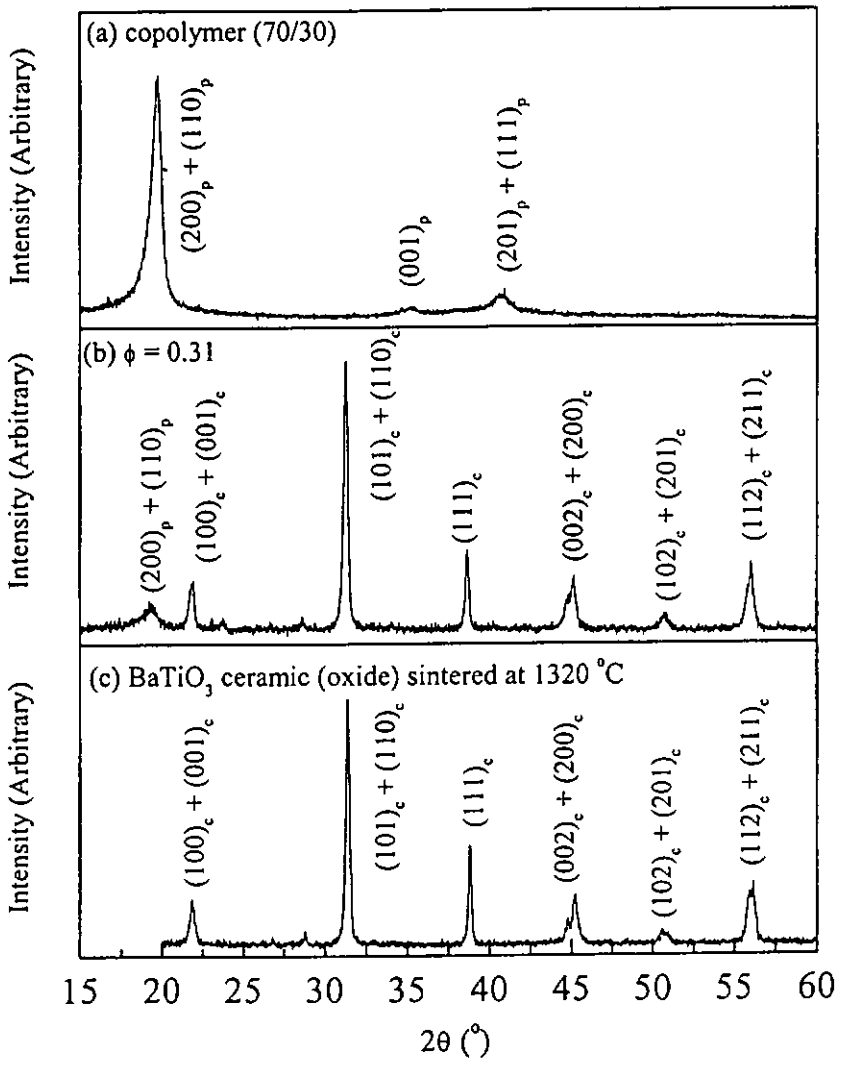


Fig. 5.2 XRD patterns of (a) P(VDF-TrFE) (70/30), (b) $BaTiO_3$/P(VDF-TrFE) 0-3 composite ($\phi$ = 0.31) and (c) $BaTiO_3$ (oxide) ceramic sintered at 1320 °C.

## 5.4 Phase Transitions

The phase transitions of the composites were analyzed by the DSC. Composites with different ceramic volume fractions were heated from 30 °C to 200 °C, then cooled to 30 °C at a rate of 10 °C/min. The sample was heated and cooled twice. The first heating process was used to remove the thermal history of the composite samples. The DSC results of the second heating and cooling process were shown in Fig. 5.3(a) and (b) respectively. Fig. 5.3 shows that the endothermic peaks (Curie temperature $T_c$, melting temperature $T_m$ and the crystallization temperature $T_s$) of the composites are closed to the peaks of the copolymer. It implied that the phase transitions of the copolymer phase are not suppressed in the composites. The melting $T_m$ and the crystallization $T_s$ temperature were slightly shifted to lower temperature when the ceramic volume fraction $\phi$ increases. There is no a systematic change in the Curie temperature $T_c$. $T_c\uparrow$ was 105 ± 1 °C and $T_c\downarrow$ were 60 and 66 ± 1 °C (Table 5.1). Fig. 5.4 shows the DSC result of $BaTiO_3$ (oxide) powder. The endothermic peak of the $BaTiO_3$ powder is broadened when the size of the powder decreases. No endothermic peak is observed when the size of the powder decreased to ~ 1 μm. However, there is a Curie point at 130 °C for the bulk $BaTiO_3$ (oxide) ceramic (shown in Fig. 3.4). Hence, unlike the bulk ceramic, $BaTiO_3$ powder below a critical size may not have a Curie transition at 130 °C. In subsequent measurement of the dielectric permittivity ε' of the composites, we found that no additional Curie transition due to the ceramic powder were observed presumably due to the small crystallite size ( 52.2 nm) of the powder.

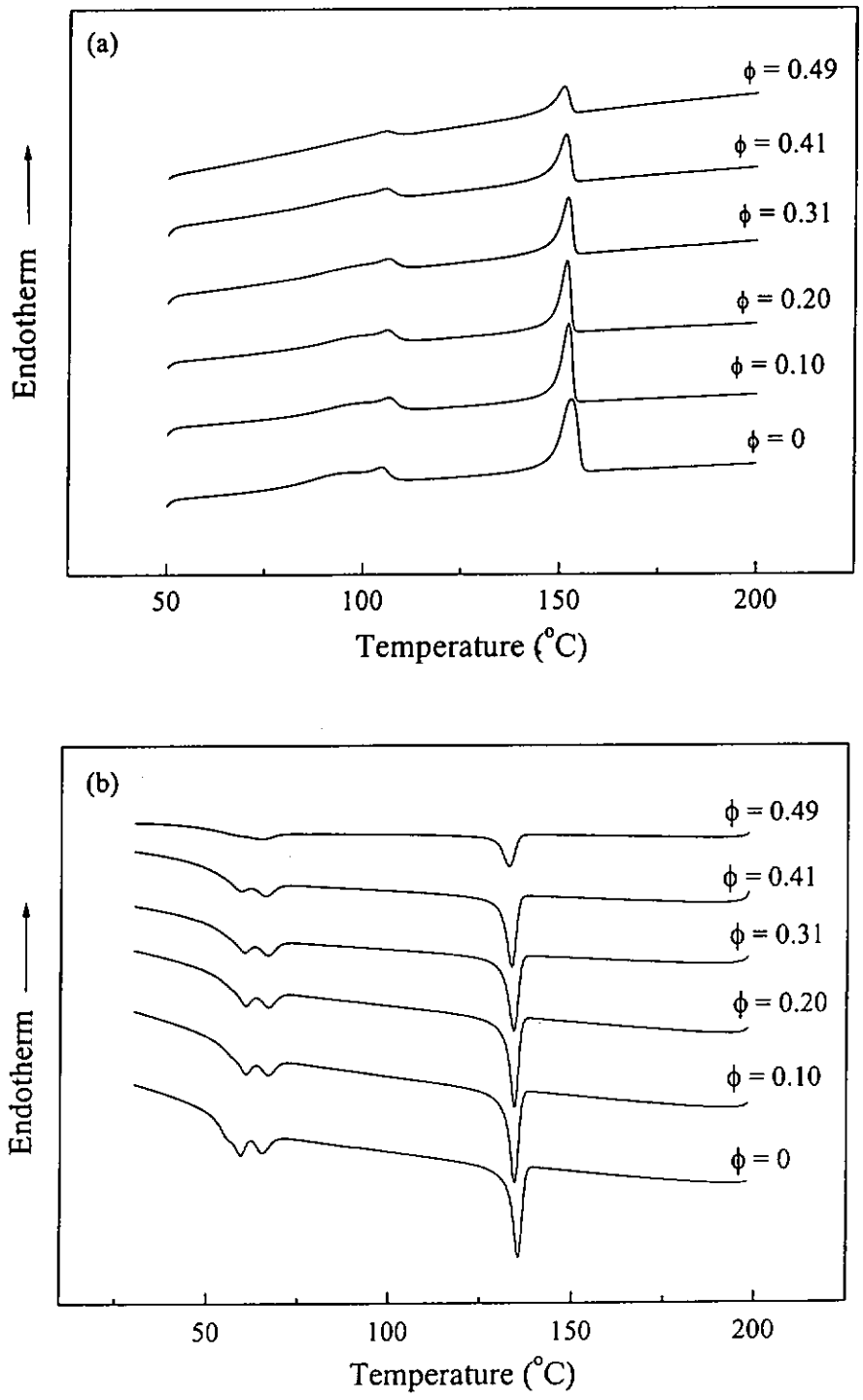


Fig. 5.3 DSC endotherms of $BaTiO_3$/P(VDF-TrFE) 0-3 composites with various $\phi$ upon (a) heating and (b) cooling.

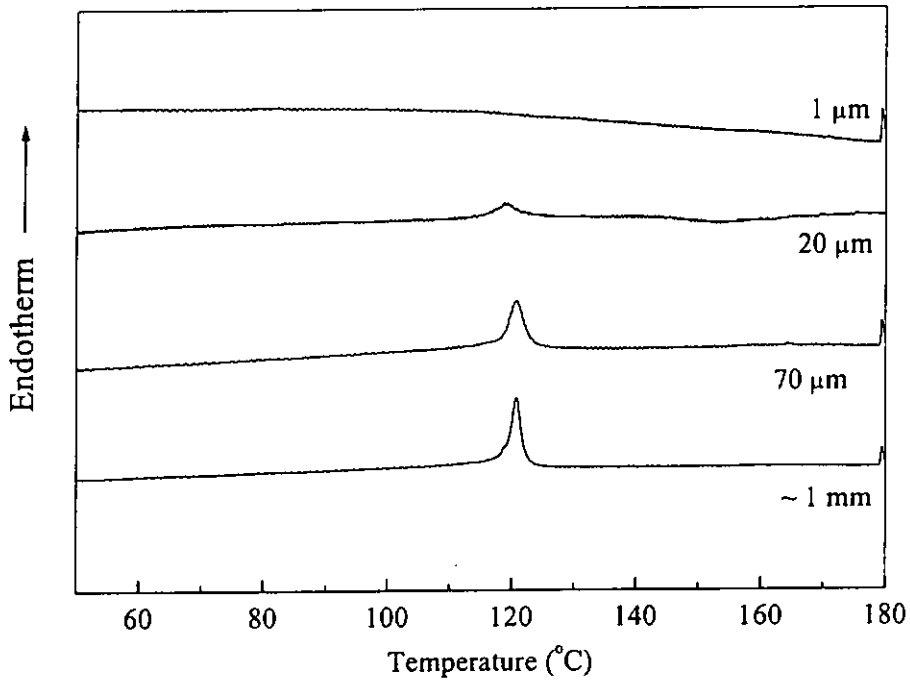


Fig. 5.4 DSC endotherms of $BaTiO_3$ (oxide) powder upon heating.

| $\phi$ | $T_c$ ( heating) (°C) | $T_c$ ( cooling) (°C) | $T_m$ (°C) | $T_s$ (°C) |
|---|---|---|---|---|
| 0 | 104.7 | 59.5, 65.3 | 153.0 | 135.5 |
| 0.10 | 106.5 | 60.8, 67.0 | 152.2 | 134.5 |
| 0.20 | 106.0 | 60.8, 67.0 | 151.2 | 134.3 |
| 0.31 | 106.0 | 60.3, 67.0 | 151.8 | 134.2 |
| 0.41 | 105.3 | 59.5, 66.2 | 151.3 | 133.5 |
| 0.49 | 105.5 | 64.7 | 150.7 | 132.0 |

Table 5.1 $T_c$, $T_m$ and $T_s$ of P(VDF-TrFE) (70/30) and $BaTiO_3$/P(VDF-TrFE) 0-3 composites with various $\phi$.

## 5.5 Dielectric Properties

### 5.5.1 Temperature and Frequency Dispersion

The dielectric permittivity ε' and ε" of the 0-3 composites were measured from -30 °C to 130 °C. Fig. 5.5 shows the dielectric permittivity ε' of the 0-3 composites with various ceramic volume fraction $\phi$ at 1 kHz as a function of temperature upon heating and cooling. From the graph, it is seen that the Curie temperature $T_c$ of the composite is close to that of the copolymer. It was about $T_c\uparrow$~ 105 °C and $T_c\downarrow$ ~ 70 °C. Fig. 5.6 shows the ε" at 1 kHz as a function of temperature. From the graph, the low-temperature non-crystalline β relaxation peaks at ~ -20 °C were observed in both the copolymer and composites upon heating and cooling. For temperature higher than 80 °C ε" increases as a result of d.c. conduction. Figs. 5.7 and 5.8 show ε' and ε" as functions of temperature at 100 kHz. It can be seen that the Curie temperature $T_c\uparrow$ and $T_c\downarrow$ are unaffected by the change in frequency, hence Fig 5.5 and Fig. 5.7 are very similar. If we compared Fig. 5.6 and Fig. 5.8, we can see that the β relaxation peaks, located at -20 °C at 1 kHz, have shifted to 10 °C at 100 kHz. The effect of d.c. conduction is not very conspicuous at 100 kHz.

Fig. 5.9 shows the dielectric permittivity ε' and ε" of the composite as a function of frequency from 500 Hz to 10 MHz at room temperature (25 °C). From the ε" frequency spectrum, it was observed that the low-temperature non-crystalline β-relaxation of the copolymer at room temperature occurs at ~ 1 MHz. This relaxation also exists in the

composites around the same frequency. The ε" peak of the 0-3 composites becomes more conspicuous and shifts to higher frequency as the ceramic volume fraction $\phi$ increases. Hence, in this study we found that, similar to the copolymer, there are two dielectric relaxations in the composites: The first relaxation is associated with the Curie transition in the crystalline regions and its temperature location is independent of the measurement frequency (Figs. 5.5 to 5.8). The second (β) relaxation is ascribed to the local motions of short chain segments in the non-crystalline regions and the temperature at which it occurs increases with increasing frequency. The β relaxation peaks of the copolymer and composites is located at about -20 °C when measured at 1 kHz, and it shifts to higher temperature with increasing frequency (Fig. 5.8).

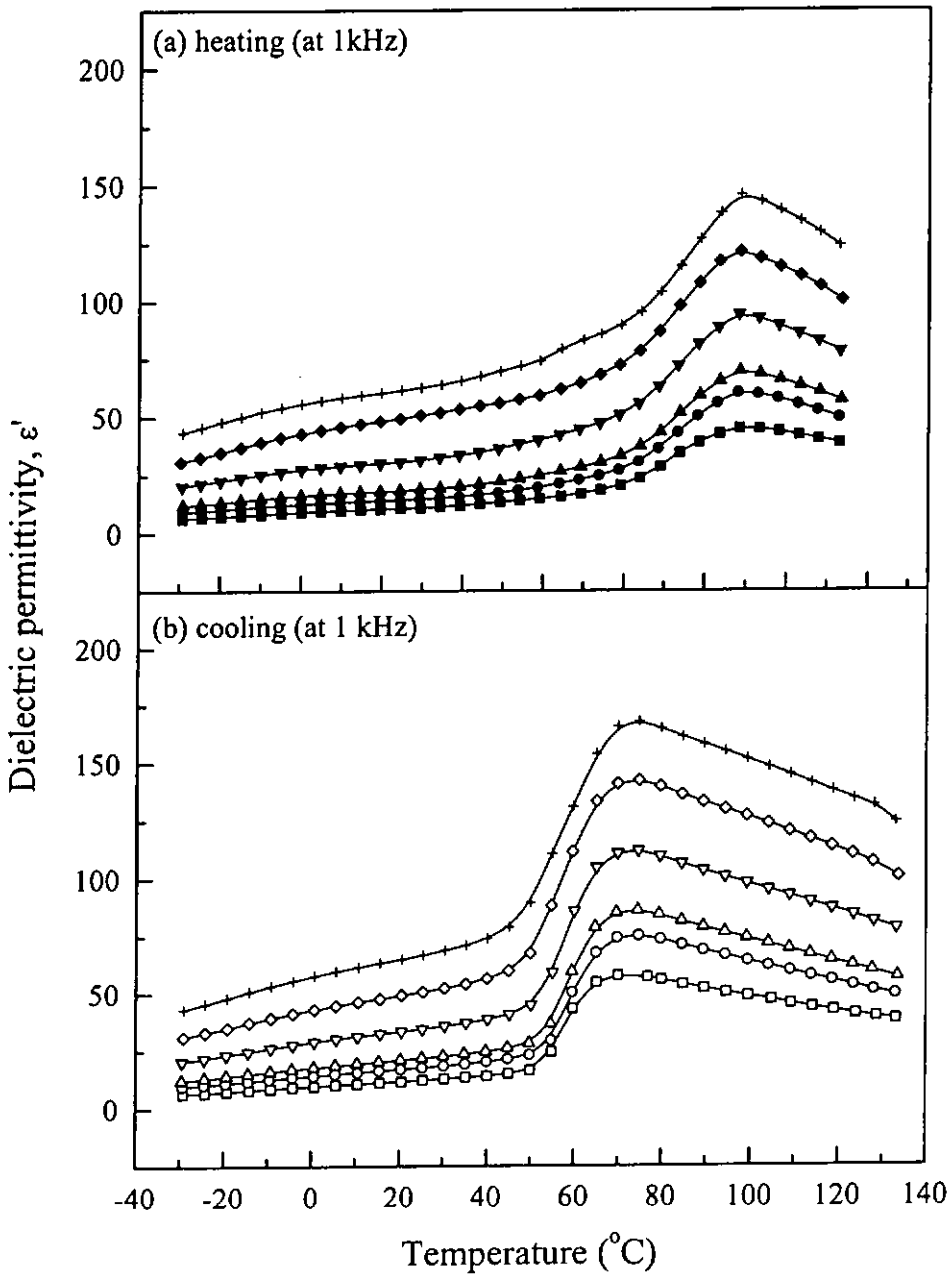


Fig. 5.5 Dielectric permittivity ε' of $BaTiO_3$/P(VDF-TrFE) with various $\phi$ at 1 kHz as a function of temperature upon (a) heating (solid symbol) and (b) cooling (open symbol). Square, circle, triangle, inverted triangle, diamond and the cross represent $\phi$ = 0, 0.10, 0.20, 0.31, 0.41 and 0.49, respectively.

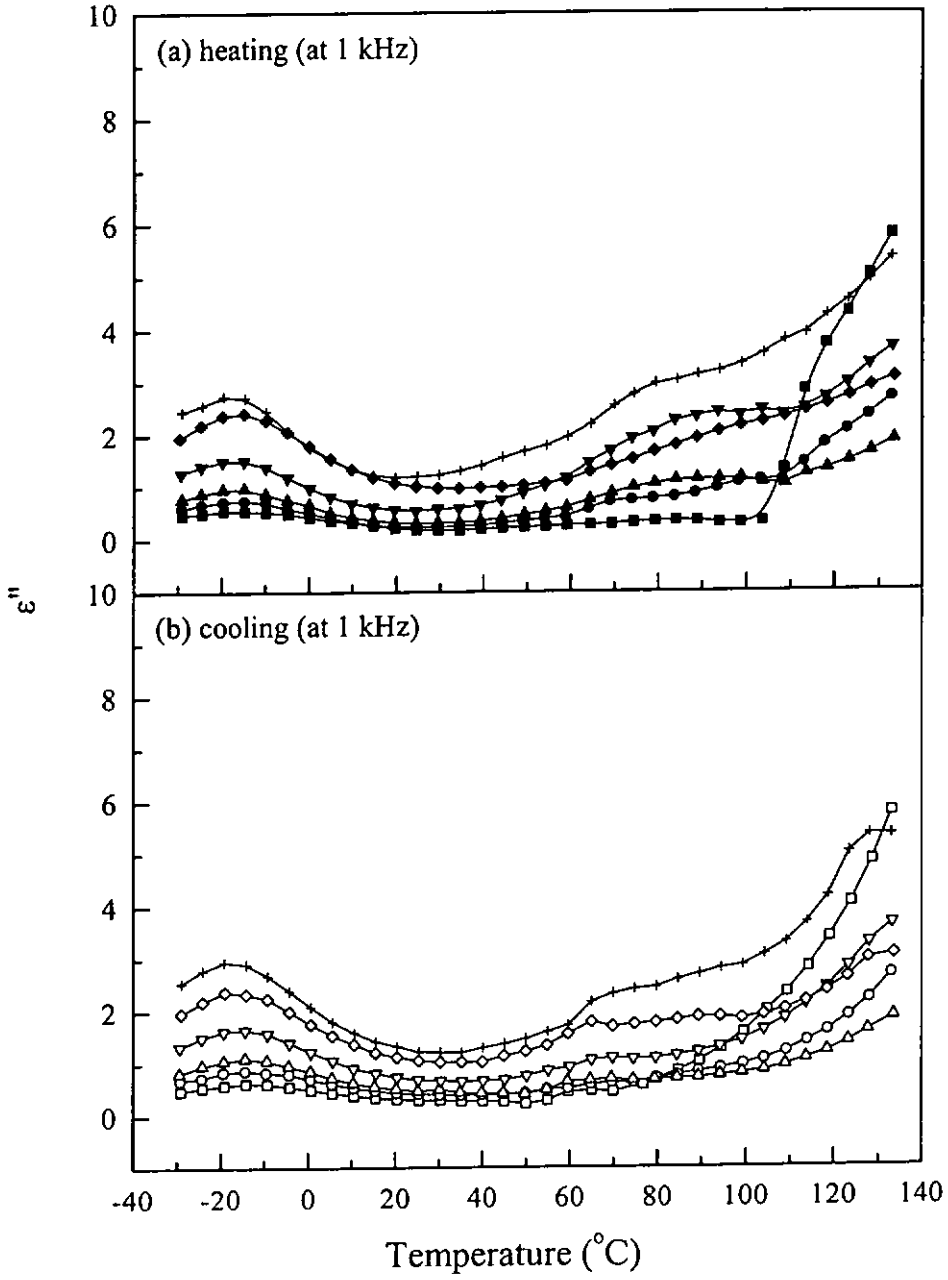


Fig. 5.6 ε" of $BaTiO_3$/P(VDF-TrFE) with various $\phi$ at 1 kHz as a function of temperature upon (a) heating (solid symbol) and (b) cooling (open symbol). Square, circle, triangle, inverted triangle, diamond and the cross represent $\phi$ = 0, 0.10, 0.20, 0.31, 0.41 and 0.49, respectively.

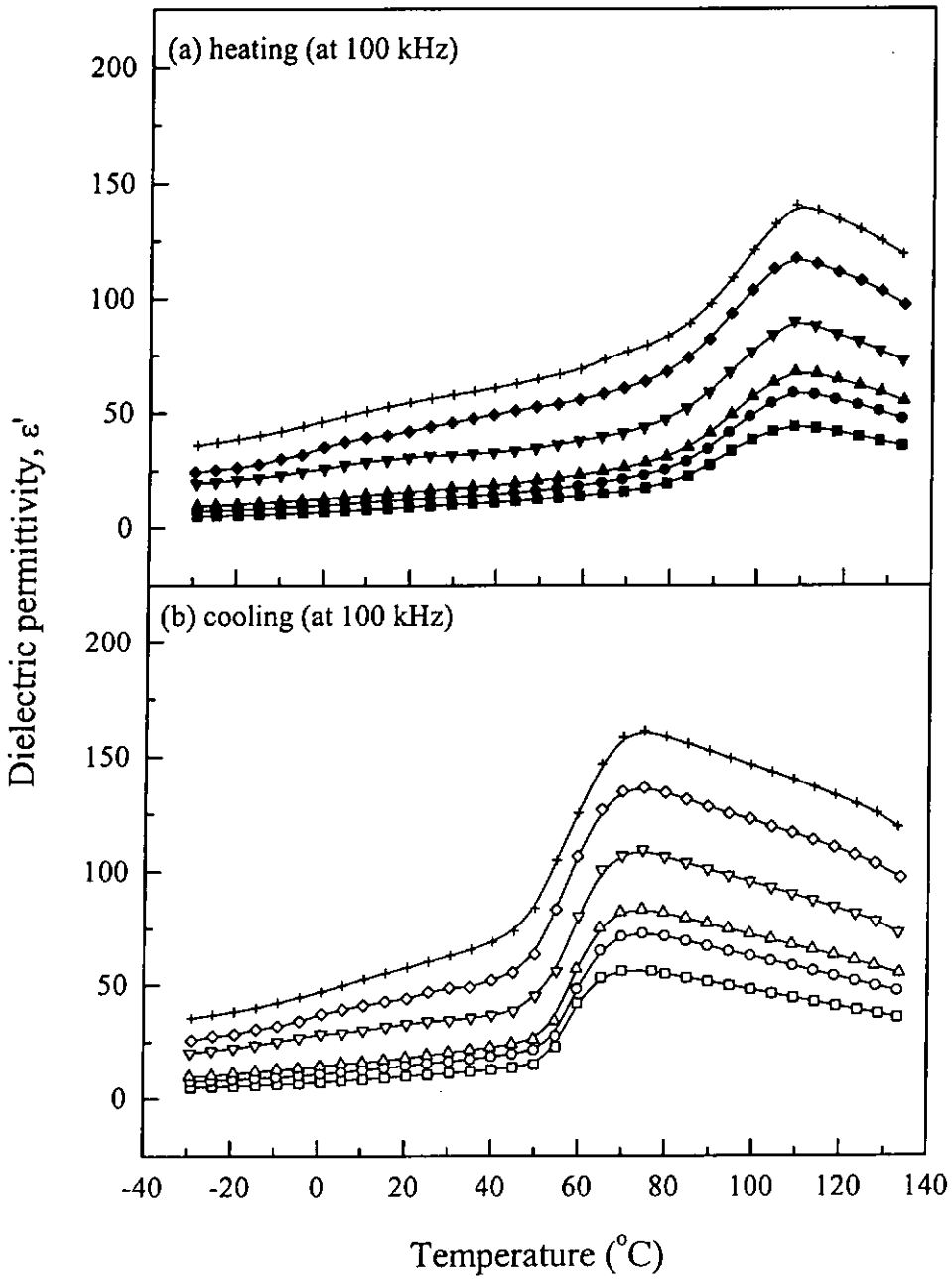


Fig. 5.7 Dielectric permittivity ε' of $BaTiO_3$/P(VDF-TrFE) with various $\phi$ at 100 kHz as a function of temperature upon (a) heating (solid symbol) and (b) cooling (open symbol). Square, circle, triangle, inverted triangle, diamond and the cross represent $\phi$ = 0, 0.10, 0.20, 0.31, 0.41 and 0.49, respectively.

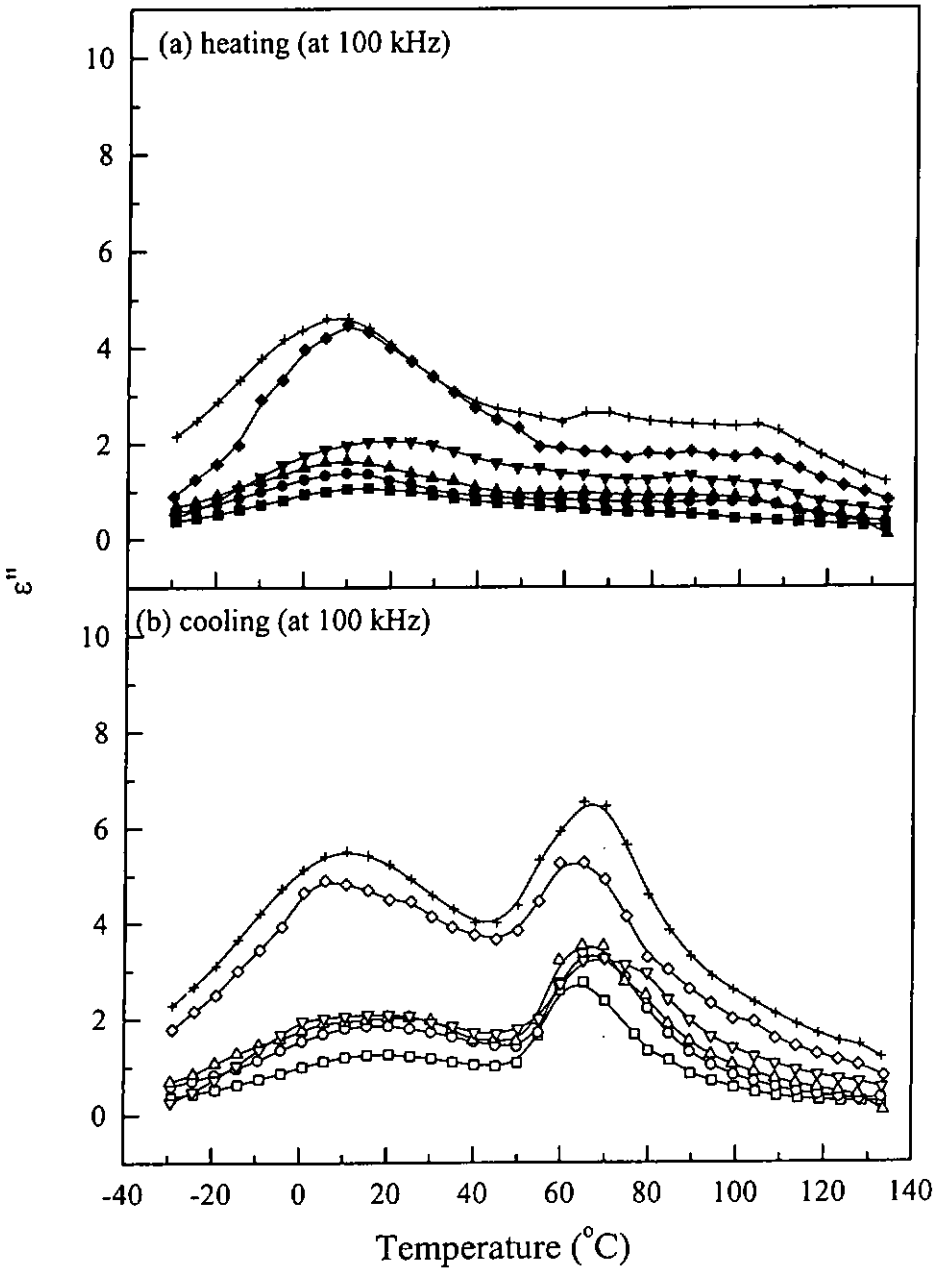


Fig. 5.8 ε" of at $BaTiO_3$/P(VDF-TrFE) with various $\phi$ at 100 kHz as a function of temperature upon (a) heating (solid symbol) and (b) cooling (open symbol). Square, circle, triangle, inverted triangle, diamond and the cross represent $\phi$ = 0, 0.10, 0.20, 0.31, 0.41 and 0.49, respectively.

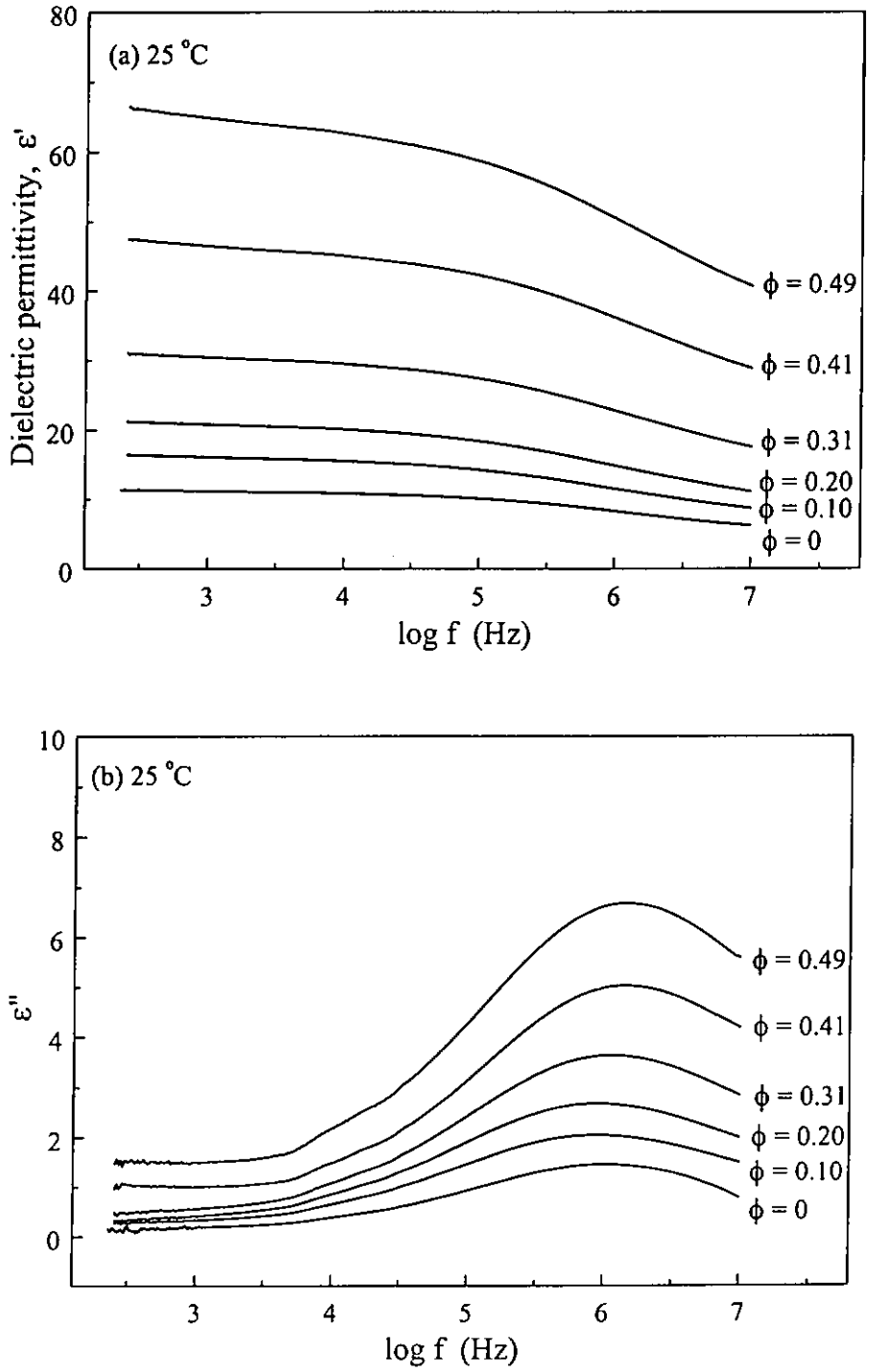


Fig. 5.9 Dielectric permittivity (a) ε' and (b) ε'' of $BaTiO_3$/P(VDF-TrFE) with various ϕ as a function of frequency at room temperature (25 °C).

### 5.5.2 Bruggeman Model

The dielectric permittivity ε' and ε" of the composites can be understood in terms of the Bruggeman mixture theory [53,54]. In the Bruggeman model, the particle embedded in the matrix is assumed to have a spherical shape. The concentration of the dispersed particle in the nearby particle was taken into account by using an integration scheme [54]. In the case of a ceramic/polymer 0-3 composite system, according to the Bruggeman's scheme, the initial low concentration of the dispersed sphere $\varepsilon_c'$ ($\varepsilon_c''$) is gradually increased. Undergoing the process that the dielectric permittivity ε' (ε") of the matrix is changed from $\varepsilon_p'$ ($\varepsilon_p''$) to ε' (ε"), the final value of the system. The Bruggeman model provides a good description of the dielectric permittivity of the ceramic/polymer 0-3 composite system [55,56]. The equations are shown as follow [54]

$$(1-\phi)=\frac{\varepsilon_c'-\varepsilon'}{\varepsilon_c'-\varepsilon_p'}\left(\frac{\varepsilon_p'}{\varepsilon'}\right)^{1/3} \tag{5.2}$$

$$\varepsilon''=\frac{(\varepsilon_c'-\varepsilon')(\varepsilon_c'+2\varepsilon_p')\varepsilon'\varepsilon_p''}{(\varepsilon_c'-\varepsilon_p')(\varepsilon_c'+2\varepsilon')\varepsilon_p'}+\frac{3(\varepsilon'-\varepsilon_p')\varepsilon'\varepsilon_c''}{(\varepsilon_c'-\varepsilon_p')(\varepsilon_c'+2\varepsilon')} \tag{5.3}$$

where ε' and ε" represent the real part and the imaginary part of the dielectric permittivity. The subscripts p and c denote the polymer phase and ceramic phase, respectively, and ϕ refer to the ceramic volume fraction.

Figs. 5.10 to 5.12 show the dielectric permittivity ε' and ε" (measured at 1 kHz) as a function of ceramic fraction $\phi$ at -30, 30 and 60 °C compared with the Bruggeman model. The $\varepsilon_c$' ($\varepsilon_c$") and $\varepsilon_p$' ($\varepsilon_p$") obtained at various temperatures from chapters 3 and 4 are used in the model calculation. The square and the circle symbols represent the measured values of ε' and ε", respectively. The solid and the dash line curves represent the theoretical value calculated from equations 5.2 and 5.3, respectively. From Fig. 5.10 (a), the experimental results of ε' and ε" fitted well to the Bruggeman model for temperature up to 60 °C. At higher temperature ( > 60 °C), due to the onset of d.c. conduction, equations 5.2 and 5.3 no longer applied.

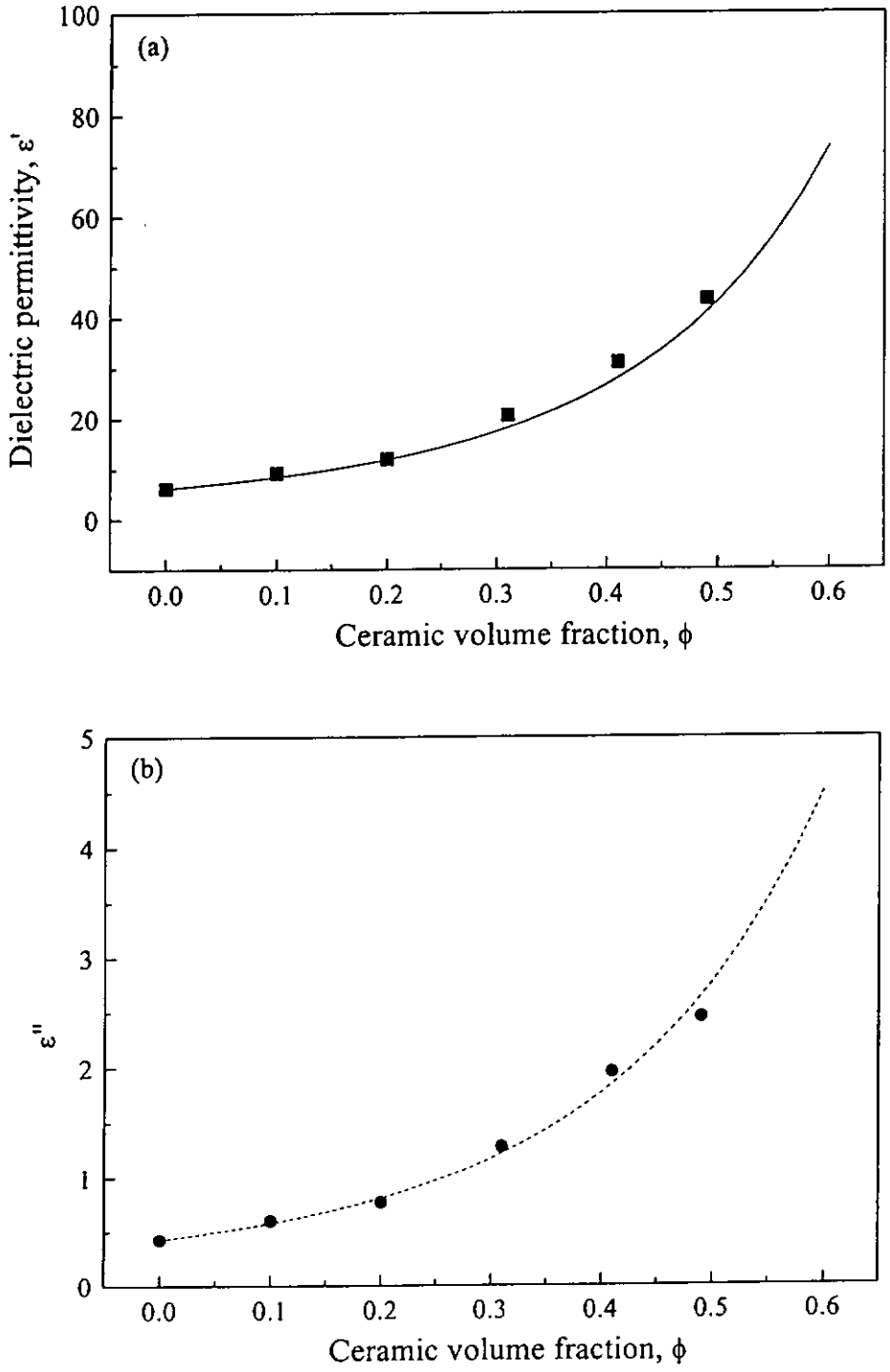


Fig. 5.10 Dielectric permittivity (a) ε' and (b) ε" of $BaTiO_3$/P(VDF-TrFE) as a function of ϕ at -30 °C upon heating. The symbols are the experimental values and the lines are model calculations using the Bruggeman equation (eqs. 5.2 and 5.3).

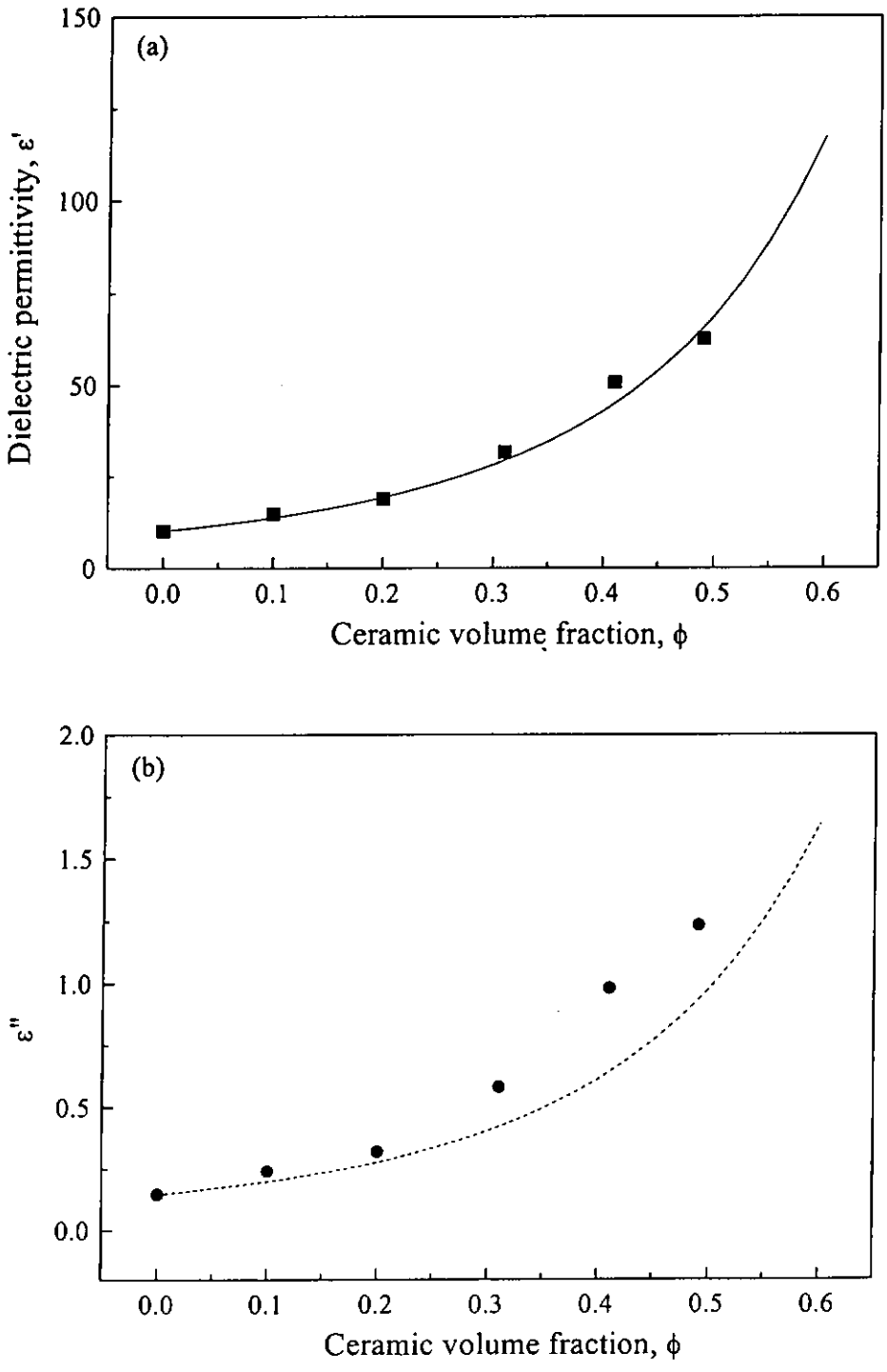


Fig. 5.11 Dielectric permittivity (a) ε' and (b) ε" of $BaTiO_3$/P(VDF-TrFE) as a function of ϕ at 30 °C upon heating. The symbols are the experimental values and the lines are model calculations using the Bruggeman equation (eqs. 5.2 and 5.3).

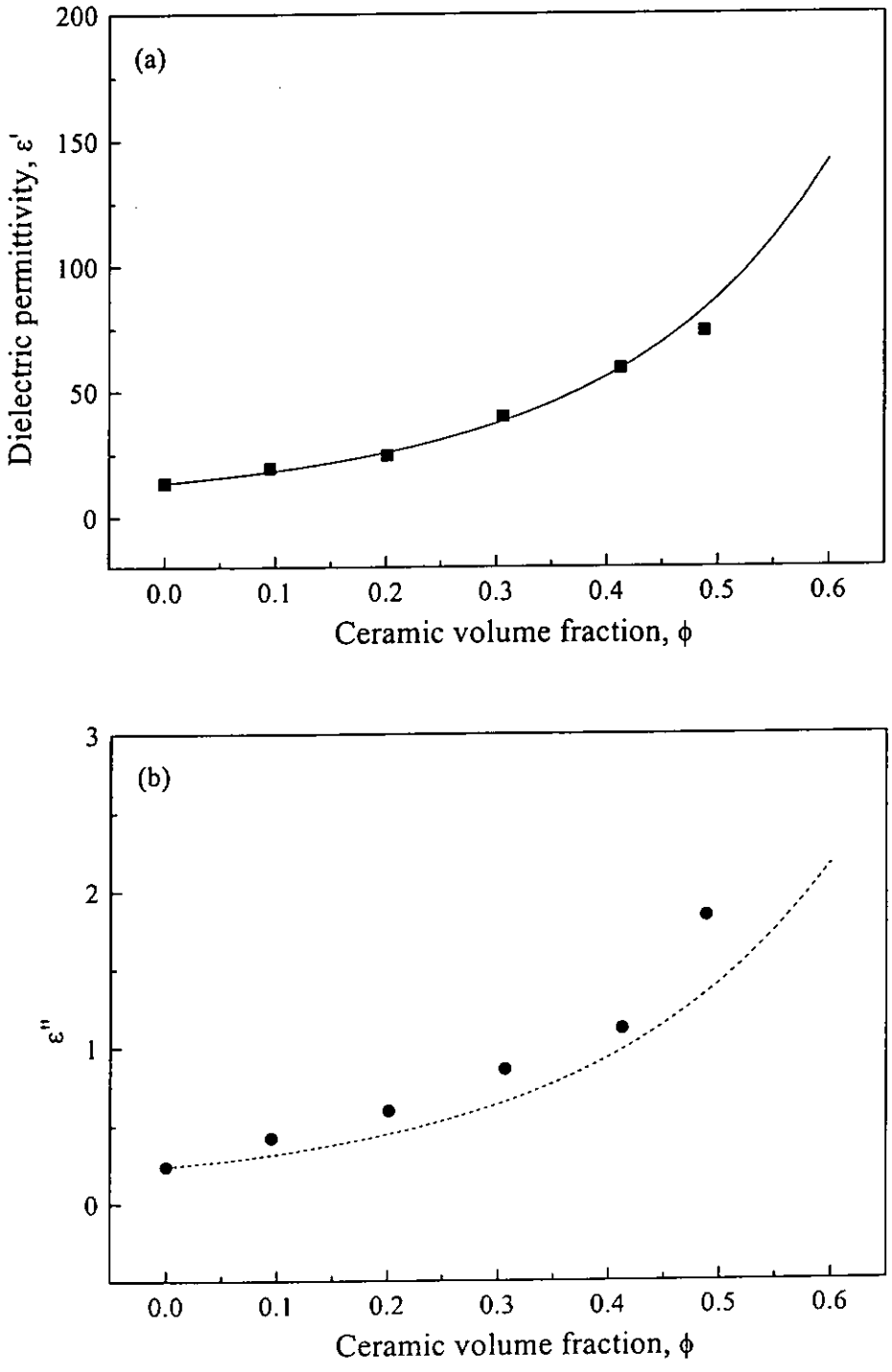


Fig. 5.12 Dielectric permittivity (a) ε' and (b) ε" of $BaTiO_3$/P(VDF-TrFE) as a function of ϕ at 60 °C upon heating. The symbols are the experimental values and the lines are model calculations using the Bruggeman equation (eqs. 5.2 and 5.3).

## 5.6 Piezoelectric and Pyroelectric Properties

### 5.6.1 Poling Process

"Poling" is a process of applying a high electric field across the thickness of the ferroelectric sample [16] to align the dipoles inside the composite [19-21,57]. After poling, the sample exhibits a net macroscopic polarization and has pyroelectric and/ or piezoelectric activities. Typically, a large degree of domain orientation in the sample would result in higher pyroelectric and piezoelectric activities.

In order to identify the pyroelectric and piezoelectric contributions from the two phases in the composites, two groups of composites were prepared. In Group 1 samples, only the ceramic phase was poled. In Group 2 samples, both of the ceramic and copolymer phases were poled in the same direction.

1. Group 1 samples (only the ceramic phase was poled)

To pole the ceramic phase only, the sample was heated to about 110 °C which was above the Cutie temperature $T_c\uparrow$ of copolymer and below the $T_c$ of $BaTiO_3$ ($T_c \sim 125$ °C) inside the oil bath. Then an electric field $E_0$ about 25 kV/mm was applied for 1 h. Finally, the field was switched off before cooling. Since, the copolymer phase was still in a paraelectric phase when the field was switched off, only the ceramic phase was poled.

2. Group 2 samples ( both ceramic and copolymer phases were poled in the same direction)

For poling both phases of the composites, the poling procedure is similar to that of poling the group 1 samples except that the electric field $E_0$ was kept on until the sample was cooled to a lower temperature, e.g. 40 °C or lower than $T_c\downarrow$ (~ 60 °C) of the copolymer phase. During the cooling process, the copolymer phase would be poled in the same direction as the ceramic phase. After poling, the samples were annealed in a short-circuited condition at 50 °C for 3 h. This can eliminate the contribution of thermally simulated current in subsequent measurements.

### 5.6.2 Electric Field Acting on the Ceramic Particle Inside the 0-3 Composites

If we assume that the composite samples contain spherical ceramic particle embedded in the copolymer matrix, the applied electric field $E_0$ acting on the ceramic particle can be estimated by [23]

$$E_c = \frac{3\varepsilon'}{2\varepsilon'+\varepsilon_c'} E_0 \tag{5.4}$$

$$L_E = \frac{E_c}{E_0} = \frac{3\varepsilon'}{2\varepsilon'+\varepsilon_c'} \tag{5.5}$$

where $E_c$, $\varepsilon'$ and $L_E$ are the electric field acting on the ceramic particle, the dielectric permittivity of the composite and the local field coefficient, respectively. The value $L_E$

for the composites were calculated using the values of $\varepsilon_c$' measured for the bulk ceramic prepared by the mixed oxide route and shown in Fig. 5.13. The close and open symbols represent data upon heating and cooling, respectively. It is seen that $L_E$ has a higher value upon cooling and the ceramic can experience higher fraction of the applied electric field and can be poled effectively. $L_E$ drops rapidly when the temperature approaches 120 °C, which is the Curie point of the ceramic. It is noted that this is only a rough estimate, the bulk ceramic $BaTiO_3$ (oxide) may not have properties identical to that of the $BaTiO_3$ powder.

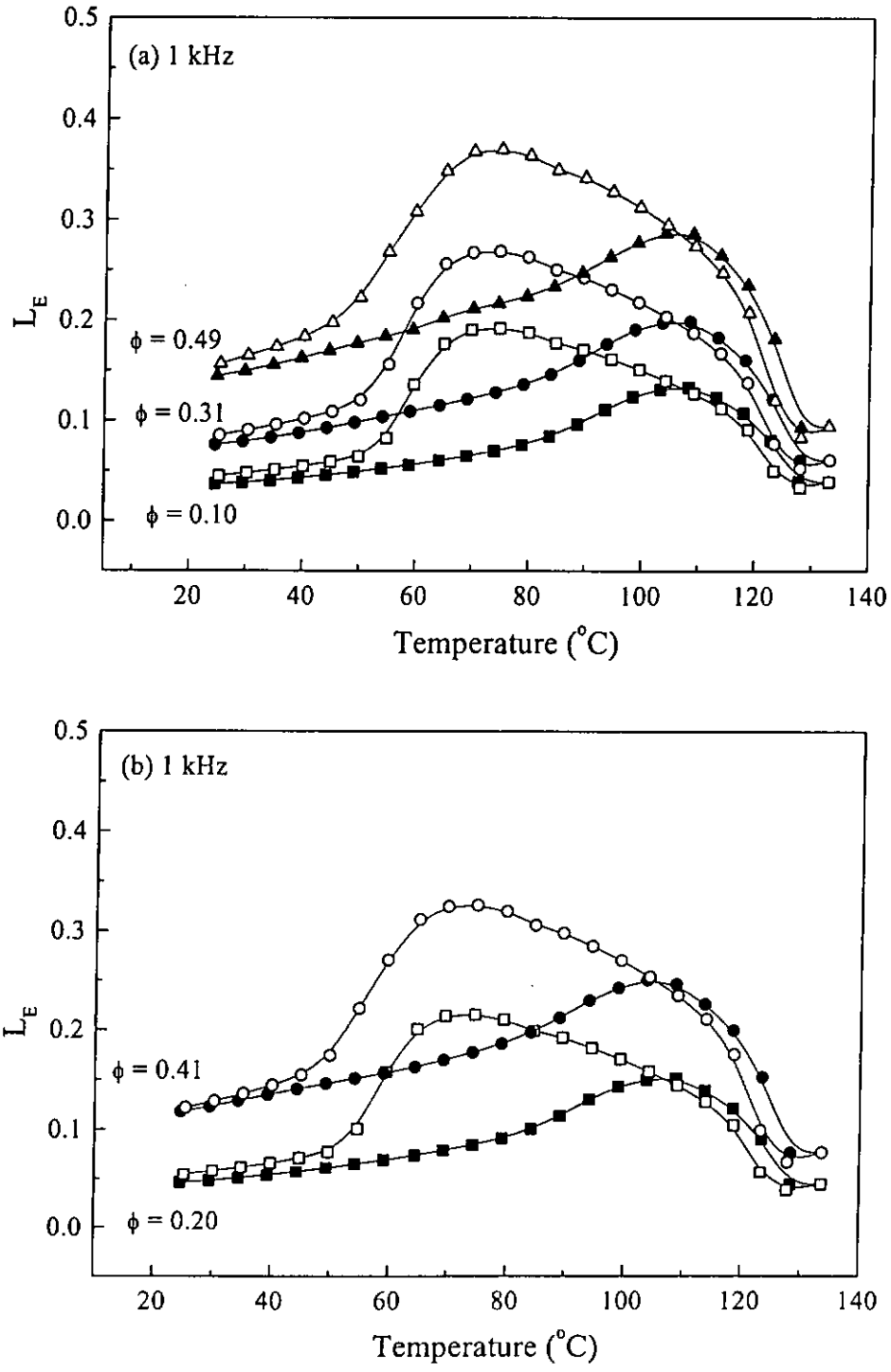


Fig. 5.13 Local field coefficient $L_E$ of various $\phi$ as a function of temperature. The solid and open symbols represent heating and cooling, respectively.

### 5.6.3 Pyroelectric and Piezoelectric Coefficients in Composites

Pyroelectric effect is the development of electric charges at the surface of a polar material when the temperature changes [58]. While piezoelectric effect is the creation of electric charges at the surface of a polar material by an applied stress [59]. In the present study, the pyroelectric p and piezoelectric $d_{33}$ coefficients of the 0-3 composites were measured and compared to the theoretical predications.

#### 5.6.3.1 Pyroelectric coefficients p

The pyroelectric coefficient p was measured using the digital integration method. Fig. 5.14 shows the results of the pyroelectric coefficient as a function of $\phi$. The pyroelectric coefficient p increases as the ceramic volume fraction increases. According to Yamazaki et al (1981) [23], the pyroelectric coefficient p can be expressed as:

$$p = \alpha_c L_E \phi \cdot p_c \tag{5.6}$$

$$p = \alpha_c L_E \phi \cdot p_c + \alpha_p (1-\phi) \cdot p_p \tag{5.7}$$

where $\alpha$, $L_E$ and $\phi$ represent the poling ratio, local field coefficient and the ceramic volume fraction, respectively. And the subscript c and p represent the ceramic phase and copolymer phase, respectively.

Equation (5.6) applied to the group 1 samples (only the ceramic phase poled). For Group 2 samples, the pyroelectric coefficient of the composites contained the contribution of the ceramic and the copolymer phases. So equation 5.7 should be used.

From Fig. 5.14, we can see that there is a reasonable agreement between the experimental results and the theoretical predication, assuming $\alpha_c p_c$ = 235 $\mu C/m^2K$, $\alpha_p p_p$ = 28 $\mu C/m^2K$. i.e. both phases are poled to an extend similar to the bulk materials.

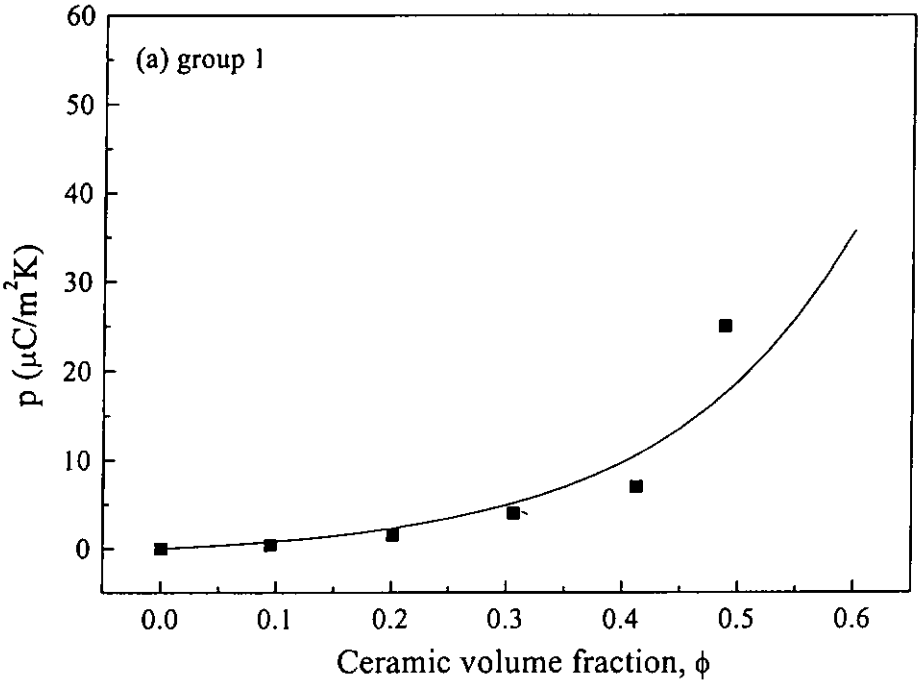


Fig. 5.14(a) Pyroelectric coefficient p of $BaTiO_3$/P(VDF-TrFE) as a function of $\phi$ for group 1 samples.

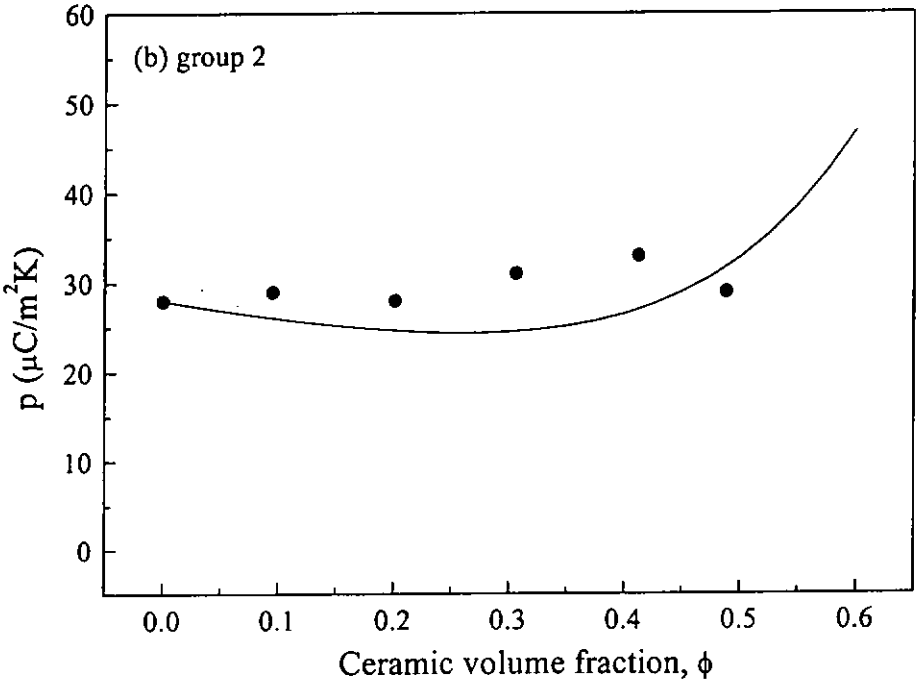


Fig. 5.14(b) Pyroelectric coefficient p of $BaTiO_3$/P(VDF-TrFE) as a function of $\phi$ for group 2 samples.

### 5.6.3.2 Piezoelectric coefficients $d_{33}$

From the direct piezoelectric effect, the piezoelectric coefficient is defined as,

$$d_{ij} = \frac{\text{dielectric displacement developed}}{\text{applied mechanical stress}},$$

the unit is C/N or from the converse piezoelectric effect,

$$d_{ij} = \frac{\text{strain developed}}{\text{applied field}},$$

the unit is m/V, where the subscript i represents the direction of dielectric displacement or electric field and j represents the direction of mechanical stress or strain. The

piezoelectric coefficient $d_{33}$ was measured directly by a Pennebaker model 8000 piezo tester (from American Piezo Ceramic, Inc), and the results are shown in Fig. 5.15.

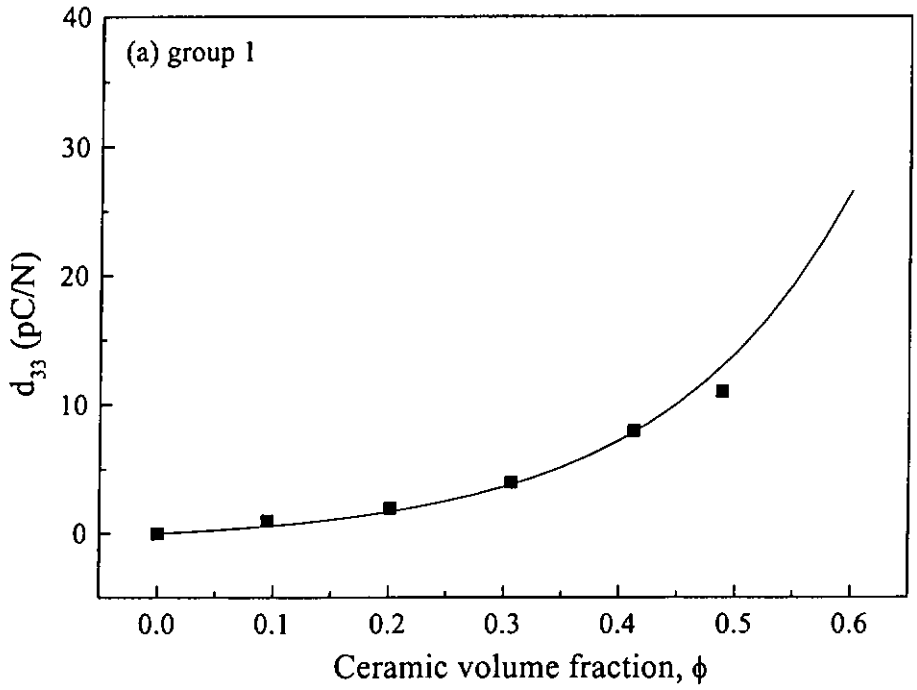


Fig. 5.15(a) Piezoelectric coefficient $d_{33}$ of $BaTiO_3$/P(VDF-TrFE) as a function of $\phi$ for group 1 samples.

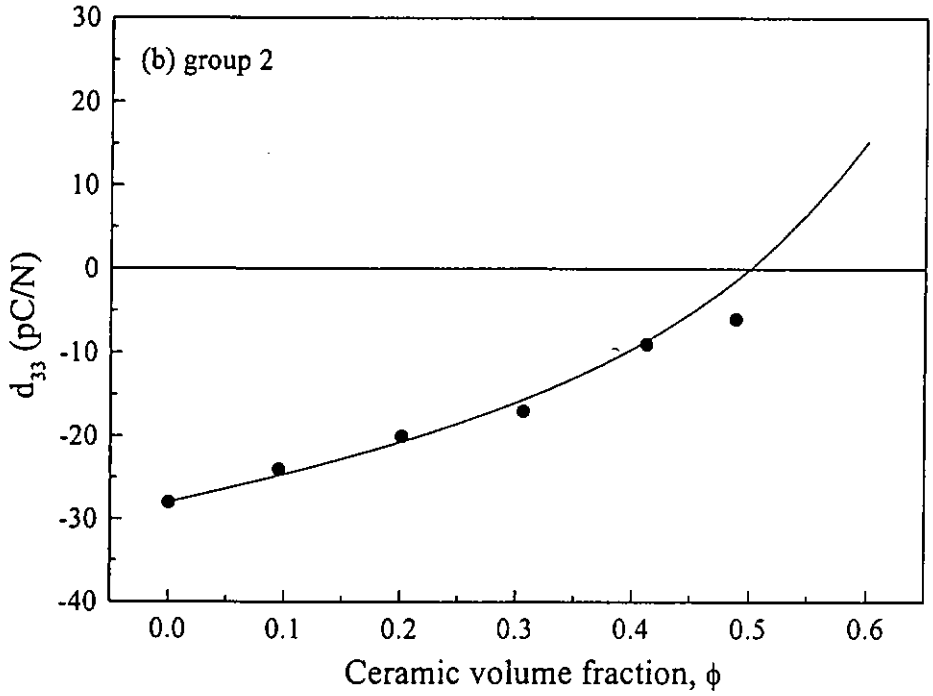


Fig. 5.15(b) Piezoelectric coefficient $d_{33}$ of $BaTiO_3$/P(VDF-TrFE) as a function of $\phi$ for group 2 samples.

Similar to the pyroelectric coefficient p, the piezoelectric coefficient $d_{33}$ can be modeled using the modified linear mixture rule (eqs. 5.8 and 5.9), the calculated values agree quite well with the experimental results.

$$d_{33} = \alpha_c L_E \phi \cdot d_{33c} \tag{5.8}$$

$$d_{33} = \alpha_c L_E \phi \cdot d_{33c} + \alpha_p (1-\phi) \cdot d_{33p} \tag{5.9}$$

In the calculation, $\alpha_c d_{33c}$ = 175 pC/N and $\alpha_p d_{33p}$ = -28 pC/N are used. The piezoelectric coefficient $d_{33}$ increases from negative to positive with increasing ceramic volume fraction $\phi$. At $\phi \sim 0.5$, the 0-3 composite would be pyroelectric but non-piezoelectric [25,26].

### 5.6.4 Polarization Distributions in 0-3 Composites

The laser induced pressure pulse (LIPP) method has been used to study the polarization distributions in the 0-3 composites. The schematic diagram for the LIPP measurement is shown in Fig. 5.16.

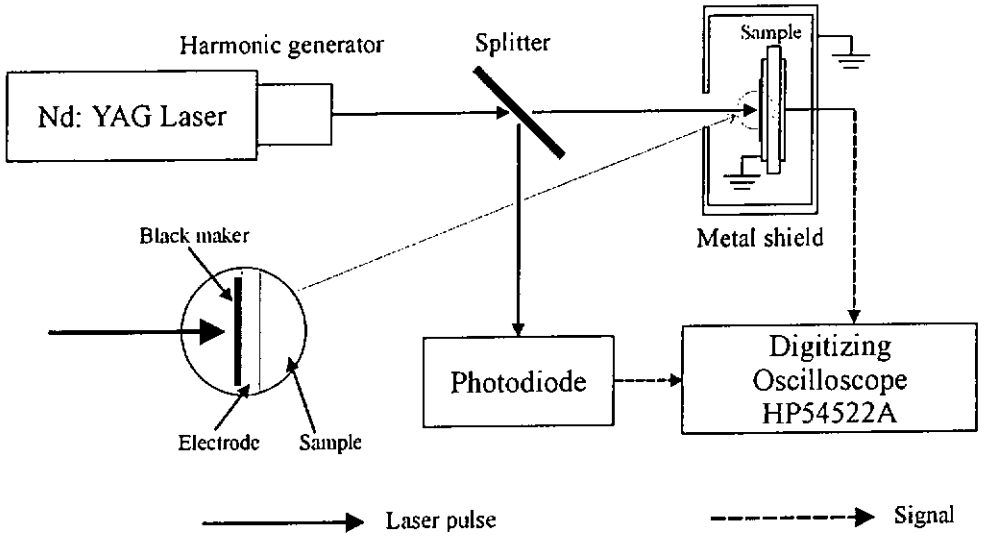


Fig. 5.16 The experimental set-up of the LIPP measurement.

The sample was enclosed in an electrically shielded sample holder. A Quantel Nd: YAG equipped with a second harmonic generator which emitted a single laser pulse of energy about 50 mJ and width 10 ns at a wavelength of 532 nm was used. The laser, with a beam diameter of 8 mm, impinged on the sample at the anode side (the side connected to positive voltage during poling). The laser was absorbed by a black marker on this surface. Due to ablation and localized heating, a pressure pulse was generated which traveled along the thickness direction (z-axis) of the sample with sound velocity.

Charges are induced in the compressed region on the electrodes. Under short-circuit conditions, the variation of the charges produced a current I(t) where the time t is related to the position of the wave front by:

$$t = \frac{\text{travelling distance along z-axis}}{\text{sound velocity}}$$

For short pressure pulses, the current I(t) measured during the penetration of the pulse into the sample or its exit is directly proportional to the piezoelectric coefficient $e_{33}$ at the interface [51]. Fig. 5.17 and Fig. 5.18 show the voltage (into a 50 Ω load) during the propagation of a pressure pulse in $BaTiO_3$, P(VDF-TrFE) copolymer and 0-3 composites of group 2 samples at the anode side. The pressure wave entered the sample at t = 0, and left the sample at t = T, marked by the arrow. Fig. 5.17 shows that the signs of the output voltages from the $BaTiO_3$ and P(VDF-TrFE) are opposite to each other. It implies that the piezoelectric coefficients of $BaTiO_3$ and P(VDF-TrFE) have opposite signs. The magnitude of the output voltage from $BaTiO_3$ was much higher than that from the copolymer. Fig. 5.18 shows the LIPP results of the 0-3 composites with various ceramic volume fraction $\phi$. From the graphs, the sign of the output voltage of the 0-3 composites were the same as the result from P(VDF-TrFE) and the magnitude of the output decreased with increasing $\phi$. This is due to the partial cancellation in the piezoelectric activities [27]. A similar trend was observed in the direct measurement of the piezoelectric coefficient $d_{33}$.

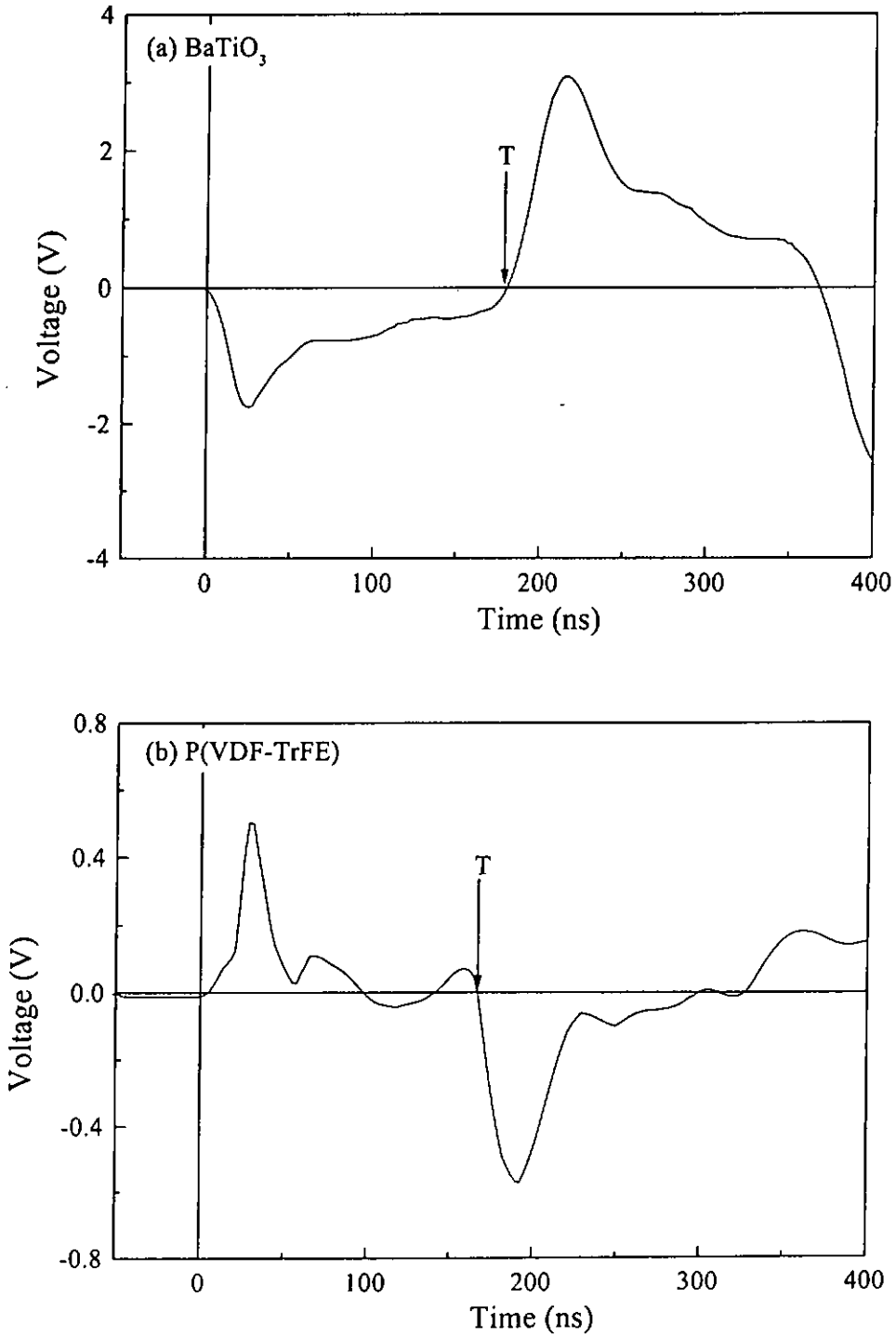


Fig. 5.17 LIPP results of (a) $BaTiO_3$ and (b) P(VDF-TrFE).

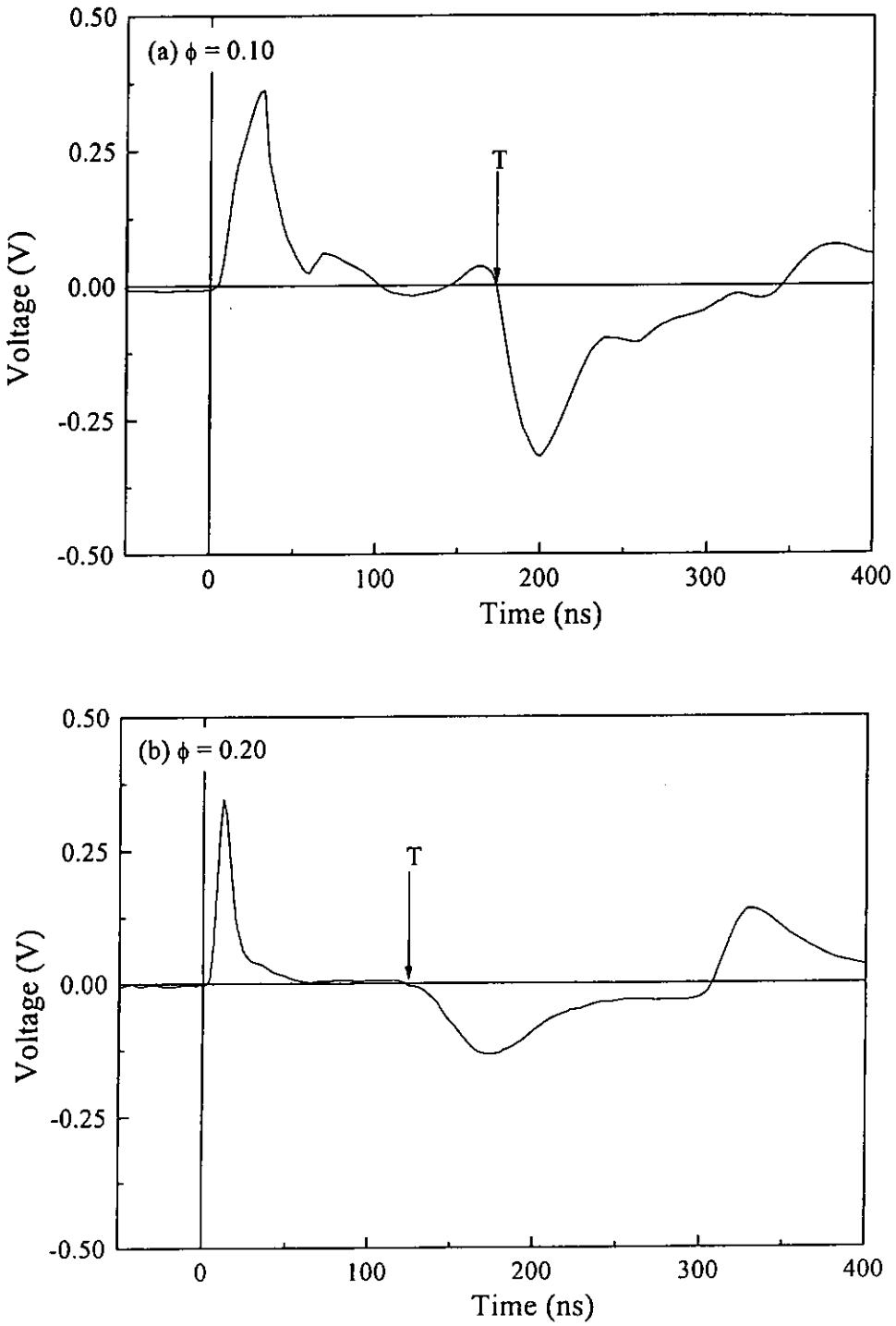


Fig. 5.18 LIPP results of $BaTiO_3$/P(VDF-TrFE) 0-3 composites with ϕ equal to (a) 0.10 and (b) 0.20.

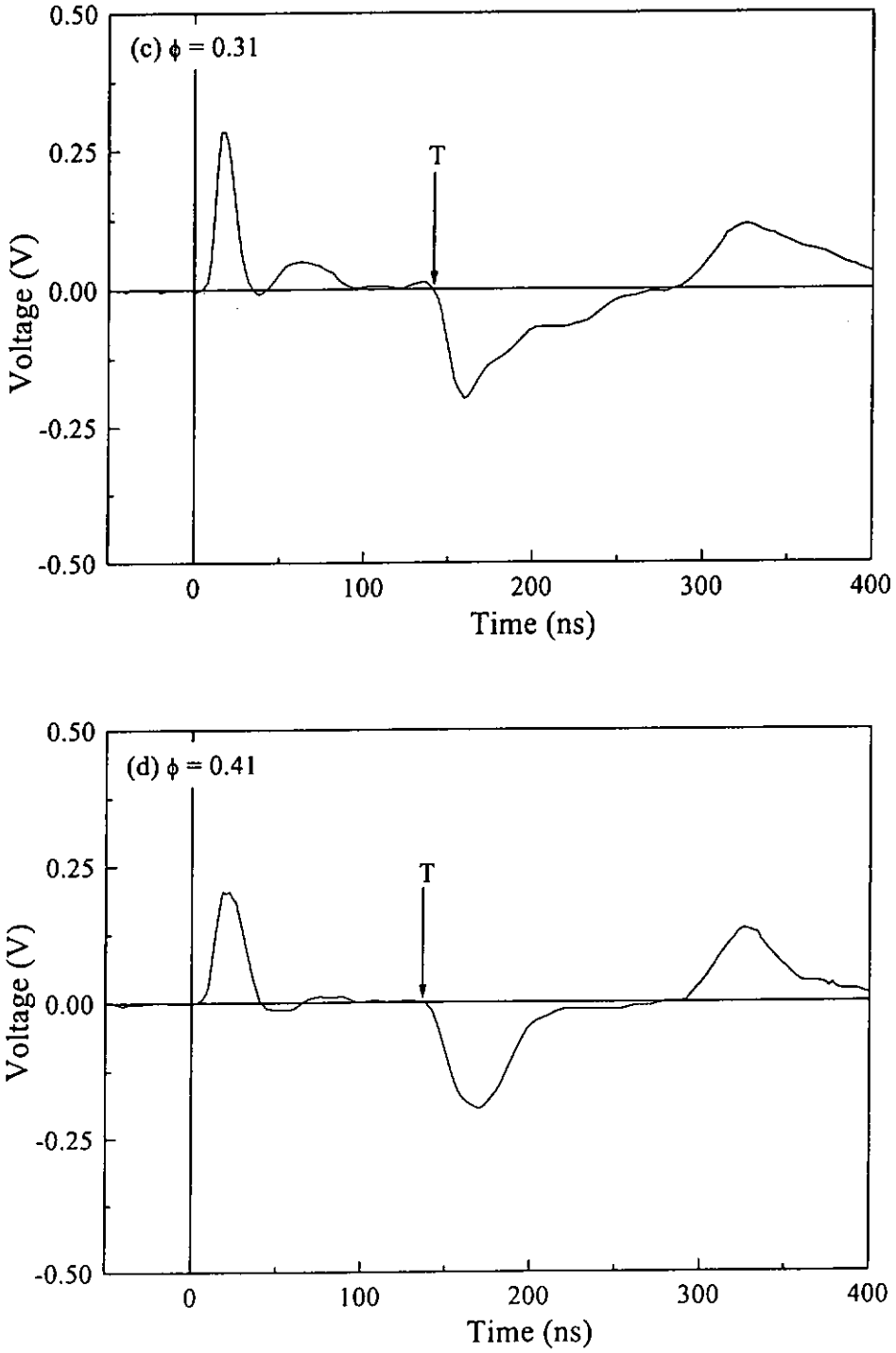


Fig. 5.18 LIPP results of $BaTiO_3$/P(VDF-TrFE) 0-3 composites with $\phi$ equal to (c) 0.31 and (d) 0.41.

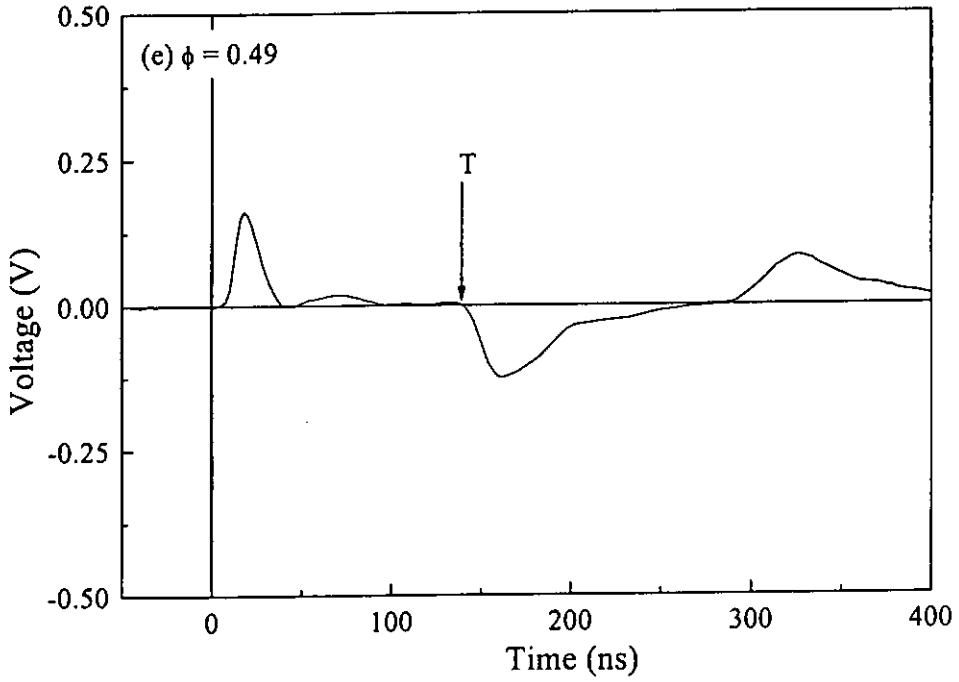


Fig. 5.18 LIPP results of $BaTiO_3$/P(VDF-TrFE) 0-3 composites with $\phi$ equal to (e) 0.49.

# CHAPTER SIX

# $BaTiO_3/BaTiO_3$ 0-3 COMPOSITES

## 6.1 Introduction

Barium titanate ceramic/ceramic 0-3 composite thick films (thickness ~16 μm) were prepared by a modified sol-gel process. Nano-sized $BaTiO_3$ powder (prepared by sol-gel method described in section 2.2.2) was dispersed in a sol-gel matrix of $BaTiO_3$ to form a composite solution. Films were prepared by spin coating and then annealed at various temperatures. The advantage of dispersing powder of the same kind of material in a sol-gel matrix is to increase the film thickness. It is difficult to prepare films with thickness up to several microns by the conventional sol-gel method. The modified sol-gel technique has been developed for preparing PZT films of thickness up to 60 μm [38]. Thick films up to several microns or more which have potential applications in pyroelectric infrared sensors and ultrasonic high frequency transducers are still in the research stage [33].

Crystallization of the powder and the composite films were studied by X-ray diffraction. The surface morphology of the composite films was investigated by SEM. The dielectric permittivity and the ferroelectric properties of the film were also measured.

## 6.2 Film Preparation

$BaTiO_3$ powder and films were prepared by a sol-gel method. The preparation of $BaTiO_3$ powder was described before. The procedure for preparing $BaTiO_3$ films by a sol-gel process was shown in Fig. 6.1. First, the $BaTiO_3$ complex solution was prepared by the procedure shown in Fig. 2.1. The complex solution was about 0.8 M. Quality of the film is affected by several parameters, namely, viscosity of the sol-gel, particle size of the powder, annealing temperature, etc. Viscosity of the solution should be high enough and the powder size should be small enough so that the powder could suspend in the solution during film coating. Glycerin was added to increase the solution viscosity and used to modify the drying sequence of the as deposited films. About 20 wt % of $BaTiO_3$ powder (annealed at 800 °C for 2 h, particle size ~100 nm) were added to a $BaTiO_3$ sol-gel solution. The composite solution was then placed in an ultrasonic bath for ultrasonic mixing to ensure that the powders were uniformly dispersed. Thick $BaTiO_3$ composite films (~ 16 μm) were fabricated by spin coating eight layers of the mixture on stainless steel substrates. Each layer, with a thickness of about 2 μm (measured by a Tencor 500 surface profiler), was fired at 500 °C. This annealing process was similar to that in a conventional sol-gel process. Finally, the eight-layer films were annealed at temperatures from 550 °C to 850 °C for 30 min. in order to crystallize the sol-gel matrix. The annealed film is a composite material consisted of a ceramic thin-film matrix with bulk ceramic powders dispersed throughout.

Gold electrodes ($1.96 \times 10^{-3}$ $cm^2$) were deposited through a mask on the top surfaces of the films. The dielectric permittivity was measured using an impedance analyzer (HP 4194A). The ferroelectric hysteresis loop was obtained using a ferroelectric test system (RT66A, Radiant Technologies) equipped with a high voltage interface.

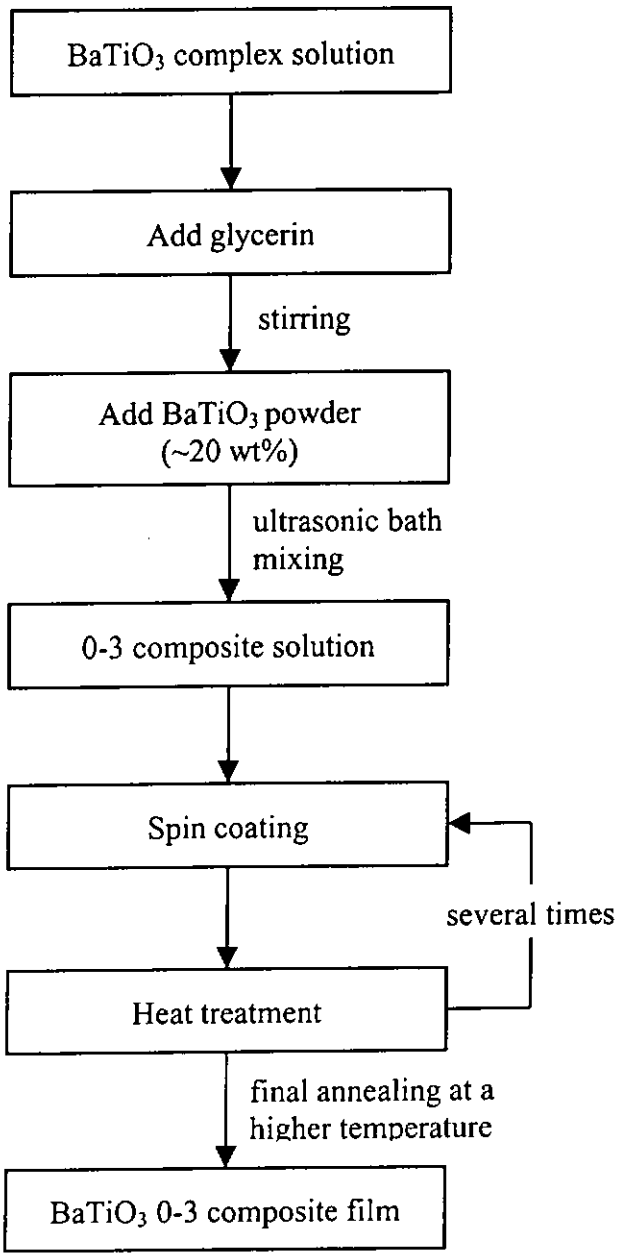


Fig. 6.1 Flowchart showing the procedure for preparing $BaTiO_3$ ceramic/ceramic 0-3 composite films by a modified sol-gel process.

## 6.3 Structure and Microstructure

Fig. 6.2 show the XRD patterns for $BaTiO_3$ powder annealed at different temperatures for 2 h. Powder annealed below 650 °C has an amorphous structure. When the annealing temperature is increased to 700 °C, crystalline peaks of $BaTiO_3$ appear. This is consistent with the thermal data which show a peak around 700 °C in the DTA curve (Fig. 6.3). In the TGA curve (Fig. 6.4), there is no weight loss at the same temperature. Fig. 6.5 gives the XRD patterns of $BaTiO_3$ 0-3 composite films annealed at different temperatures. The peaks at $2\theta = 44°$ and 50 ° are due to the stainless steel substrate. They overlap with the (002) (200) and (210) peaks of $BaTiO_3$. These peaks become more prominent when the films were annealed at a higher temperature (i.e. 700 °C or above).

The average crystallite size in the powder and the composite films was calculated using Scherrer's equation [39]

$$D = \frac{K\lambda}{B\cos\theta} \tag{6.1}$$

where D is the crystallite diameter, K is the Scherrer's constant (K = 0.89), $\lambda$ is the wavelength of the X-ray, B is the FWHM of a diffraction peak and $\theta$ is the Bragg angle. By comparing with the widths of diffraction peaks of a standard material, Si, the true width arising from the finite crystallite size in the powder and films were obtained. Table 6.1 and 6.2 show the crystallite size of the powder and the films as a function of annealing temperature.

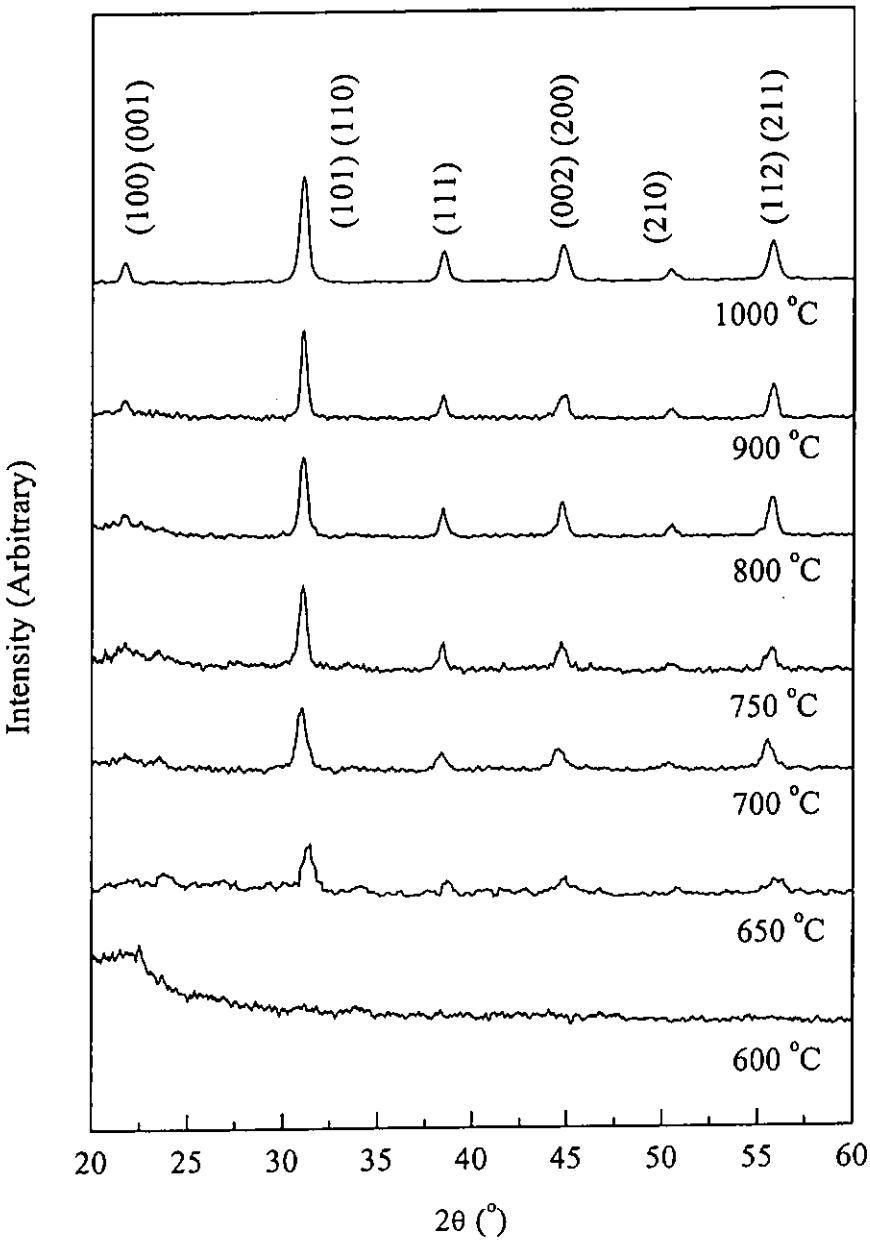


Fig. 6.2 XRD patterns for $BaTiO_3$ powder annealed at different temperature.

| Annealing temperature (°C) | 650 | 700 | 750 | 800 | 900 |
|---|---|---|---|---|---|
| Crystallite size (nm) | 28.44 | 30.18 | 44.76 | 46.40 | 61.11 |

Table 6.1 Variation of the average crystallite size of $BaTiO_3$ powder.

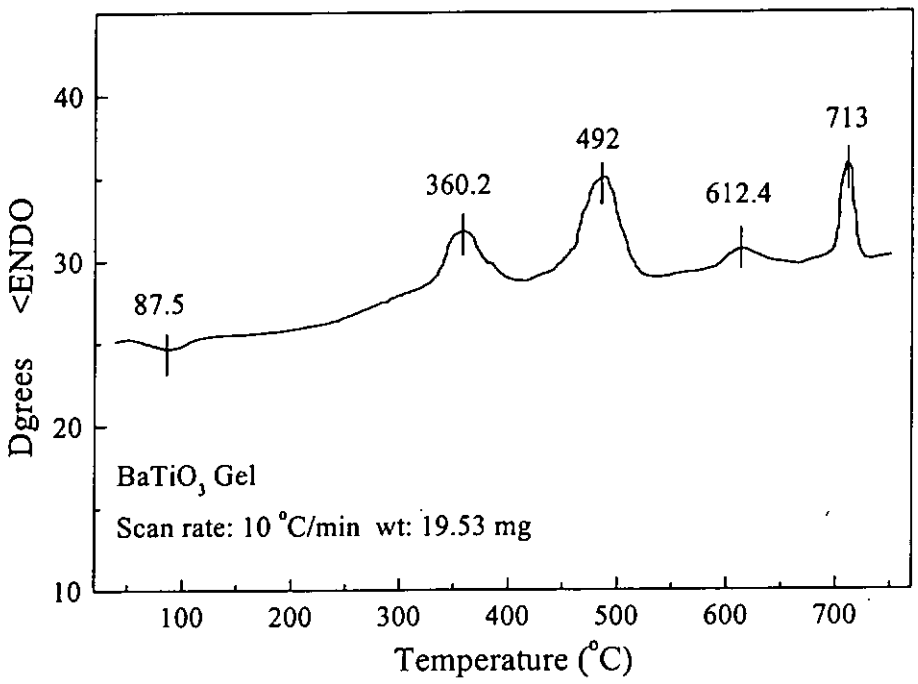


Fig. 6.3 DTA curve for $BaTiO_3$ powder.

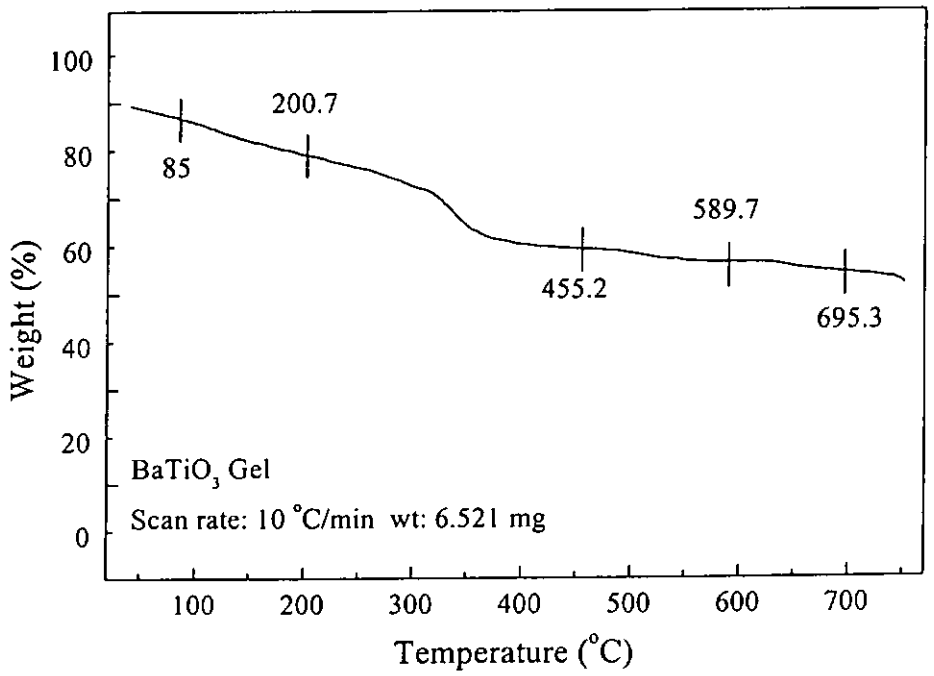


Fig. 6.4 TGA curve for $BaTiO_3$ powder.

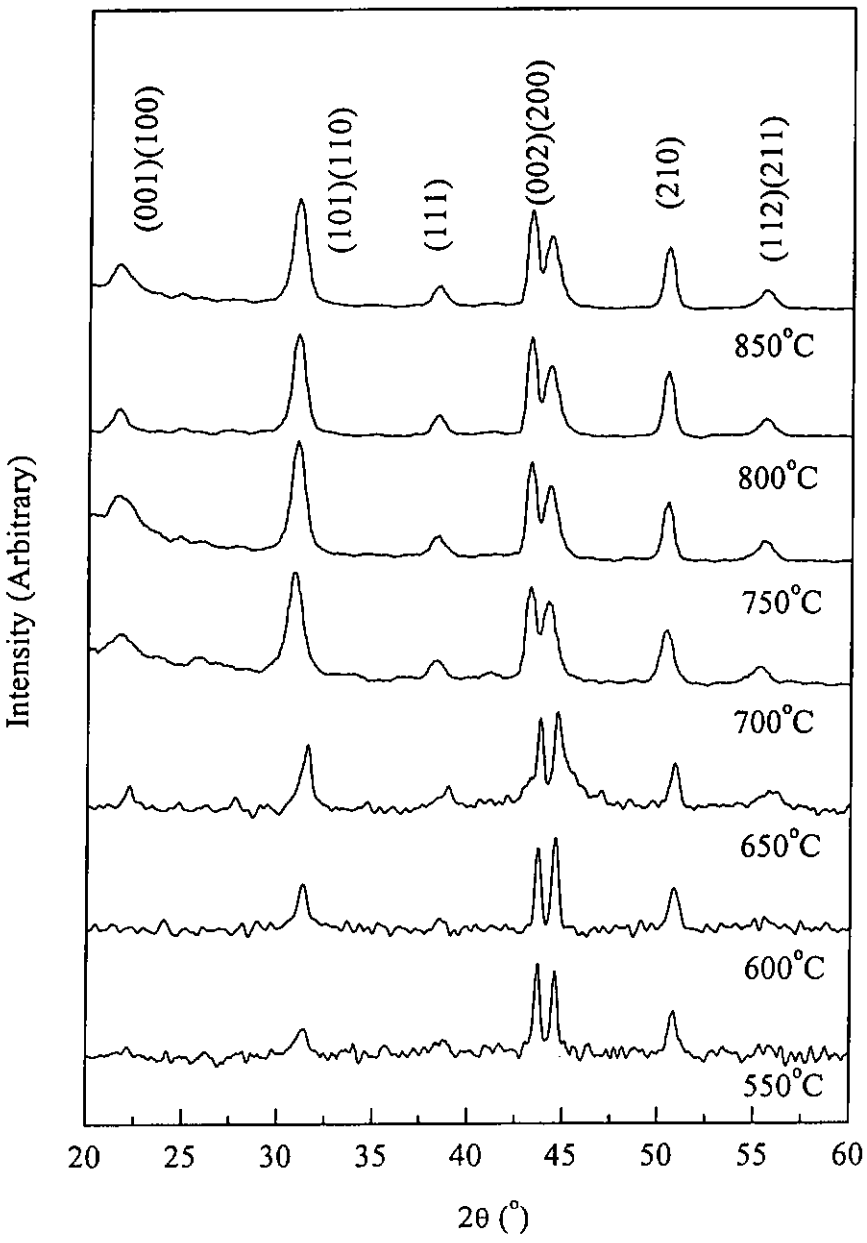


Fig. 6.5 XRD patterns for $BaTiO_3$ 0-3 composite film annealed at different temperatures.

| Annealing temperature (°C) | 700 | 750 | 800 | 850 |
|---|---|---|---|---|
| Crystallite size (nm) | 19.15 | 21.00 | 24.90 | 31.66 |

Table 6.2 Variation of the average crystallite size of $BaTiO_3$ 0-3 composite films.

Fig. 6.6 shows the surface morphology of the $BaTiO_3$ ceramic/ceramic 0-3 composite films heat treated at 550 °C and 850 °C. For the films annealed at 550 °C (Fig. 6.6(a)), it is seen that the ceramic powder dispersed uniformly in an amorphous matrix and has a 0-3 structure. After annealing at 850 °C (Fig. 6.6(b)), the matrix had also crystallized (granular grains with size ~ 40nm), so it was difficult to distinguish the powder from the crystalline grains in the matrix.

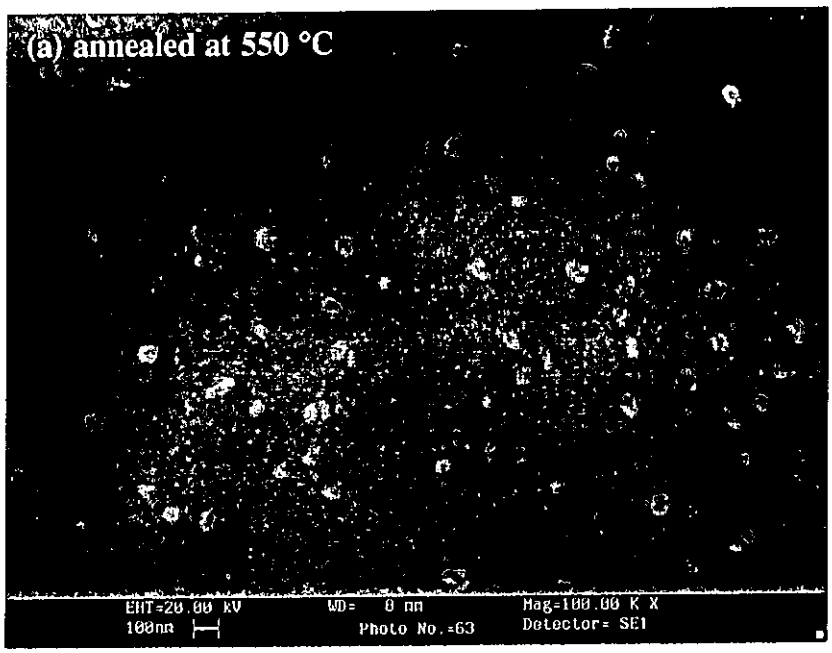


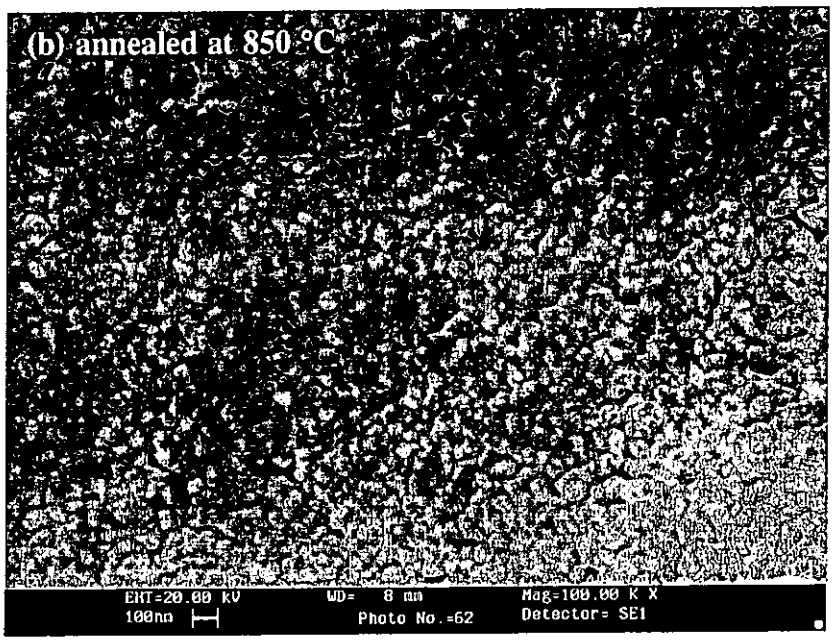


Fig. 6.6 Surface morphology of $BaTiO_3$ ceramic/ceramic 0-3 composite film heat-treated at (a) 550 °C and (b) 850 °C for 30 min.

## 6.4 Dielectric and Ferroelectric Properties

### 6.4.1 Dielectric Permittivity

Fig. 6.7 shows the frequency spectra of the dielectric permittivity ε' of $BaTiO_3$ thick (16 μm) films annealed at different temperatures. ε' of the films annealed at higher temperature decreases more significantly as frequency increases. The dielectric permittivity of the film annealed at 850 °C decreased from 401 to 349 as the frequency increased from 1 kHz to 10 MHz. The dielectric permittivity increased as the annealing temperature increased (see Fig. 6.8). This may due to the fact that higher annealing temperature leads to a larger grain size [60]. The value of the dielectric permittivity of the thick film is much smaller than the reported value ε' ~ 1700 for bulk $BaTiO_3$ [1,46]. The experimental result in section 3.3 gives ε' ~ 1905 for bulk $BaTiO_3$ (sol-gel) ceramic with grain size larger than 1 μm.

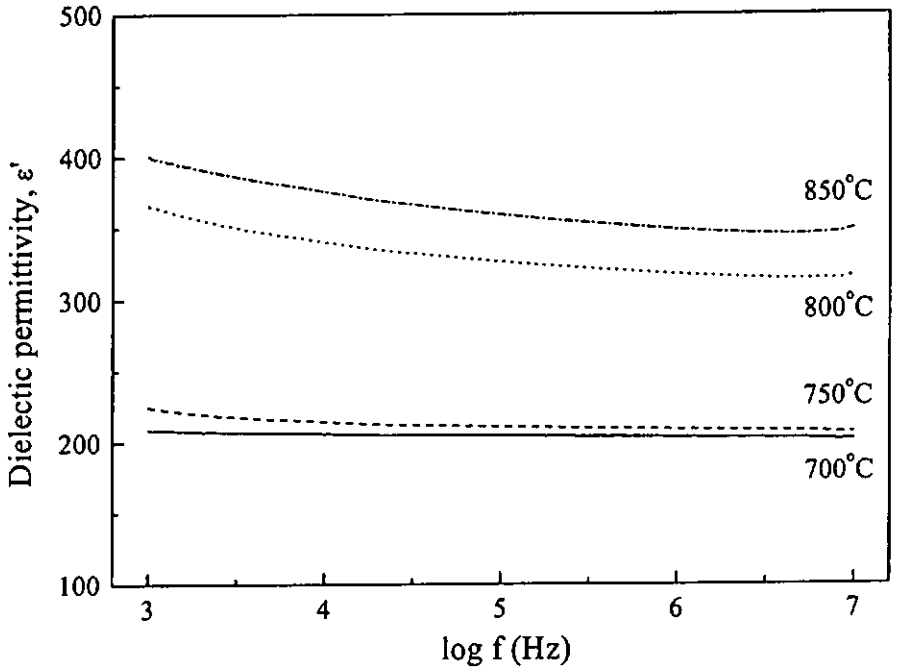


Fig. 6.7 Frequency dependence of dielectric permittivity ε' of $BaTiO_3$ composite films annealed at various temperatures.

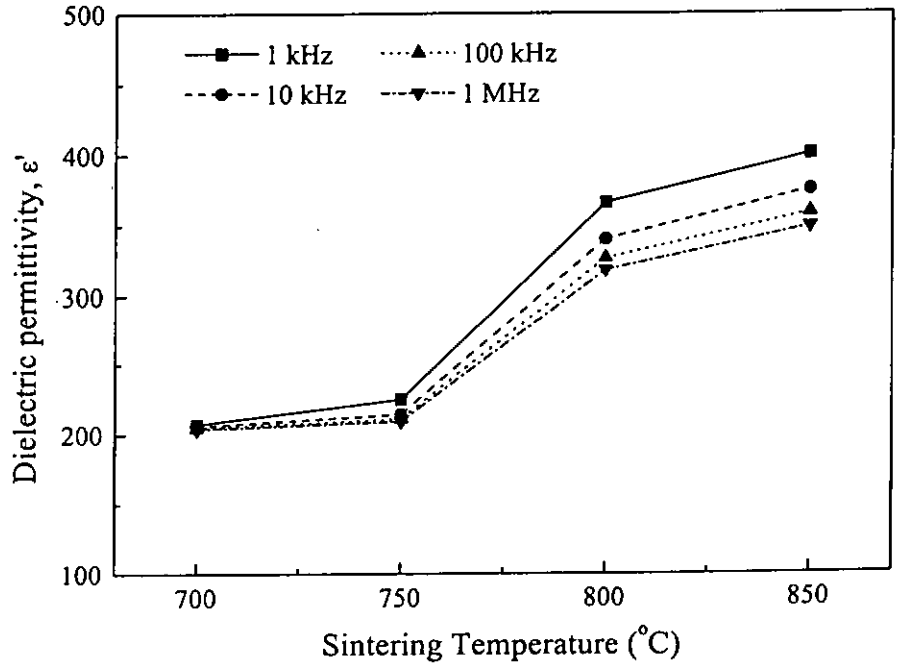


Fig. 6.8 Effect of annealing temperature on dielectric permittivity ε' of $BaTiO_3$ composite films measured at various frequencies.

### 6.4.2 Ferroelectric Hysteresis Loop

The ferroelectric hysteresis loop of the 0-3 composite films sintered at 700 °C to 850 °C was measured at room temperature (25 °C). The results are shown in Fig. 6.9. The value of spontaneous polarization $P_s$, remanent polarization $P_r$ and coercive field $E_c$ were shown in Table 6.3. The value of $P_s$ is smaller while that of $E_c$ is higher than those reported value for $BaTiO_3$ single crystal ($P_s$ = 26 μC/cm2, $E_c$ = 1.5 kV/cm) [1]. The experimental results in section 3.3.3 give $P_s$ = 16.8 μC/cm$^2$, $P_r$ = 6.5 μC/cm$^2$ and $E_c$ = 0.8 kV/mm for bulk $BaTiO_3$ (sol-gel) ceramic sintered at 1200 °C. The lower $P_s$ and the higher $E_c$ values for the films may arise from the smaller grain size and the clamping of the films to the substrate [61,62]. No ferroelectric hysteresis loops were observed when the films were annealed at 700 °C and 750 °C, probably because of the small crystallite size.

| Annealing temperature °C | $P_s$ μC/cm$^2$ | $P_r$ μC/cm$^2$ | $E_c$ kV/mm |
|---|---|---|---|
| 800 | 8.0 | 6.5 | 8.0 |
| 850 | 10.0 | 5.0 | 7.0 |

Table 6.3 Spontaneous polarization $P_s$, remanent polarization $P_r$ and coercive field $E_c$ of $BaTiO_3$ 0-3 composite films annealed at 800 °C and 850 °C.

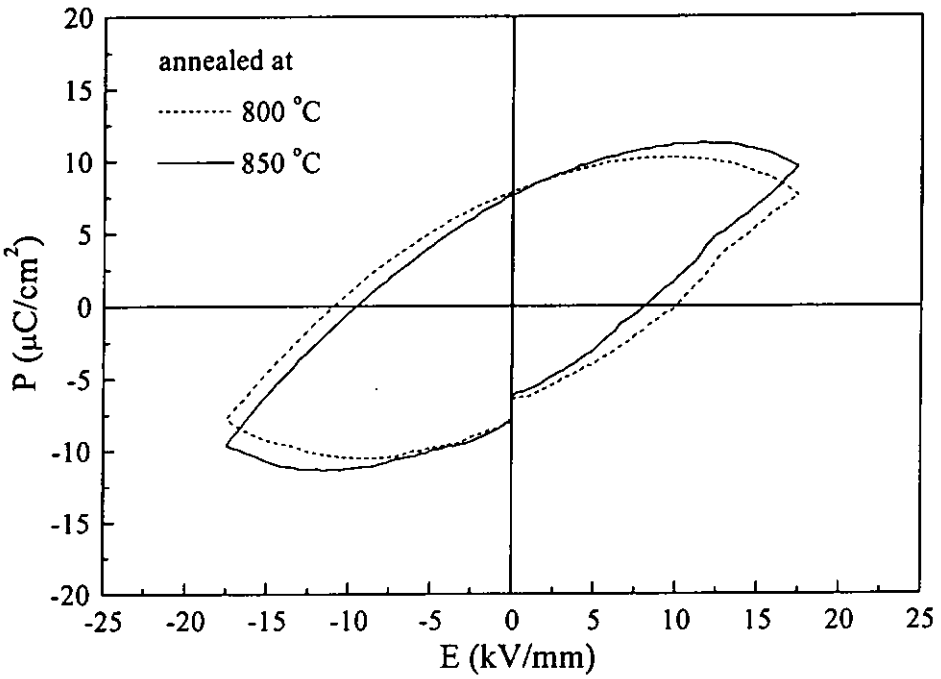


Fig. 6.9 Hysteresis loops measured at room temperature for $BaTiO_3$ 0-3 composite films annealed at 800 °C and 850 °C.

For the RT66A ferroelectric test system, a pulse response measurement is automatically performed after each hysteresis measurement. The pulse response is measured using triangular pulses in a five-pulse set with 1 sec delay between each pulse. A total of eight measurements are made over the last four pulses. The first pulse is used to reset the internal capacitor. The profile is list in Table 6.4.

| Pulse # | Voltage Applied | Parameter Measured |
|---|---|---|
| 1 | -Vmax | - |
| 1 | 0 | - |
| 2 | Vmax | P* |
| 2 | 0 | P*r |
| 3 | Vmax | P^ |
| 3 | 0 | P^r |
| 4 | -Vmax | -P* |
| 4 | 0 | -P*r |
| 5 | -Vmax | -P^ |
| 5 | 0 | -P^r |

Table 6.4 List of the pulse profile of the pulse measurement.

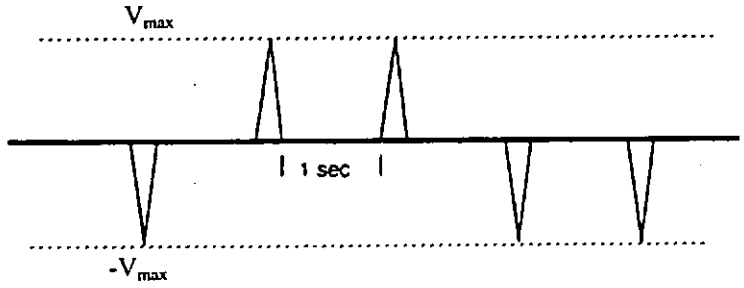


Fig. 6.10 The pulse profile of the pulse measurement.

| Annealing temperature (°C) | P* | P*r | P^ | P^r | Switchable polarization* |
|---|---|---|---|---|---|
| 800 | 14.22 | 13.36 | 11.53 | 10.66 | 2.7 |
| 850 | 15.75 | 15.52 | 11.35 | 10.22 | 4.9 |

*switchable polarization is equal to P* – P^ ( P*r – P^r)

Table 6.5 Result of pulse measurements.

where Pr(x) = remanent polarization state at zero volts after application of x colts.

Ps(x) = the polarization state at x volts

P* Ps (Vmax) - Pr(-Vmax) :

The polarization transferred out of the capacitor traversing from zero to Vmax volts when the capacitor starts at Pr(-Vmax).

P*r Pr(Vmax) – Pr(-Vmax) :

The polarization remaining out of the sample capacitor after returning to zero volts from Vmax, when the capacitor starts Pr(-Vmax).

P^ Ps(Vmax) – Pr(Vmax):

The polarization transferred out of the capacitor traversing from zero to Vmax volts when the capacitor starts at Pr(Vmax).

P^r Pr(Vmax) – Pr(Vmax):

The polarization remaining out of the sample capacitor starts at Pr(Vmax).

# Chapter Seven

# Conclusion

In the present study, barium titanate/poly(vinylidene fluoride trifluoroethylene) $BaTiO_3$/P(VDF-TrFE) 0-3 composite and barium titanate ceramic/ceramic 0-3 composites were fabricated.

$BaTiO_3$/P(VDF-TrFE) 0-3 composites with various ceramic volume fractions were fabricated by compression molding. The dielectric permittivities were measured as a function of temperature and thermal hysteresis was observed upon heating ($T_c\uparrow \sim 105$ °C) and cooling ($T_c\downarrow \sim 70$ °C). The Curie point upon heating and cooling are comparable to the phase transitions obtained by DSC. The dielectric permittivity as a function of ceramic volume fraction was compared to the Bruggeman model. The experimental results agreed quite well with the model predication for temperature up to 80 °C.

A poling treatment was used to induce the pyroelectric and piezoelectric properties. In order to investigate the contribution of each phase in the composite, two groups of composites are prepared. Group 1 samples have only the ceramic phase poled and group 2 samples have both the ceramic and copolymer phase poled in the same direction. The pyroelectric and piezoelectric coefficients of the composites of the two

group of samples are measured and compared with the Yamazaki equations. A good agreement was found between the experimental results and the calculated values. The equations are extended based on the additive property of the contributions from the two phases in the composite. The calculated values using this modified linear mixture equation are used to calculation p and $d_{33}$ of the composites and compared to the experimental results of group two samples and good agreement is also observed. Both the experimental results and the calculated values of the piezoelectric activities of the ceramic phase and the copolymer phase shows that they partially cancel each other. On the other hand, the pyroelectric coefficient of the two phases reinforces. Therefore, as a particular value of ceramic volume fraction $\phi$ ($\phi \sim 0.5$), the composite is pyroelectric but non-piezoelectric when the ceramic phase and copolymer phase are poled in the same direction. It is anticipated that at a certain value of $\phi$, the composite will be piezoelectric but non-pyroelectric when the two phases of composites are poled in opposite directions.

For the barium titanate ceramic/ceramic 0-3 composites, about 20 wt% of ceramic powder was dispersed into a $BaTiO_3$ sol-gel matrix to form a 0-3 complex solution. Films were prepared by spin coating multiple layers (total eight layers with thickness of about 16 μm) on stainless steel substrate. The films were annealed at 700 °C to 850 °C for 30 min. to crystallize the sol-gel matrix. The room temperature (25 °C) dielectric permittivity of the films (measured at 1 kHz) annealed at 700, 750, 800 and 850 °C were 207, 225, 367 and 401, respectively. $\varepsilon'$ for the films annealed at higher temperature exhibit stronger frequency dependence. The dielectric permittivity of the film annealed at 850 °C decreased from 401 to 349 as the frequency increased from

1 kHz to 10 MHz. The values of the spontaneous polarization, remanent polarization and the coercive field of the film annealed at 850 °C were 10 $\mu C/cm^2$, 5 $\mu C/cm^2$ and 7 kV/mm, respectively.

The $BaTiO_3$-based composites will be used in various sensor and transducer applications and the present work provides useful information for the fabrication and properties of these composites.

# REFERENCES


1. Jaffe, B., Cook, W.R. and Jaffe, H. "Barium titanate". Roberts, J.P. and Popper, P., eds., *Piezoelectric Ceramics*, Academic Press Inc. (London) Ltd., London, pp.53-114 (1971)
2. Xu, Y. "Perovskite-type ferroelectric: part I". *Ferroelectric Materials and Their Applications*, Elsevier Science Publishers B.V., Amsterdam, pp.101-159 (1991)
3. Arlt, G., Hennings, D. and de With, G. "Dielectric properties of fine-grained barium titanate ceramic". *Journal of Applied Physics*, Vol. 58, pp.1619-1625 (1985)
4. McNeal, M.P., Jang, S.J. and Newnham, R.E. "The effect of grain and particle size on the microwave properties of barium titanate ($BaTiO_3$)". *Journal of Applied Physics*, Vol. 83, pp.3288-3297 (1998)
5. Bell, A.J. " Grain size effect in barium titanate-revisited". In Pandey, R.K., Liu, M. and Safari, A. eds., Proceeding of the Ninth IEEE international Symposium, 7-10 August 1994, pp.14-17 (1994)
6. Shaikh, A.S. Vest, R.W. and Vest, G.M. "Dielectric properties of ultrafine grained $BaTiO_3$". *IEEE Transactions on Ultrasonic, Ferroelectrics, and Frequency Control*, Vol.36, pp.407-412 (1989)
7. Kawai, H. "The piezoelectricity of poly(vinylidene fluoride)". *Japanese Journal of Applied Physics*, Vol. 8, pp.975-976 (1969)

8. Koga, K.K. and Ohigashi, H. "Piezoelectricity and related properties of vinylidene fluoride and trifluoroethylene copolymers". *Journal of Applied Physics*, Vol. 59, pp.2142-2150 (1986)

9. Furukawa, T. "Ferroelectric properties of vinylidene fluoride copolymers". *Phase Transitions*, Vol. 18, pp.143-211 (1989)

10. Furukawa, T. "Structure and properties of ferroelectric polymer". Das-Gupta, D.K., eds., *Ferroelectric Polymers and Ceramic-Polymer Composites*, Trans Tech Publications, Switzerland, pp.15-30 (1994)

11. Yamazaki, H., Ohwaki, J., Yamada, T. and Kitayama, T. "Temperature dependence of the pyroelectric response of vinylidene fluoride-trifluoroethylene copolymer and the effect of its poling conditions". *Applied Physics letters*, Vol. 39, pp.772-773 (1981)

12. Neummann, N., Köhler, R. and Hofmann, G. "Application of P(VDF/TrFE) thin films in pyroelectric detectors", *Ferroelectrics*, Vol. 118, pp.319-324 (1991)

13. Tajitus, Y., Ogura, H., Chiba, A. and Furukawa, T. "Investigation of switching characteristics of vinylindene fluoride/trifluoroethylene copolymer in relation to their structures". *Japanese Journal of Applied Physics*, Vol. 26. pp.554-560 (1987)

14. Newnham, R.E., Skinner, D.P. and Cross, L.E. "Connectivity patterns for piezoelectric composites". *Materials Research Bulletin*, Vol. 13, pp.525-536 (1978)

15. Furukawa, T., Ishida, K. and Fukada, E. "Piezoelectric properties in the composite system of polymers and PZT ceramic". *Journal of Applied Physics*, Vol. 50, pp.4904-4912 (1979)

16. Dias, C.J. and Das-Gupta, D.K. "Inorganic ceramic/polymer ferroelectric composite electrets". *IEEE Transactions on Dielectrics and Electrical Insulation*, Vol.3, pp.706-734 (1996)

17. Lovinger, A.J. "Ferroelectric polymers". *Science*, Vol.220, pp.1115-1121 (1983)

18. Takeuchi, H., Jyomura, S. and Nakaya, C. "New piezoelectric materials for ultrasonic transducers". *Japanese Journal of Applied Physics*, Vol. 24(Suppl. 2), pp.36-40 (1985)

19. Dias, C.J. and Das-Gupta, D.K. "Piezo- and pyroelectricity in ferroelectric cermiac-polymer composites". Das-Gupta, D.K., eds., *Ferroelectric Polymers and Ceramic-Polymer Composites*, Trans Tech Publications, Switzerland, pp.217-248 (1994)

20. Dias, C.J. and Das-Gupta, D.K. "Poling behavior of ceramic/polymer ferroelectric composites". *Ferroelectrics*, Vol. 157, pp.405-410 (1994)

21. Chan, H.L.W., Chen Y. and Choy C.L. "A poling study of PZT/P(VDF-TrFE) 0-3 composites". *Integrated Ferroelectrics*, Vol. 9, pp.207-14 (1995)

22. Landau L.D. and Lifshitz E.M. "Course of theatrical physics". *Electrodynamics of Continuous Media*, Pergamen Press, Oxford, pp.36-91 (1960)

23. Yamazaki, H. and Kitayama, T. "Pyroelectric properties of polymer-ferroelectric composites". *Ferroelectrics*, Vol. 33, pp.147-153 (1981)

24. Sessler, G.M. "Poling and properties of polarization of ferroelectric copolymers and composites". Das-Gupta, D.K., eds., *Ferroelectric Polymers and Ceramic-Polymer Composites*", Trans Tech Publications, Switzerland, pp.249-274 (1994)

25. Chen, Y. "Studies on Lead zirconate titanate (PZT)/Polyvinylidene fluoride and trifluoroethylene ($VF_2/VF_3$) copolymer 0-3 composites". *MPhil Thesis*, PolyU (1995)

26. Chan, E.W.K. "Lead titanate ($PbTiO_3$)/piezoelectric copolymer P(VDF-TrFE) 0-3 composites". *MPhil Thesis*, PolyU (1997)

27. Chan, H.L.W., Ng, P.K.L. and Choy, C.L. "Effect of poling procedure on the properties of lead zirconate titanate/vinylidene fluoeide-trifluoroethylene composites". *Applied Physics Letters*, Vol.74, pp.3029-3031 (1999)

28. Muralidhar, C. and Pillai, P.K.C. "Dielectric behavior of barium titanate-polyvinylidene fluoride composites". *Journal of Materials Science*, Vol.23, pp.1071-1076 (1988)

29. Muralidhar, C. and Pillai, P.K.C. "Pyroelectric behavior in barium titanate/ polyvinylidene fluoride composites". IEEE Transactions on Electrical Insulation, Vol. EI-21, pp.501-504 (1986)

30. Takeuchi, M., Miyamoto, Y. and Nagasaka, H. "Effective dielectric constant of $BaTiO_3$-PVDF systems". *Japanese Journal of Applied Physics*, Vol.24, pp451-453 (1985)

31. Jones, R.E., Mainar, P.D., Olowolafe, J.O., Campbell, J.O. and Mogab, C.J. "Electrical characteristics of paraelectric lead lanthanum zirconium titanate thin films for dynamic random access memory applications". *Applied Physics Letters*, Vol. 60, pp.1022-1024 (1992)

32. Hu, H. and Krupanidhi, S.B. "Enhanced electrical properties of ferroelectric $Pb(Zr_{0.5},Ti_{0.5})O_3$ thin films grown with low energy oxygen ion assistance.". *Journal of Applied Physics*, Vol.74, pp.3373-3382 (1993)

33. Tu, Y.L. and Milne, S. J. "Processing and characterization of $Pb(Zr,Ti)O_3$ films, up to 10 μm thick, produced from a diol sol-gel route". *Journal of Materials Research*, Vol. 11, pp.2556-2564 (1996)

34. Kushida, K. and Takeuchi, H. "Piezoelectricity of c-Axis oriented $PbTiO_3$ thin films". *Applied Physics Letters*, Vol. 50, pp.1800-1801 (1987)

35. Ramesh, R., Sands, T., Keramidas, V.G. and Fork, D.K. "Epitaxial ferroelectric thin films for memory applications". *Materials Science Engineering B*, Vol. B22, pp.283-289 (1994)

36. Mohallem, N.D. S. and Aegerter, M. A. "Sol-gel processed $BaTiO_3$". *Materials Research Society Symposium Proceedings*, Vol. 121, pp.515-518 (1988)

37. Zhou, Q.F., Chan, H.L.W. and Choy, C.L. "Nanocrystalline powder and fibres of lead zirconate titanate prepared by the sol gel process". *Journal of Materials Processing Technology*, Vol. 63, pp.281-285 (1997)

38. Barrow, D.A., Petroff, T.E., Tandon, R.P. and Sayer, M. "Characterization of thick lead zirconate titanate films fabricated using a new sol gel based process". *Journal of Applied Physics*, Vol. 81, pp.876-881 (1997)

39. Birks, L.S. and Friedman, H. "Particle size determination from X-ray line Broadening". *Journal of Applied Physics*, Vol. 17, pp.687-692 (1946)

40. Aegerter M.A., Charbouillot, Y., Mohallem, N. and De Godoy, L.H. "Synthesis, characterization, and applications of lead and barium titanate materials prepared by the sol-gel method". Uhlmann, D.R. Ulrich, D.R., eds., *Ultrastructure Processing of Advanced Materials*, A Wiley-Interscience Publication, New York, pp.613-627 (1992)

41. Fang, T.T., Lin, H.B. and Hwang, J.B. "Thermal analysis of precursors of barium titanate prepared by coprecipitation". *Journal of the American Ceramic Society*, Vol.73, pp.3363-3367 (1990)

42. Jaffe, B., Cook, W.R. and Jaffe, H. "Measurement techniques". Roberts, J.P. and Popper, P., eds., *Piezoelectric Ceramics*, Academic Press Inc. (London) Ltd., London, pp.23-47 (1971)

43. Xu, Y. "Methods for measuring the physical properties of ferroelectric materials". *Ferroelectric Materials and Their Applications*, Elsevier Science Publishers B.V., Amsterdam, pp.37-100 (1991)

44. Haertling, G.H. "Piezoelectric and electrooptic ceramics". Buchanan, R.C., eds., *Ceramic Materials for Electronics*, Marcel DekkerInc., New York, pp.129-206 (1991)

45. Beauger, A., Mutin, J.C. and Niepce, J.C. "Synthesis reaction of barium titanate $BaTiO_3$ ---Part 2, Study of solid-solid interfaces". *Journal of Materials Science*, Vol.25, pp.1169-1183 (1990)

46. Haertling, G.H. "Ferroelectric ceramics: history and technology". *Journal of the American Ceramic Society*, Vol.82, pp.797-818 (1999)

47. Furukawa, T. and Johnson, G.E. "Dielectric relaxations in a copolymer of vinylidene fluoride and trifluoroethylene". *Journal of Applied Physics*, Vol. 52, pp.940-943 (1981)

48. Furukawa, T., Chuchi. M., Chiba A. and Date M. "Dielectric Relaxations and Molecular Motions in Homopolymers and Copolymers of Vinylidene Fluoride and Trifluoroethylene". *Macromolecules*, Vol. 17, pp.1384-1390 (1984)

49. Chan, H.L.W., Zhao, Z., Kwok, K.W., Choy, C.L., Alquié, C., Boué, C. and Lewiner, J. "Polarization of thick polyvinylidene fluoride/trifluoroethylene copolymer films". *Journal of Applied Physics*, Vol.80, pp.3982-3991 (1996)

50. Gerhard-Multhaupt, R., Sessler, G.M. and West, J.E. "Investigation of piezoelectricity distributions in poly(vinylidene fluoride) by means of quartz of laser- generated pressure pulses". *Journal of Applied Physics*, Vol. 55, pp.2769-2775 (1984)

51. Sessler, G.M., West, J.E., Gerhard-Multhaupt, R. and von Seggern, H. "Nondestructive laser method for measuring charge profiles in irradiated polymer films". IEEE Transactions on Nuclear Science, Vol. NS29, pp.1644-1649 (1982)

52. Chan, H.L.W., Zhao, Z. and Choy, C.L. "Effect of wavelength on pressure wave progration measurements of thick VF2/VF3 copolymer films". *Ferroelectrics*, Vol. 186, pp.247-250 (1996)

53. van Beek, L.K.H. "Dielectric behavior of heterogeneous systems". *Progress in Dielectrics Vol. 7*, Heywood, London, pp.69-114 (1967)

54. Bruggeman, D.A.G. "Berechnung verschiedener physikalischer konstanten von heterogenen substanzen". *Annalen der Physik.*, Vol. 24, pp.636-679 (1935)

55. Chan, H.L.W., Chan, W.K., Zhang, Y. and Choy, C.L. "Pyroelectric and piezoelectric properties of lead titanate/polyvinylidene fluoride-trifluoroethylene 0-3 composites". *IEEE Transaction on Dielectrics and Electrical Insulation*, Vol. 5, pp.501-512 (1998)

56. Chan, H.L.W., Ng, P.K.L. and Choy, C.L. "Permittivity and electrical conductivity of PZT/P(VDF-TrFE) 0-3 composites". *Ferroelectrics*, Vol. 201, pp.225-234 (1997)

57. Lee, M.H., Halliyal, A. and Newnham, R.E. "Poling of coprecipitated lead-titanate-epoxy 0-3 piezoelectric composites". *Journal of American Ceramic Society*, Vol. 72, pp.986-990 (1989)

58. *IEEE Standard Definitions of Primary Ferroelectric Terms*, ANSI/IEEE Std 180, Institute of Electrical and Electronics Engineers, New York, (1986)

59. Jaffe, B., Cook, W.R. and Jaffe, H. "The piezoelectric effect in ceramic". Roberts, J.P. and Popper, P., eds., *Piezoelectric Ceramics*, Academic Press Inc. (London) Ltd., London, pp.7-22 (1971)

60. Wada, S., Suzuki, T. and Noma, T. "Preparation of barium titanate ceramics from amorphous fine particles of the Ba-Ti-O system and its dielectric properties". *Journal of Materials Research*, Vol. 10,pp.306-311 (1995)

61. Sharma, H.B. and Mansingh, A. "Sol-gel processed barium titanate thin films". *Ferroelectrics letters*, Vol.22, pp.75-82 (1997)

62. Li, A.D., Ge, C.Z., Lü, P., Wu, D. and Xiong, S.B. "Fabrication and electrical properties of sol-gel derived $BaTiO_3$ films with metallic $LaNiO_3$ electrode". *Applied Physics Letters*, Vol.70, pp.1616-1618 (1997)

# List of Publications

1. Chan, H.L.W., Cheung, M.C. and Choy, C.L. "Study on $BaTiO_3$/P(VDf-TrFE) 0-3 composites". *Ferroelectrics*, Vol.224, pp.113-120 (1999)
2. Cheung, M.C., Chan, H.L.W., Zhou, Q.F. and Choy, C.L. "Barium titanate ceramic/ceramic 0-3 composites for ultrasonic transducer application". *to be published in Proceedings 1999 Spring Meeting Symposium.*
3. Cheung, M.C., Chan, H.L.W., Zhou, Q.F. and Choy, C.L. "Characterization of barium titanate ceramic/ceramic nanocomposite films prepared by a sol-gel process". *accepted by Nanostructured Materials.*
4. Cheung, M.C., Chan, H.L.W. and Choy, C.L. "Study on barium titanate ceramics prepared by various methods". *Submitted to Journal of Materials Science.*